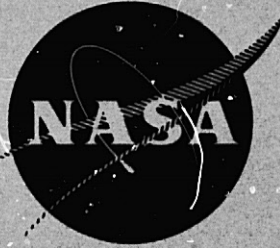


## **General Disclaimer**

### **One or more of the Following Statements may affect this Document**

- This document has been reproduced from the best copy furnished by the organizational source. It is being released in the interest of making available as much information as possible.
- This document may contain data, which exceeds the sheet parameters. It was furnished in this condition by the organizational source and is the best copy available.
- This document may contain tone-on-tone or color graphs, charts and/or pictures, which have been reproduced in black and white.
- This document is paginated as submitted by the original source.
- Portions of this document are not fully legible due to the historical nature of some of the material. However, it is the best reproduction available from the original submission.



# OSCILLATORY COMBUSTION OF LIQUID MONOPROPELLANT DROPLETS

by

S. P. Chanin and G. M. Faeth

Mechanical Engineering Department  
The Pennsylvania State University  
University Park, Pennsylvania

prepared for

NATIONAL AERONAUTICS AND SPACE ADMINISTRATION

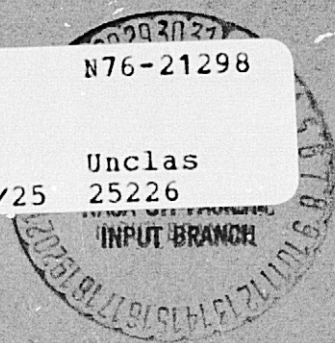
NASA Lewis Research Center  
Contract NGR 39-009-077

Richard J. Priem, Program Manager and Technical Monitor

(NASA-CR-134983) OSCILLATORY COMBUSTION OF  
LIQUID MONOPROPELLANT DROPLETS (Pennsylvania  
State Univ.) 129 p HC \$6.00 CSCL 21B

N76-21298

Unclas  
G3/25 25226



1. Report No. NASA CR-134983		2. Government Accession No.		3. Recipient's Catalog No.	
4. Title and Subtitle  Oscillatory Combustion of Liquid Monopropellant Droplets				5. Report Date March 1976	
				6. Performing Organization Code	
7. Author(s) S. P. Chanin and G. M. Faeth				8. Performing Organization Report No.	
9. Performing Organization Name and Address Mechanical Engineering Department The Pennsylvania State University University Park, Pennsylvania 16802				10. Work Unit No.	
				11. Contract or Grant No. NGR 39-009-077	
12. Sponsoring Agency Name and Address National Aeronautics and Space Administration Washington, D. C. 20546				13. Type of Report and Period Covered Contractor Report	
				14. Sponsoring Agency Code	
15. Supplementary Notes Program Manager and Technical Monitor, Richard J. Priem, Chemical Rocket Division NASA Lewis Research Center, Cleveland, Ohio					
16. Abstract  A theoretical investigation was conducted on the open-loop combustion response of monopropellant droplets and sprays to imposed pressure oscillations. The theoretical model was solved as a perturbation analysis through first order, yielding linear response results. Unsteady gas phase effects were considered in some cases, but the bulk of the calculations assumed a quasi-steady gas phase. Calculations were conducted using properties corresponding to hydrazine decomposition. Zero-order results agreed with earlier measurements of hydrazine droplet burning in combustion gases. The droplet response was greatest (exceeding unity in some cases) for large droplets with liquid phase temperature gradients; at frequencies near the characteristic frequency of the liquid phase thermal wave. The response of a spray is less than that of its largest droplet, however, a relatively small percentage of large droplets provides a substantial response (exceeding unity in some cases).					
17. Key Words (Suggested by Author(s)) Hydrazine fuel combustion Burning rate response Spray combustion				18. Distribution Statement  Unclassified-Unlimited	
19. Security Classif. (of this report) Unclassified		20. Security Classif. (of this page) Unclassified		21. No. of Pages 129	22. Price* \$ 3.00

\* For sale by the National Technical Information Service, Springfield, Virginia 22151

## SUMMARY

The objective of this study was to theoretically examine the open-loop combustion response of monopropellant droplets and sprays to imposed pressure oscillations. The theoretical model is an extension of an earlier response model developed for one-dimensional liquid monopropellant strand combustion. The theoretical approach employed perturbation analysis through first order, yielding linear response results.

The major assumptions of the analysis were: a one-step, irreversible gas phase reaction; phase equilibrium at the liquid surface; constant liquid phase physical properties; variable gas phase physical properties; and negligible forced convection. The latter assumption is known to be valid at high reactivities, where the reaction zone is close to the liquid surface. Transient liquid phase analysis was coupled with both transient and quasi-steady gas phase models. The calculations emphasized the quasi-steady gas phase case, since unsteady gas phase effects largely became important at frequencies greater than the most probable frequency range for combustion instability. The calculations were conducted using properties corresponding to hydrazine decomposition.

The results of the study may be summarized as follows:

### STEADY COMBUSTION

1. The zero-order or steady state calculations gave predictions in good agreement with earlier measurements of liquid surface temperatures and droplet burning rates in combustion gases, for hydrazine.

2. Small droplets essentially evaporate with little reaction effects while large drops (about two orders of magnitude larger) burn with surface mass fluxes equivalent to liquid strands. A simple approximate formula was developed which estimates burning rates for all sizes with maximum errors on the order of 10%.

### DROPLET RESPONSE

1. Small drops give low or negative response at all frequencies.

2. Large drops provide a response near unity at low frequencies. Response declines at frequencies somewhat in excess of the characteristic frequency of the liquid phase thermal wave. If temperature gradients of sufficient magnitude are present in the liquid phase, this decline is preceded by a response peak in excess of unity.

3. If a response peak occurs at liquid phase thermal wave frequencies, it is associated with a frequency regime where the surface temperature oscillation leads the pressure oscillation. At higher frequencies the temperature oscillation lags the pressure oscillation, and this behavior is associated with declining response.

4. Large drops have a second response peak of order unity at frequencies associated with the gas phase thermal wave; however, the frequency range of this peak is generally higher than frequencies associated with combustion instability.

#### SPRAY RESPONSE

1. The total response of a monodisperse injected spray is less than the response of the initial droplet size; although the frequency range of response peaking is similar.

2. For a polydisperse injected spray, the response depends strongly on the spray distribution. Even a low percentage of large droplets can yield an appreciable response, due to their long lifetime and high response.

3. At high pressures and low frequencies in the range associated with combustion instability, droplet lifetimes approach the cycle period for drop sizes of technological importance. The response associated with the lifetime was not considered in this investigation, and deserves further study.

## ACKNOWLEDGMENTS

The financial support of the National Aeronautics and Space Administration under Contract Number NGR 39-009-077, with Dr. R. J. Priem of the Lewis Research Center serving as contract monitor, is gratefully acknowledged.



## TABLE OF CONTENTS (CONTINUED)

	<u>Page</u>
III. STEADY STATE DROPLET RESULTS . . . . .	39
3.1 Introduction . . . . .	39
3.2 Temperature Distribution . . . . .	39
3.3 Mass Burning Rates . . . . .	45
IV. FIRST-ORDER RESULTS . . . . .	54
4.1 Introduction . . . . .	54
4.2 Small Drop, Low Frequency Limit . . . . .	55
4.3 Large Drop Limit . . . . .	57
4.4 Complete Solution . . . . .	68
V. SPRAY COMBUSTION MODEL . . . . .	82
5.1 Description of the General Model . . . . .	82
5.2 Life History Analysis . . . . .	86
VI. SPRAY COMBUSTION RESULTS . . . . .	91
6.1 Droplet Burning Time . . . . .	91
6.2 Quasi-Steady Gas Phase Spray Response . . . . .	96
VII. SUMMARY AND CONCLUSIONS . . . . .	102
7.1 Summary . . . . .	102
7.2 Conclusions . . . . .	103
7.2.1 Steady State Combustion . . . . .	104
7.2.2 Oscillatory Combustion . . . . .	105
7.2.3 Spray Combustion . . . . .	106
BIBLIOGRAPHY . . . . .	107

LIST OF TABLES

<u>Table</u>	<u>Title</u>	<u>Page</u>
1	Properties Used in the Theoretical Model. . . . .	40
2	Steady Droplet Burning Rate Data (Non-Wet Bulb) . . . .	49
3	Summary of Steady State Calculations. . . . .	51
4	Droplet Size Range of Transition Region . . . . .	53
5	Critical Frequency Ranges for Hydrazine Strand Combustion. . . . .	66
6	Frequencies of the Unsteady Gas and Liquid Phase Response Peaks. . . . .	67
7	Dimensional Droplet Lifetimes as a Function of Initial Radius and Pressure . . . . .	95

## LIST OF FIGURES

<u>Figure</u>	<u>Caption</u>	<u>Page</u>
1	Sketch of the Droplet Combustion Response Model . . .	11
2	Theoretical and Experimental Liquid Surface Temperatures as a Function of Pressure. . . . .	42
3	Steady State Liquid Phase Temperatures as a Function of A at Approximately 10 Atm. Pressure (Non-Wet Bulb Conditions) . . . . .	43
4	Steady State Gas Phase Temperatures as a Function of A at Approximately 10 Atm. Pressure (Non-Wet Bulb Conditions) . . . . .	44
5	Steady State Gas Phase Temperatures as a Function of A at Approximately 10 Atm. Pressure (Wet Bulb Conditions). . . . .	46
6	Theoretical and Experimental Steady State Droplet Gasification Rates at Approximately 1 Atm. Pressure (Non-Wet Bulb Conditions). . . . .	48
7	Theoretical Steady State Droplet Gasification Rates at Approximately 1 Atm. Pressure (Wet Bulb Conditions) . . . . .	50
8	Response and Perturbation Surface Temperature as a Function of Pressure at the Small Droplet Limit for Wet and Non-Wet Bulb Conditions . . . . .	56
9	Response as a Function of Frequency at the Large Droplet Limit at Approximately 1 Atm. Pressure (Non-Wet Bulb Conditions) . . . . .	58
10	Response as a Function of Frequency at the Large Droplet Limit at Approximately 10 Atm. Pressure (Non-Wet Bulb Conditions) . . . . .	59
11	Response as a Function of Frequency at the Large Droplet Limit at Approximately 100 Atm. Pressure (Non-Wet Bulb Conditions) . . . . .	60
12	Response as a Function of Frequency at the Large Droplet Limit at Approximately 1 Atm. Pressure (Wet Bulb Conditions) . . . . .	62

## LIST OF FIGURES (CONTINUED)

<u>Figure</u>	<u>Caption</u>	<u>Page</u>
13	Response as a Function of Frequency at the Large Droplet Limit at Approximately 10 Atm. Pressure (Wet Bulb Conditions) . . . . .	63
14	Response as a Function of Frequency at the Large Droplet Limit at Approximately 100 Atm. Pressure (Wet Bulb Conditions) . . . . .	64
15	Quasi-Steady Gas Phase Response as a Function of Frequency and A at Approximately 1 Atm. Pressure (Non-Wet Bulb Conditions) . . . . .	69
16	Quasi-Steady Gas Phase Response as a Function of Frequency and A at Approximately 10 Atm. Pressure (Non-Wet Bulb Conditions) . . . . .	70
17	Quasi-Steady Gas Phase Response as a Function of Frequency and A at Approximately 100 Atm. Pressure (Non-Wet Bulb Conditions) . . . . .	71
18	Quasi-Steady Gas Phase Response as a Function of Frequency and A at Approximately 1 Atm. Pressure (Wet Bulb Conditions) . . . . .	72
19	Quasi-Steady Gas Phase Response as a Function of Frequency and A at Approximately 10 Atm. Pressure (Wet Bulb Conditions) . . . . .	73
20	Quasi-Steady Gas Phase Response as a Function of Frequency and A at Approximately 100 Atm. Pressure (Wet Bulb Conditions) . . . . .	74
21	Perturbation Surface Temperature Magnitude and Phase Angle as a Function of Frequency and Pressure (Non-Wet Bulb Conditions) . . . . .	75
22	Perturbation Liquid Phase Temperature Distribution for a Sinusoidal Pressure Oscillation and a $T_{1s}$ Phase Lead of Approximately 4 Degrees (Non-Wet Bulb Conditions). . . . .	77
23	Perturbation Surface Temperature Magnitude and Phase Angle as a Function of Frequency and Pressure (Wet Bulb Conditions). . . . .	78

## LIST OF FIGURES (CONTINUED)

<u>Figure</u>	<u>Caption</u>	<u>Page</u>
24	Perturbation Liquid Phase Temperature Distribution for a Sinusoidal Pressure Oscillation and a $T_{1s}$ Phase Lag of Approximately 5.5 Degrees (Wet Bulb Conditions) . . . . .	79
25	Spray Combustion Model. . . . .	87
26	Nondimensional Droplet Lifetimes as a Function of $A_o/A_s$ . . . . .	92
27	Nondimensional Droplet Burning Time as a Function of Nondimensional Droplet Radius at Approximately 10 Atm. Pressure (Non-Wet Bulb Conditions) . . . . .	93
28	Nomdimensional Droplet Burning Time as a Function of Nondimensional Droplet Radius at Approximately 10 Atm. Pressure (Wet Bulb Conditions). . . . .	94
29	Total Response as a Function of $\omega_o$ for a Monodisperse Spray at Approximately 10 Atm. Pressure (Non-Wet Bulb Conditions) . . . . .	97
30	Total Response as a Function of $\omega_o$ for a Monodisperse Spray at Approximately 10 Atm. Pressure (Wet Bulb Conditions) . . . . .	99
31	Total Response as a Function of $\omega_o$ for a Polydisperse Spray at Approximately 10 Atm. Pressure for Varying Spray Set Mass Fractions and Injection Rates (Non-Wet Bulb Conditions) . . . . .	100

## NOMENCLATURE

<u>Symbol</u>	<u>Description</u>
a	Vapor pressure parameter, Equation (2-20)
A	Parameter, Equation (2-30)
A <sub>s</sub>	Parameter for strand case, Equation (2-76)
A <sub>o</sub>	Initial A injected into chamber, Equation (5-15)
A <sub>1-5</sub>	Constants in first-order solution, Equations (2-107)-(2-111)
B	Pre-exponential factor, Equation (2-7)
C	Constant, Equation (2-73)
C <sub>f</sub>	Specific heat of liquid, Equation (2-2)
C <sub>p</sub>	Specific heat of gas, Equation (2-5)
D	Binary diffusivity, Equation (2-4)
D <sub>1-3</sub>	Constants used in first-order solution, Equations (2-115)-(2-117)
E	Activation energy, Equation (2-7)
f	Spray droplet distribution function, Equation (5-3)
F	Fraction, Equation (5-21)
F <sub>1-4</sub>	Constants used in first-order solution, Equations (2-118)-(2-121)
g	Spray injection distribution function, Equation (5-11)
G <sub>1-2</sub>	Constants used in first-order solution, Equations (2-122)-(2-123)
h <sub>i</sub> <sup>o</sup>	Heat of formation, Equation (2-9)
H <sub>1-5</sub>	Constants used in first-order solution, Equations (2-92)-(2-94), (2-101), (2-102)
i	$\sqrt{-1}$ , Equations (2-52)
I	Total number of drops injected per unit time into a combustion chamber
J <sub>11-23</sub>	Constants used in first-order solution, Equations (2-132)

## NOMENCLATURE (CONTINUED)

<u>Symbol</u>	<u>Description</u>
$K_T$	Constant used in first-order solution, Equations (2-99)
$K_L$	Constant, Equation (2-89)
$L$	Linear operator, Equation (2-91)
$L'$	Linear operator, Equation (2-106)
$L$	Heat of vaporization, Equation (2-18)
$L_e$	Lewis number, Equation (2-13)
$L_f$	Vapor pressure parameter, Equation (2-20)
$\dot{m}$	Mass flow per unit solid angle, Equation (2-1)
$M$	Molecular weight, Equation (2-7)
$n$	Reaction order, Equation (2-7)
$N$	Total number of species $i$ , Equation (2-4)
$N$	Total number of drops in a spray set, Equation (5-3)
$p$	Pressure, Equation (2-5)
$P_r$	Open-loop response, Equation (4-4)
$P_{rt}$	Total (spray) response, Equation (5-2)
$q$	Energy of reaction, Equation (2-5)
$r$	Strand burning rate, Equation (4-4)
$r$	Radial distance, Equation (2-1)
$r_{so}$	Initial radius injected into combustion chamber, Equation (5-7)
$R$	Universal gas constant, Equation (2-7)
$Re$	Real part, Equation (4-1)
$R_s$	Radius, Equation (5-7)
$R_{so}$	Radius, Equation (5-10)
$R_s'$	Beginning of drop size group (radius), Equation (5-21)

## NOMENCLATURE (CONTINUED)

<u>Symbol</u>	<u>Description</u>
$R_s$	End of drop size group (radius), Equation (5-21)
$t$	Time, Equation (2-2)
$T$	Temperature, Equation (2-2)
$T_o$ (1)	Expansion variable, Equation (2-69)
$v_r$	Radial velocity, Equation (2-1)
$w$	Reaction rate, Equation (2-4)
$Y_i$	Mass fraction of species $i$ , Equation (2-4)
$\alpha$	Thermal diffusivity, Equation (2-22)
$\alpha'$	Constant, Equation (2-70)
$\beta$	Ratio of specific heats, Equation (2-22)
$\gamma$	Specific heat ratio, Equation (2-28)
$\delta$	Temperature dependence of pre-exponential factor, Equation (2-7)
$\delta_f$	Ratio of thermal diffusivities, Equation (2-22)
$\epsilon$	Amplitude of oscillatory pressure, Equation (2-52)
$\xi$	Small parameter, Equation (2-69)
$\eta$	Stretched radial distance coordinate, Equation (2-70)
$\theta$	Combined variable, Equation (2-40)
$\lambda$	Thermal conductivity, Equation (2-2)
$v_i, v_i''$	Stoichiometric parameters, Equation (2-6)
$v_i$	Parameter, Equation (2-8)
$\rho$	Density, Equation (2-1)
$\tau$	Time, Equation (5-17)
$\omega$	Frequency, Equation (2-52)
$\omega_o$	Frequency, Equation (5-22)

## NOMENCLATURE (CONTINUED)

<u>Symbol</u>	<u>Description</u>
$\omega_j$	Frequency, Equation (5-23)
$\omega_s$	Frequency for strand case, Equation (4-5)

Subscripts

f	Liquid
F	Fuel
H	Homogeneous solution
i	Center of droplet
j	Size group j
L	Lifetime
LDL	Large drop limit
ref	Reference to largest drop injected into combustion chamber
s	Liquid surface
s-	Inner side of liquid surface
s+	Outer side of liquid surface
SDL	Small drop limit
T	Total
o	Steady state quantities
p	Particular solution
l	First-order quantities
$\infty$	Ambient conditions, far from liquid surface

Superscripts

*	Dimensional quantities
*	Symbol used in first-order solution

## NOMENCLATURE (CONTINUED)

<u>Symbol</u>	<u>Description</u>
$\hat{\phantom{x}}$	Symbol used in first-order solution
-	Symbol used in first-order solution
-	Steady State
'	Instantaneous perturbation

## CHAPTER I

### INTRODUCTION

#### 1.1 General Statement of the Problem

The phenomenon of rocket combustion instability is the direct result of the coupling between the combustion and fluid dynamics of the overall combustion system. This coupling enables oscillatory energy from the combustion process to sustain these instabilities. The oscillations will decay only by decreasing the coupling mechanism or by insuring the damping process, either natural or man-made, has sufficient magnitude to dissipate the supplied oscillatory energy at a faster rate than it is produced.

Almost every rocket engine development program has encountered combustion instabilities in one form or other; thus, understanding this phenomena is of major importance. These oscillations, which have frequencies in the range of 500-30000 Hz [1], are capable of producing vibrations, increased heat transfer rates, decreased performance, uncontrolled impulses, and variations in the thrust vectors of rocket combustion chambers [1]. Since rockets often carry humans and/or expensive and very sensitive equipment, the understanding and prevention of these destructive oscillations are of utmost concern.

Instabilities can be initiated spontaneously from the inherent noise in the combustion and mechanical processes, or they can be activated by a finite disturbance such as a chamber pressure fluctuation or an explosion of accumulated propellants [1].

Combustion instabilities can be suppressed by the use of acoustic liners, Helmholtz resonators, baffles, other damping devices, or by the redesign of the combustion chamber, in order to eliminate resonant modes. The only true test of the stability of a rocket engine, however, is from an actual test firing. This further underscores the importance of understanding the coupling mechanism between the combustion process and the fluid dynamics.

The objective of the present study is to investigate one aspect of the combustion instability problem, namely, the response of a burning liquid monopropellant to imposed pressure oscillations. The response of a single droplet is considered first, followed by an estimation of the response of an entire spray.

Hydrazine is selected as the monopropellant fuel in this study, since the hydrazine family of fuels are extensively used in today's space rocket programs. For example, the Apollo command module thruster and the lunar ascent and descent engines use hydrazine fuels. The major emphasis of this study concerns the theoretical analysis of hydrazine droplet combustion and burning rate response to fluctuations in pressure.

## 1.2 Previous Related Studies

Consideration of previous work is divided into three categories; liquid monopropellant droplet combustion, quasi-steady monopropellant spray combustion, and oscillatory combustion.

1.2.1 Monopropellant Droplet Combustion. A detailed summary of experimental hydrazine droplet and strand (large drop limit) combustion has been presented by Allison [2, 3].

Fendell [4] obtained a closed form analytical solution for the burning of monopropellants in an inert atmosphere at the zero activation energy limit.

Williams [5] restricted his approach to adiabatic burning with a low reaction rate and a one-step overall reaction. He developed an analytical solution for small drops having low chemical reaction rates and large activation energies. His analysis is limited by the adiabatic and low reaction rate assumptions.

Spalding and Jain [6], Jain [7], Tarifa [8], and Allison and Faeth [9] have investigated monopropellant droplet combustion using the thin flame approximations. Spalding and Jain [6] and Jain [7] used the thin flame approximation in order to obtain an analytical solution for monopropellant droplet burning rates. The energy release of the decomposition reaction is assumed to occur in a thin shell at some distance from the drop. The reaction rate dependence on temperature is quite strong for large activation energies, and the flame surface is located where the unreacted gas flows into the thin shell at the laminar burning velocity of the mixture. Spalding and Jain [6] were able to estimate the droplet burning rate as a function of the laminar flame speed, which is known from experiment, for adiabatic combustion.

Tarifa [8] assumed an Arrhenius global reaction rate in a flame zone of finite thickness, and obtained an analytical solution for monopropellant combustion in an atmosphere of inert gases. Allison and Faeth [9] used Spadling's [6] thin flame approximation in order to relate flame position to the laminar burning velocity. An Arrhenius correlation with two adjustable parameters was used to approximate the

laminar burning velocity. Allison and Faeth [9] also obtained experimental droplet burning rate results which compare favorably with results obtained in the present study.

Lorell and Wise [10] considered the case of a single, unimolecular overall reaction with no backward reaction. A two point boundary value problem was numerically solved in order to find the burning rate eigenvalue.

Later work by Allison and Faeth [11] employed one-step kinetics to describe the combustion of a liquid hydrazine strand. The steady state conservation equations were integrated numerically, using an asymptotic expansion to formally satisfy the boundary conditions at large distances from the liquid surface. This procedure does not involve any approximate mathematical treatment of the combustion process, and since it minimizes uncertainties in the model, this approach was employed in the present study.

1.2.2 Quasi-Steady Monopropellant Spray Combustion. The problem of combustion instability is very complicated and contains many variables. There are several analytical methods to describe combustion instabilities in combustion chambers; however, they are severely limited to idealized problems, and almost none have been applied to the monopropellant case. A review of the current literature on this subject can be found in Reference [1].

The present theoretical study uses a one dimensional, spray combustion model. This model considers several drop size groups, in order to simulate actual spray characteristics. The response

contribution from each of these groups is summed to obtain the overall spray response.

1.2.3 Oscillatory Combustion. A description of much of the available literature on combustion instability is given in Reference [1]. The present summary primarily considers liquid burning rate response to imposed pressure oscillations.

Crocco [12, 13, 14] uses the sensitive time lag theory in which a time lag exists between the time a fuel particle is injected into the combustion chamber and the time it is burned to form the final combustion products. With this approach, the combustion-gas dynamic coupling process is not explicitly considered, and the time lag can only be found from experimental observations.

Priem [15, 16, 17] realized that the thermal energy and the gas release rates are of utmost importance in analyzing the combustion process, and he numerically solved the gas dynamic equations for the combustion chamber to determine these factors. Fluctuations in the surrounding gaseous flow field and the unsteady burning rate response of the droplets, which is the source term in the gas dynamic equations, were also investigated by Priem.

Williams [18] and Strahle [19, 20] used a bipropellant fuel and assumed the Burke-Schumann thin diffusion flame model in the leading edge boundary layer of the burning droplet. The droplet was subjected to longitudinal standing wave fluctuations while the liquid temperatures were assumed to be constant. The response curves, which depend on frequency, were flat with a peak at extremely high frequencies. The difficulty with this analysis arises from the fact

that liquid temperatures are not constant for oscillatory combustion, even at low frequencies, while the gas phase can be considered to be quasi-steady except at very high frequencies and pressures [21].

Heidmann and Wieber [22] also investigated bipropellant droplets, assuming that at each point in time, the gas phase combustion rate equalled the vaporization rate of the liquid fuel. This is not a good assumption at high frequencies where gas phase transient effects become important. However, they did find response peaks for quasi-steady drops.

In the bipropellant analysis of T'ien and Sirignano [23], the gas phase was considered to be quasi-steady with respect to the liquid phase at low frequencies. The peaks in the response function were caused by the liquid phase thermal lag; however, the response was not large enough to provide a mechanism for instability. While the liquid phase thermal wave does not give sufficient peaks for bipropellants, this may not be the case for monopropellants, which were not considered in Reference [23].

Allison and Faeth [11] used a monopropellant hydrazine strand model, similar to a model used by T'ien [24] for a solid propellant response study. They assumed low pressure phase equilibrium at the liquid surface, unsteady liquid phase, and both quasi-steady and unsteady gas phase. The liquid phase thermal wave for strand combustion yielded peaks capable of causing instability. Liquid fuel response was measured at frequencies representative of the response of the liquid phase thermal wave. Agreement between theory and experiment regarding both the magnitude and phase lag of the combustion response was found to be good. The next logical step in this analysis

would be the investigation of oscillatory combustion of droplets. The present study seeks to complete this extension.

### 1.3 Specific Statement of the Problem

The development of a mathematical model of oscillatory combustion of liquid monopropellant droplets is of significant value due to the application of these propellants in actual rocket engines.

Very few, if any, experimental studies of nonsteady liquid droplet combustion have been conducted. The past procedure has been to obtain pressure-time data from actual rocket engine tests and then attempt to deduce burning rate response.

Allison and Faeth [11] studied steady and unsteady burning of liquid strands of hydrazine, and were able to obtain very good agreement between experiment and theory. These one-dimensional strands approximate the large drop limit, since the curvature effect of a large spherical drop is negligible.

The present study will extend the work of Allison and Faeth [9, 11] to derive a mathematical model for unsteady oscillatory droplet burning. The large drop values will be compared with the one-dimensional strand burning results of Allison and Faeth [11]. The forcing function will be the gas phase pressure oscillations, and the burning rate or open-loop response will be examined.

Thus, the specific objectives of the present study are:

1. Develop a mathematical model for the burning of a liquid monopropellant droplet for both steady state and oscillatory pressure conditions.

2. Theoretically investigate the steady state droplet burning for both wet and non-wet bulb conditions, and compare the results with available measurements.
3. Investigate the theoretical burning rate response for wet and non-wet bulb conditions.
4. Develop a mathematical model for one-dimensional, quasi-steady spray combustion, and calculate the overall spray combustion response for both wet and non-wet bulb conditions.

## CHAPTER II

### THEORETICAL CONSIDERATIONS

#### 2.1 General Model and Assumptions

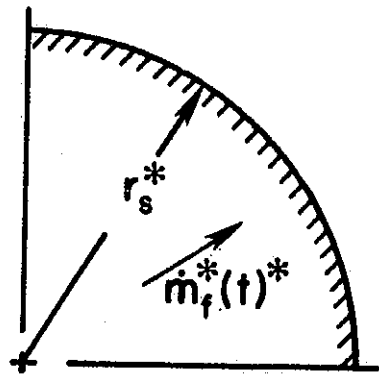
The theoretical model under consideration involves a droplet that is burning in the absence of convection, yielding a spherically symmetric flow field. While convection is important under actual combustion chamber conditions, there is evidence to indicate that the region where the droplet has a low (or zero) relative velocity with respect to the ambient gas, is a very critical zone in determining combustion instability characteristics [1]. For simple evaporation without decomposition, the response due to velocity effects has been found to be quite low [23]. In addition, the decomposition process near the droplet surface reduces the influence of convection over a fairly wide range of conditions [25], [26]. This occurs since convection only affects the process when the outer edge of the flow field interacts with the reaction zone, a situation that is limited to very weak reactivity or very high Reynolds numbers. Therefore, neglecting convection for monopropellant droplets puts fewer limitations on the practicality of the calculations, than would be the case for bipropellants.

Similar to earlier response studies [11], [23], the ambient pressure is assumed to be oscillating with a wavelength that is long in comparison to the dimensions of the combustion field of the droplet. The period of oscillation, however, is assumed to be short in comparison to the total droplet lifetime so that consideration does

not have to be given to large changes in the position of the surface during a pressure oscillation. This assumption allows the analysis to proceed while only examining oscillatory solutions. The frequency regime where this assumption breaks down will be discussed later.

Since the combustion rate of monopropellant droplets is much higher than bipropellants, the usual assumption of a constant liquid phase temperature (in the zero order) is less valid than for bipropellants. Therefore, the presence of mean liquid phase temperature gradients must be considered in the analysis. Also, examination of constant mean temperatures will be made, in order to include the conventional steady combustion model, by equating the bulk liquid temperature to the wet bulb temperature at a given pressure.

A sketch of the theoretical model is shown in Figure 1. The process is examined at an instant of time when the droplet radius is  $r_s^*$ . Formally, this radius is taken to be fixed so that the mass flux of fuel is time varying. This actually corresponds to porous sphere combustion; however, the two cases are equivalent as long as the density in the liquid phase is large compared to that of the gas phase; and the period of oscillation is small in comparison to the lifetime of the droplet [27]. When this is true, the motion of the surface with respect to the mean surface position is negligible and can be ignored. Exceptions to this assumption arise near the critical point and the present analysis is not valid in this regime. The response portion of the analysis is invalid at frequencies having an oscillation period comparable to the lifetime of the droplet.



REPRODUCIBILITY OF THE  
ORIGINAL PAGE IS POOR

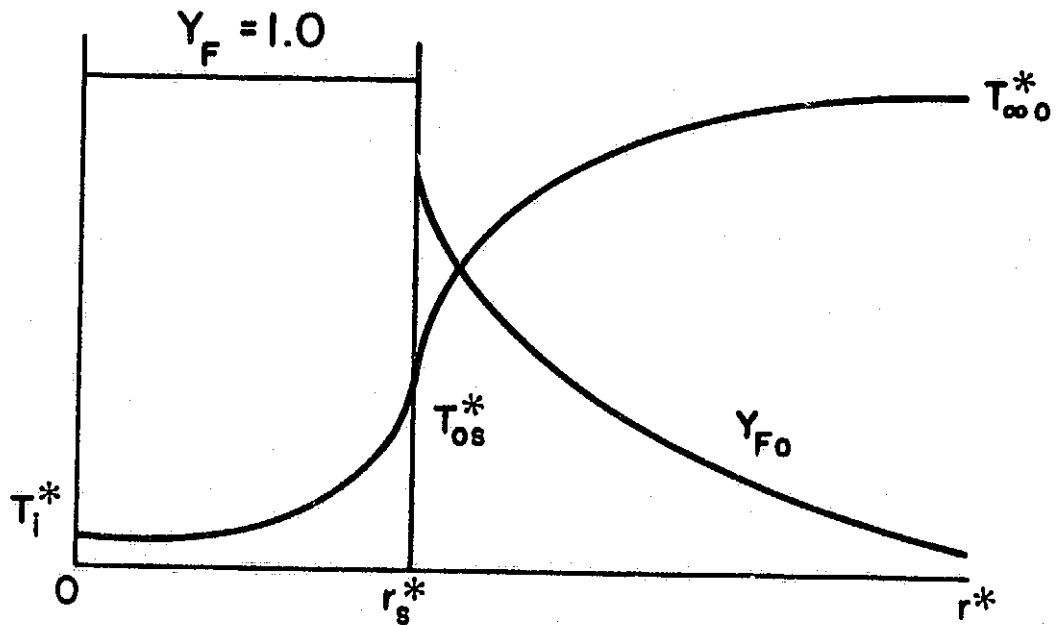


Figure 1 Sketch of the Droplet Combustion Response Model

In the true model of monopropellant droplet combustion, the radius is not constant, but decreases with time, while  $\dot{m}_f^*$  is zero. Also, as the droplet becomes smaller due to gasification, the temperature throughout the droplet tends to approach the surface or wet bulb temperature.

For generality, gas phase transient effects are included in the model. The effect of variable properties is also included, so that the model is equivalent to the earlier strand combustion analysis [11].

The remaining assumptions of the analysis are similar to those of Reference [11]. They are as follows:

1. The process is spherically symmetric with a Mach number less than unity and negligible body forces. Inertial and viscous terms in the momentum equation are neglected.
2. The reaction process is premixed and laminar. A one-step, irreversible chemical reaction takes place in the gas phase and any time lags associated with the chemical reaction itself are negligible, i.e., the chemical reaction is locally quasi-steady and obeys an Arrhenius equation. Chemical reaction is neglected in the liquid phase.
3. Radiation heat transfer is neglected.
4. The gas phase is taken to be an ideal gas and the Lewis number is assumed to be unity.
5. All gas diffusion coefficients are equal, all molecular weights are equal, all gas phase specific heats are equal and constant, the gas phase thermal conductivity is independent of composition and varies linearly with

temperature, and the liquid is composed of a single chemical species having constant properties.

6. The combustion products are assumed to be insoluble in the liquid phase and the gas phase fuel mass fraction at the liquid surface is given by the Clausius-Clapeyron equation. As in the case of the gas phase reaction, the equilibrium at the surface is assumed to occur rapidly in comparison to other transient effects in the system.
7. The wavelength of any periodic pressure disturbance is assumed to be long compared with the diameter of the zone involving active combustion. Consideration of the momentum equation, along with Assumption 1, then implies that pressure is only a function of time.

A discussion of the applicability of these assumptions is provided in References [3] and [11].

## 2.2 Governing Equations

2.2.1 Dimensional Equations. Considering the above assumptions, the dimensional conservation equations can be obtained in spherical coordinates from the general equations given in Reference [28].

Liquid Phase             $a \geq r^* \geq r_s^*$

Conservation of Mass

$$\rho_f^* r^{*2} v_{fr}^* = \dot{m}_f^* = \text{constant} \quad (2-1)$$

Conservation of Energy

$$\rho_f^* C_f^* r^{*2} \frac{\partial T^*}{\partial t^*} + \rho_f^* C_f^* r^{*2} v_r^* \frac{\partial T^*}{\partial r^*} = \lambda_f^* \frac{\partial}{\partial r} \left( r^{*2} \frac{\partial T^*}{\partial r^*} \right) \quad (2-2)$$

where  $\dot{m}_f^*$ , the mass flow rate per unit solid angle, is only a function of time.

Gas Phase  $r^* < r^* < \infty$

Conservation of Mass

$$\frac{\partial \rho^*}{\partial t^*} + \frac{1}{r^{*2}} \frac{\partial}{\partial r^*} (\rho^* r^{*2} v_r^*) = 0 \quad (2-3)$$

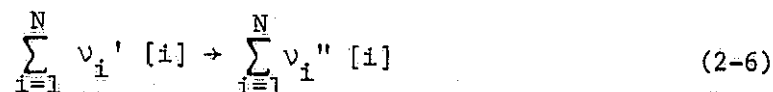
Conservation of Species

$$\rho^* \frac{\partial Y_i}{\partial t^*} + \rho^* v_r^* \frac{\partial Y_i}{\partial r^*} = \frac{1}{r^{*2}} \frac{\partial}{\partial r^*} \left( r^{*2} \rho^* D^* \frac{\partial Y_i}{\partial r^*} \right) + v_i w_F^* \quad i=1, N \quad (2-4)$$

Conservation of Energy

$$\rho^* C_P^* \frac{\partial T^*}{\partial t^*} + \rho^* v_r^* C_P^* \frac{\partial T^*}{\partial r^*} = \frac{1}{r^{*2}} \frac{\partial}{\partial r^*} \left( r^{*2} \lambda^* \frac{\partial T^*}{\partial r^*} \right) + \frac{\partial P^*}{\partial t^*} + q^* w_F^* \quad (2-5)$$

where the stoichiometry of the one-step gas phase reaction is assumed to have the form



The other terms in Equations (2-4) and (2-5) are defined as

$$w_F^* = B^* T^* \delta \left[ \frac{P^* Y_F}{M^* R^* T^*} \right]^n \exp \left[ \frac{-E^*}{R^* T^*} \right] \quad (2-7)$$

$$v_i = \frac{v_i'' - v_i'}{v_F'} \quad (2-8)$$

$$q^* = - \sum_{i=1}^N h_i^{*0} v_i \quad (2-9)$$

where  $v_F = -1$ . Since the gas is ideal

$$P^* = \rho^* R^* T^* / M^* \quad (2-10)$$

The gas phase mass flow rate per unit solid angle is defined as

$$\dot{m}^* = \rho^* r^{*2} v_r^* \quad (2-11)$$

The thermal conductivity is taken to be proportional to temperature

$$\lambda^* = \lambda_{\infty}^* (T^*/T_{\infty}^*) \quad (2-12)$$

The unity Lewis number assumption provides

$$Le = \frac{\lambda^*}{\rho^* D^* C_P^*} = 1 \quad (2-13)$$

#### Boundary Conditions

Since the liquid is incompressible, it has a constant temperature at the origin or center of the drop.

$$r^* = 0 \quad T^* = T_i^* \quad (2-14)$$

In the case of steady combustion at the wet bulb temperature of the droplet,  $T_i^*$  would be equal to the wet bulb temperature. However, since monopropellants have higher gasification rates than most bipropellants, cases exist where temperature gradients are present in the liquid phase throughout the lifetime of the droplet. Therefore,  $T_i^*$  is taken as a parameter for the analysis in order to investigate the effect of these gradients on the response.

Temperature and pressure are continuous across the liquid-gas interface.

$$T_{s-}^* = T_{s+}^* \quad (2-15)$$

REPRODUCIBILITY OF THE  
ORIGINAL PAGE IS POOR

$$P_{s-}^* = P_{s+}^* \quad (2-16)$$

Conservation of mass at the interface reduces to

$$\rho_f^* v_{r_{fs}}^* = \rho^* v_{r_s}^* \quad (2-17)$$

The conservation of energy equation, where the heat flux reaching the surface goes into the heat flux in the liquid phase and the heat of vaporization of the gasifying fuel, reduces to

$$\lambda_f^* \left. \frac{\partial T^*}{\partial r^*} \right]_{s-} = \lambda^* \left. \frac{\partial T^*}{\partial r^*} \right]_{s+} - \rho_f^* v_{r_{fs}}^* [(C_p^* - C_f^*) T_s^* + L^*] \quad (2-18)$$

The insolubility of the product species in the liquid phase implies that the total mass flux of the non-fuel species is zero at the surface of the droplet. The conservation of species equation then reduces to

$$\rho^* D^* \left. \frac{\partial Y_{Fs}}{\partial r^*} \right]_{s+} = \rho_f^* v_{r_{fs}}^* (Y_{Fs} - 1) \quad (2-19)$$

The fuel mass fraction is related to the temperature at the surface by the Clausius-Clapeyron equation.

$$Y_{Fs} = \frac{a^*}{P^*} \exp \left[ \frac{-L_f^*}{R^* T_s^*} \right] \quad (2-20)$$

Far from the drop surface all the fuel is consumed and the temperature is only a function of time.

$$r^* = \infty \quad Y_F = 0 \quad T^* = T^*(t^*) \quad (2-21)$$

where  $T^*(t^*)$  is a known function depending upon the specified pressure variation.

2.2.2 Nondimensional Equations. The previous equations are simplified by transformation into the following dimensionless variables.

$$\begin{aligned}
 a &= a^*/p_o^* & r &= r^*/r_s^* \\
 D &= D^*/D_{\infty o}^* & t &= t^*\lambda_{\infty o}^*/\rho_{\infty o}^*C_p^*r_s^{*2} \\
 E &= E^*/R^*T_{\infty o}^* & T &= T^*/T_{\infty o}^* \\
 L &= L^*/C_p^*T_{\infty o}^* & v_r &= v_r^*\rho_{\infty o}^*C_p^*r_s^*/\lambda_{\infty o}^* \\
 L_f &= L_f^*/R^*T_{\infty o}^* & \beta &= C_f^*/C_p^* \\
 \dot{m} &= \dot{m}^*C_p^*/r_s^*\lambda_{\infty o}^* & \delta_f &= \alpha_f^*/\alpha_{\infty o}^* \\
 p &= p^*/p_o^* & \lambda &= \lambda^*/\lambda_{\infty o}^* \\
 q &= q^*/C_p^*T_{\infty o}^* & \rho &= \rho^*/\rho_{\infty o}^*
 \end{aligned} \tag{2-22}$$

The conservation equations can now be rewritten in dimensionless form as follows:

Liquid Phase  $r \leq 1$

$$\rho_f r^2 v_{fr} = \dot{m}_f \tag{2-23}$$

$$\frac{\partial T}{\partial t} + v_{fr} \frac{\partial T}{\partial r} = \frac{\delta_f}{r^2} \frac{\partial}{\partial r} \left( r^2 \frac{\partial T}{\partial r} \right) \tag{2-24}$$

Gas Phase  $r > 1$

$$\frac{\partial \rho}{\partial t} + \frac{1}{r^2} \frac{\partial}{\partial r} (\rho r^2 v_r) = 0 \tag{2-25}$$

$$\dot{m} = \rho r^2 v_r \quad (2-26)$$

$$\rho \left( \frac{\partial Y_i}{\partial t} + v_r \frac{\partial Y_i}{\partial r} \right) = \frac{1}{r^2} \frac{\partial}{\partial r} \left( r^2 \rho D \frac{\partial Y_i}{\partial r} \right) + v_i w \quad i = 1, N \quad (2-27)$$

$$\rho \left( \frac{\partial T}{\partial t} + v_r \frac{\partial T}{\partial r} \right) = \frac{1}{r^2} \frac{\partial}{\partial r} \left( r^2 \lambda \frac{\partial T}{\partial r} \right) + \left( \frac{\gamma - 1}{\gamma} \right) \frac{dp}{dt} + q w \quad (2-28)$$

where the dimensionless reaction rate is defined as

$$w = A p^{n_p} T^{\delta} Y_F^{n_Y} \exp(-E/T) \quad (2-29)$$

and A is a reaction parameter which is related to the drop size

$$A = \frac{C_p^* B^* r_s^* T_{\infty 0}^{\delta}}{\lambda_{\infty 0}^*} \left[ \frac{P_o^*}{M^* R^* T_{\infty 0}^*} \right]^n \quad (2-30)$$

The assumptions of an ideal gas, unity Lewis number, and thermal conductivity proportional to temperature, reduce to the following relationship

$$T = \lambda = \rho D = p/\rho \quad (2-31)$$

### Boundary Conditions

The dimensionless boundary condition equations are:

At the center of the drop,  $r = 0$

$$T = T_i \quad (2-32)$$

At the drop surface,  $r = 1$

$$T_{s-} = T_{s+} \quad (2-33)$$

$$P_{s-} = P_{s+} \quad (2-34)$$

$$\lambda_f \left. \frac{\partial T}{\partial r} \right|_{s-} = \lambda \left. \frac{\partial T}{\partial r} \right|_{s+} - \rho v_r [(1-\beta)T + L] \quad (2-35)$$

$$\rho D \left. \frac{\partial Y_F}{\partial r} \right|_{s+} = \rho v_r (Y_F - 1) \quad (2-36)$$

$$Y_F = a \exp(-L_f/T) \quad (2-37)$$

Far from the drop surface  $r = \infty$

$$Y_F = 0 \quad (2-38)$$

$$T = T(t) \quad (2-39)$$

The above equations can be further simplified by introducing the Shvab-Zeldovich variable,  $\theta$ , a new dependent variable based on the fuel mass fraction

$$\theta = q Y_F + T \quad (2-40)$$

After substituting Equation (2-40) into Equations (2-27) to (2-29) and (2-36) to (2-38), along with some minor simplifications, the pertinent equations can be summarized as follows:

Liquid Phase  $r \leq 1$

$$\frac{\partial T}{\partial t} + v_{fr} \frac{\partial T}{\partial r} = \frac{\delta_f}{r^2} \frac{\partial}{\partial r} \left( r^2 \frac{\partial T}{\partial r} \right) \quad (2-41)$$

Gas Phase  $r > 1$

$$\frac{\partial \rho}{\partial t} + \frac{1}{r^2} \frac{\partial}{\partial r} (\rho r^2 v_r) = 0 \quad (2-42)$$

$$\rho \left( \frac{\partial \theta}{\partial t} + v_r \frac{\partial \theta}{\partial r} \right) = \frac{1}{r^2} \frac{\partial}{\partial r} \left( r^2 T \frac{\partial \theta}{\partial r} \right) + \left( \frac{\gamma - 1}{\gamma} \right) \frac{d\rho}{dt} \quad (2-43)$$

$$\rho \left( \frac{\partial T}{\partial t} + v_r \frac{\partial T}{\partial r} \right) = \frac{1}{r^2} \frac{\partial}{\partial r} \left( r^2 T \frac{\partial T}{\partial r} \right) + \left( \frac{\gamma - 1}{\gamma} \right) \frac{d\rho}{dt} + q w \quad (2-44)$$

$$w = A q^{-n} p^n T^{\delta-n} (\theta - T)^n \exp(-E/T) \quad (2-45)$$

Boundary Conditions

$$r = 0$$

$$T = T_i \quad (2-46)$$

$$r = 1$$

$$T = T_s \quad (2-47)$$

$$\lambda_f \left. \frac{\partial T}{\partial r} \right|_{s-} = T \left. \frac{\partial T}{\partial r} \right|_{s+} - \rho v_r [(1-\beta)T + L] \quad (2-48)$$

$$T \left. \frac{\partial(\theta - T)}{\partial r} \right|_{s+} = \rho v_r (\theta - T - q) \quad (2-49)$$

$$\theta - T = aq \exp(-L_f/T) \quad (2-50)$$

$$\theta = T = T(t) \quad (2-51)$$

2.2.3 Perturbation Analysis. The imposed pressure oscillations can be decomposed into a constant mean pressure and an oscillatory component having a small amplitude,  $\epsilon$ . Transforming the dependent variables in the same manner, substituting into the conservation and boundary equations, and separating into like powers of  $\epsilon$ , results in zero-order or steady state equations ( $\epsilon^0$ ) and first-order or oscillatory equations ( $\epsilon^1$ ). The higher powers of  $\epsilon$  are disregarded in the present analysis, which considers only linear response. The assumed pressure oscillation and the dependent variables are represented as follows:

$$p(t) = 1 + \varepsilon e^{i\omega t}$$

$$T(r, t) = T_o(r) + \varepsilon T_1(r) e^{i\omega t}$$

$$\theta(r, t) = \theta_o(r) + \varepsilon \theta_1(r) e^{i\omega t}$$

$$\dot{m}(r, t) = \dot{m}_o(r) + \varepsilon \dot{m}_1(r) e^{i\omega t}$$

$$\dot{m}_f(t) = \dot{m}_{fo} + \varepsilon \dot{m}_{f1} e^{i\omega t} \quad (2-52)$$

where  $T_1$ ,  $\theta_1$ ,  $\dot{m}_1$ , and  $\dot{m}_{f1}$  are complex quantities.

### 2.3 Zero-Order Problem (Steady State)

2.3.1 Equations. Substituting Equations (2-52) into Equations (2-41) to (2-51), yields the following zero-order, steady state equations:

Liquid Phase       $r \leq 1$

$$\frac{d}{dr} \left( r^2 \frac{dT_o}{dr} - \frac{\dot{m}_o}{\rho_f \delta_f} T_o \right) = 0 \quad (2-53)$$

$$\dot{m}_{fo} = \dot{m}_o = \text{constant} \quad (2-54)$$

Gas Phase       $r > 1$

$$\frac{d}{dr} \left( r^2 T_o \frac{d\theta_o}{dr} - \dot{m}_o \theta_o \right) = 0 \quad (2-55)$$

$$\frac{d}{dr} \left( r^2 T_o \frac{dT_o}{dr} - \dot{m}_o T_o \right) + r^2 q^{1-n} A T_o^{\delta-n} (\theta_o - T_o)^n \exp(-E/T_o) = 0 \quad (2-56)$$

Boundary Conditions

$$r = 0$$

$$T_o = T_i \quad (2-57)$$

$$r = 1$$

$$\lambda_f \left( \frac{dT_o}{dr} \right)_{s-} = T_o \left( \frac{dT_o}{dr} \right)_{s+} - \dot{m}_o [(1-\beta)T_o + L] \quad (2-58)$$

$$T_o \left( \frac{d(\theta_o - T_o)}{dr} \right)_{s+} = \dot{m}_o (\theta_o - T_o - q) \quad (2-59)$$

$$\theta_o - T_o = a q \exp(-L_f/T_o) \quad (2-60)$$

$$r = \infty$$

$$\theta_o = T_o = 1 \quad (2-61)$$

These zero-order equations are sufficiently general to allow for any ambient conditions, either adiabatic or non-adiabatic. Since most combustion chambers are essentially adiabatic, and monopropellants do not involve a local enthalpy defect in any stream, a condition of adiabatic combustion can be applied to simplify the calculations. (This is only strictly true under the conditions of the present model which allows for temperature gradients in the liquid phase. If there is bulk heating of the liquid, small enthalpy defects will arise in the spray.) This leads to the zero-order compatibility condition between dimensionless properties as follows:

$$q = 1 - \beta T_1 + L \quad (2-62)$$

The flame temperature can be computed from the dimensional form of Equation (2-62).

2.3.2 Liquid Phase Solution. An analytical solution can be obtained for the zero-order liquid phase Equation (2-53) from the

boundary conditions  $T_o = T_i$  at  $r = 0$  and  $T_o = T_{os}$  at  $r = 1$ , as follows:

$$\frac{T_o - T_i}{T_{os} - T_i} = \exp \left\{ \frac{\dot{m}_o}{\rho_f \delta_f} \left( 1 - \frac{1}{r} \right) \right\} \quad (2-63)$$

The boundary condition of Equation (2-58) can now be simplified by substituting the derivative of Equation (2-63) at  $r = 1$ , and noting that  $\beta = (\lambda_f / \rho_f \delta_f)$ .

$$\left( T_o \frac{dT_o}{dr} \right)_{s+} = \dot{m}_o (T_o - \beta T_i + L) \quad (2-64)$$

2.3.3 Gas Phase Solution. For the case of adiabatic combustion, integration of Equation (2-55) once; application of the boundary conditions at the liquid surface; and simplifying through the use of Equation (2-62), yields

$$r^2 T_o \frac{d\theta_o}{dr} - \dot{m}_o \theta_o = - \dot{m}_o \quad (2-65)$$

Integrating Equation (2-65) again, after transformation to eliminate explicit dependent on  $T_o$ , yields after application of the outer boundary condition

$$\theta_o = 1 \quad (2-66)$$

as a consequence of adiabatic combustion. Substituting Equation (2-66) into Equations (2-59) and (2-60) yields

$$\left( T_o \frac{dT_o}{dr} \right)_{s+} = \dot{m}_o (q + T_o - L)_s \quad (2-67)$$

$$T_{os} = 1 - a q \exp(-L_f / T_{os}) \quad (2-68)$$

Equation (2-68) may be solved with an iteration procedure for the temperature at the liquid surface. The outer boundary condition, Equation (2-61) is unchanged.

The zero order problem is now reduced to the solution of a single, nonlinear, second order, ordinary differential equation, Equation (2-56). Equations (2-61), (2-67) and (2-68) provide three boundary conditions to define the problem and determine the eigenvalue,  $\dot{m}_0$ .

In the general case, Equation (2-56) is nonlinear and must be integrated numerically. Since any practical range of numerical integration must be finite with respect to  $r$ , the outer boundary condition, Equation (2-61) was handled by considering the asymptotic behavior of Equation (2-56) for large  $r$ .

To find the form of Equation (2-56) for large  $r$ , let

$$T_o = 1 - \xi T_o^{(1)} \quad (2-69)$$

where  $\xi$  is a small parameter. The radial coordinate is also stretched by defining

$$r = \xi^{\alpha'} \eta \quad (2-70)$$

where  $\alpha'$  is a constant to be determined by proper matching. Keeping the lowest order terms, in  $T_o^{(1)}$ , the equation becomes:

$$\frac{d}{d\eta} \left( \eta^2 \frac{dT_o^{(1)}}{d\eta} \right) - \dot{m}_0 \xi^{-\alpha'} \frac{dT_o^{(1)}}{d\eta} - \xi^{2\alpha'} + n - 1 \eta^2 A \exp(-E) T_o^{(1)n} = 0 \quad (2-71)$$

The form of the asymptotic solution depends upon the reaction order,  $n$ . The combustion of hydrazine which was considered in

References [3] and [11], was best represented by  $n = 2$ , which is also generally true for other monopropellants. In this case, a proper match of terms can be achieved by setting  $\alpha' = 0$ , and balancing convection against diffusion. The resulting asymptotic equation is:

$$\frac{d}{dr} \left( r^2 \frac{dT_o^{(1)}}{dr} - \dot{m}_o T_o^{(1)} \right) = 0 \quad (2-72)$$

with the outer boundary condition  $T_o^{(1)} = 0$ ,  $r = \infty$  from Equation (2-69). Therefore, unlike the strand combustion case [3, 11] the asymptotic solution for droplets for  $n = 2$  does not involve the reaction rate term. This occurs since the area for heat conduction increases as  $r^2$  rather than remaining constant, increasing the significance of heat conduction at large distances from the liquid surface.

The solution of Equation (2-72) satisfying the outer boundary condition yields:

$$T_o = 1 - C[1 - \exp(-\dot{m}_o/r)] \quad (2-73)$$

at large  $r$ , where the small parameter  $\xi$  has been absorbed into the unknown constant,  $C$ . The constant  $C$  must be determined by matching Equation (2-73) with the numerical solution of Equation (2-56) in conjunction with the appropriate boundary conditions at the liquid surface.

Given  $A$ , the solution procedure involves guessing values for  $C$  and  $\dot{m}_o$ . Starting values for the numerical solution  $\left( T_o, \frac{dT_o}{dr} \right)$  are determined from Equation (2-73) at some large but finite value of  $r$ . Equation (2-56) is then integrated to the droplet surface,  $r = 1$ ,

using the fourth order Hamming predictor-corrector method. At  $r = 1$ , Equations (2-67) and (2-68) must be satisfied, determining  $\dot{m}_0$  and  $C$  uniquely. Since Equation (2-56) is nonlinear, a double iteration technique must be used. The present procedure employed the Newton-Raphson method for this iteration. Once  $\dot{m}_0$  and  $C$  are determined, the outer boundary condition, Equation (2-61), is only satisfied at the true mathematical infinity, through Equation (2-73).

2.3.3.1 Solution for Small A (Small Drop Limit). For a second order reaction, the parameter  $A$  in Equation (2-56) is proportional to  $(p_0 * r_s^*)^2$ . Therefore, for small droplet sizes,  $A$  approaches zero and the reaction terms may be neglected in the conservation equations. Under these conditions, Equation (2-56) may be integrated to yield the following implicit equation for the temperature distribution.

$$\dot{m}_0 \left( 1 - \frac{1}{r} \right) = T_0 - T_{os} + (q - 1) \ln \left\{ \frac{T_{os} + q - 1}{T_0 + q - 1} \right\} \quad (2-74)$$

The gasification rate  $\dot{m}_0$ , may be determined by applying the outer boundary condition,  $T_0 = 1$  when  $r = \infty$ , in Equation (2-74) to yield

$$\dot{m}_0 = 1 - T_{os} + (q - 1) \ln [1 - (1 - T_{os})/q] \quad (2-75)$$

The liquid surface temperature,  $T_{os}$ , can be determined from Equation (2-68).

2.3.3.2 Solution for Large A (Large Drop Limit). At any pressure,  $A$  increases as the size of the droplet increases. With increasing  $A$ , the zero-order reaction zone moves closer to the droplet, reducing the influence of curvature on the solution. This is also accompanied by an increase in  $\dot{m}_0$ , although  $T_{os}$  remains

unchanged. Reference to the liquid phase solution, Equation (2-63), indicates a rapid decay of temperature as one moves into the liquid phase, reducing the effect of curvature in this region as well.

The above discussion indicates that at large  $A$ , the process approaches a condition where temperature variation and reaction effects are confined to a thin region surrounding the liquid surface, with little effect of curvature in the spherical coordinate system. Under these conditions, the characteristics of droplet combustion and strand combustion approach one another and the results of References [3] and [11] can be applied directly to the droplet combustion problem. Therefore, it is only necessary to convert the earlier zero-order results to the present notation.

In References [3] and [11], the expression for the liquid surface temperature is equivalent to Equation (2-68) and no change is required. Under the present assumptions, particularly unity Lewis number, the curvilinear coordinate system has no influence on the surface temperature. This is also true in cases where the Lewis number is not unity at the high activation energy limit where the reaction zone is collapsed to a flame sheet [29].

In the case of strand combustion, the burning rate eigenvalue is given in terms of a parameter  $A_s$  as follows:

$$A_s = \frac{B^* T_{\infty}^{*\delta} \lambda_{\infty}^*}{(\rho_{\infty}^* v_{\infty}^*)^2 C_p^*} \left[ \frac{P_o^*}{M^* R^* T_{\infty}^*} \right]^n \quad (2-76)$$

At the large droplet limit, with the combustion zone close to the surface,

$$\dot{m}_o^* = r_s^{*2} \rho_{\infty o}^* v_{\infty o}^* \quad (2-77)$$

Therefore,  $\dot{m}_o$  is given by

$$\dot{m}_o = (A/A_s)^{1/2} \quad (2-78)$$

Knowledge of the droplet size and the chemical kinetic parameters provides A; the quantity  $A_s$  is given as the eigenvalue of the zero order solution in References [3] and [11], completing the determination of  $\dot{m}_o$ .

#### 2.4 First-Order Problem

2.4.1 Equations. Utilizing the general zero-order results, the first order equations reduce to the following.

Liquid Phase  $r < 1$

$$\dot{m}_{f1} = \text{constant} \quad (2-79)$$

$$\frac{d}{dr} \left( r^2 \frac{dT_1}{dr} \right) - \frac{\dot{m}_o}{\rho_f \delta_f} \frac{dT_1}{dr} - \frac{i\omega r^2}{\delta_f} T_1 = \frac{\dot{m}_{f1}}{\rho_f \delta_f} \frac{dT_o}{dr} \quad (2-80)$$

Gas Phase  $r > 1$

$$T_o^2 \frac{d\dot{m}_1}{dr} - i\omega r^2 T_1 = -i\omega r^2 T_o \quad (2-81)$$

$$\frac{d}{dr} \left( r^2 T_o \frac{d\theta_1}{dr} \right) - \dot{m}_o \frac{d\theta_1}{dr} - \frac{r^2 i\omega \theta_1}{T_o} = -r^2 \left( \frac{\gamma - 1}{\gamma} \right) i\omega \quad (2-82)$$

$$\begin{aligned} & \frac{d}{dr} \left( r^2 T_o \frac{dT_1}{dr} \right) - \dot{m}_o \frac{dT_1}{dr} + \frac{d}{dr} \left( r^2 T_1 \frac{dT_o}{dr} \right) \\ & + r^2 q w_o \left[ (\delta - n) \frac{T_1}{T_o} + n \left( \frac{\theta_1 - T_1}{\theta_o - T_o} \right) + \frac{ET_1}{T_o^2} \right] - \frac{r^2 i\omega T_1}{T_o} = \\ & \dot{m}_1 \frac{dT_o}{dr} - r^2 \left( \frac{\gamma - 1}{\gamma} \right) i\omega = r^2 q w_o n \quad (2-83) \end{aligned}$$

Boundary Conditions

$$r = 0 \quad T_1 = 0 \quad (2-84)$$

$$r = 1$$

$$\dot{m}_{f1} = \dot{m}_1 \quad T_{1s} = T_{1s+} \quad (2-85)$$

$$\lambda_f \left. \frac{dT_1}{dr} \right|_{s-} = T_1 \left. \frac{dT_o}{dr} \right|_{s+} + T_o \left. \frac{dT_1}{dr} \right|_{s+} - \dot{m}_1 [(1-\beta)T_o + L] - \dot{m}_o (1-\beta)T_1 \quad (2-86)$$

$$T_o \left. \frac{d(\theta_1 - T_1)}{dr} \right|_{s+} - T_1 \left. \frac{dT_o}{dr} \right|_{s+} = \dot{m}_o (\theta_1 - T_1) + \dot{m}_1 (1 - T_o - q) \quad (2-87)$$

$$\theta_1 - T_1 = a q \exp(-L_f/T_o) \left[ \frac{L_f T_1}{T_o} - 1 \right] \quad (2-88)$$

Far from the droplet,  $\theta_1$  and  $T_1$  must approach a constant value.

$$r = \infty$$

$$\theta_1 = T_1 = K_1 \quad (2-89)$$

The value of  $K_1$  depends upon the case under consideration. For an unsteady gas phase, since  $\theta_1 = \theta_1(t)$  at large  $r$ , the constant can be determined by considering the behavior of Equation (2-82) at large  $r$ . In this case,  $K_1 = (\gamma-1)/\gamma$  which is the form for isentropic flow.

In the case of a quasi-steady gas phase, with transient effects still important in the liquid phase,  $K_1$  is the amplitude of the ambient temperature variation due to the varying energy content of the liquid at the surface of the droplet (resulting from transient energy storage in the liquid phase). In this case,  $K_1$  becomes a second eigenvalue in the solution to be determined along with  $\dot{m}_1$ . At

the limit where the liquid phase also becomes quasi-steady, the value of  $K_1$  goes to zero, since in the absence of transient energy storage in the liquid phase, Equation (2-62) must be satisfied.

The equations for the first order are linear. Therefore, solutions can be combined to eliminate the need for iteration in order to determine  $\hat{m}_1$  and  $K_1$ . Since the limits of integration extend to infinity, asymptotic gas phase solutions are employed so that numerical computations can be confined to a finite region. Numerical difficulties are encountered when integrating the liquid phase solution to  $r = 0$ , therefore an asymptotic analysis is employed in this region as well.

2.4.2 Liquid Phase Solution. Similar to the zero-order case, the liquid phase solution is completed by applying the boundary condition  $T_1 = T_{1s}$  at  $r = 1$ , although  $T_{1s}$  is not generally known until the gas phase solution is complete. This procedure allows the liquid phase solution to be decoupled from the gas phase.

In order to simplify the subsequent discussion, Equation (2-80) may be rewritten as:

$$L\{T_1\} = \hat{m}_{f1} H_3 \quad (2-90)$$

where

$$L = \frac{d^2}{dr^2} + H_1 \frac{d}{dr} + H_2 \quad (2-91)$$

is a linear operator, and

$$H_1 = \frac{2}{r} - \frac{\hat{m}_o}{\rho_f \delta_f r^2} \quad (2-92)$$

$$H_2 = -\frac{i\omega}{\delta_f} \quad (2-93)$$

$$H_3 = (T_{os} - T_1) \frac{\dot{m}_o}{(\rho_f \delta_f r^2)^2} \exp \left\{ \frac{\dot{m}_o}{\rho_f \delta_f} \left( 1 - \frac{1}{r} \right) \right\} \quad (2-94)$$

The boundary conditions on Equation (2-90) are

$$r = 0, \quad T_1 = 0; \quad r = 1, \quad T_1 = T_{1s} \quad (2-95)$$

The quantity  $\dot{m}_1$  is an eigenvalue to be determined from the complete gas and liquid phase solutions. Exploiting the linearity of Equation (2-90), let

$$T_1 = \hat{T}_1 + \dot{m}_{f1} T_1^* \quad (2-96)$$

Equation (2-96) can be divided into homogeneous and particular parts

$$\begin{aligned} \hat{T}_1 &= \hat{K}_T T_{1H} \\ T_1^* &= T_{1P}^* + K_T^* T_{1H} \end{aligned} \quad (2-97)$$

where  $\hat{K}_T$  and  $K_T^*$  are constants to be determined from the boundary conditions. The differential equations then become

$$L\{T_{1H}\} = 0; \quad L\{T_{1P}^*\} = H_3 \quad (2-98)$$

The values of  $\hat{K}_T$  and  $K_T^*$  are selected to match the boundary condition at  $r = 1$ , to yield

$$\begin{aligned} \hat{K}_T &= T_{1s} / T_{1Hs} \\ K_T^* &= -T_{1Ps}^* / T_{1Hs} \end{aligned} \quad (2-99)$$

In order to match the liquid and gas phase solutions, the derivative of  $T_1$  at the liquid surface is required. Combining Equations (2-96), (2-97) and (2-99) this quantity is

$$\lambda_f \left( \frac{dT_1}{dr} \right)_{s-} = H_4 T_{1s} + H_5 \dot{m}_{f1} \quad (2-100)$$

where

$$H_4 = \frac{\lambda_f}{T_{1Hs-}} \left( \frac{dT_{1H}}{dr} \right)_{s-} \quad (2-101)$$

$$H_5 = \lambda_f \left[ \left( \frac{dT_{1P}}{dr} \right)_{s-} - \left( \frac{T_{1Ps-}^*}{T_{1Hs-}} \right) \left( \frac{dT_{1H}}{dr} \right)_{s-} \right] \quad (2-102)$$

The behavior of Equation (2-98) at small  $r$  yields the following asymptotic forms for  $T_{1H}$  and  $T_{1P}^*$ , as  $r \rightarrow 0$

$$T_{1H} = \exp\{-\dot{m}_o / \rho_f \delta_f r\} \quad (2-103)$$

$$T_{1P}^* = \frac{1}{\rho_f \delta_f} (T_{os} - T_i) \left( 1 - \frac{1}{r} \right) \exp \left\{ \frac{\dot{m}_o}{\rho_f \delta_f} \left( 1 - \frac{1}{r} \right) \right\} \quad (2-104)$$

Equations (2-103) and (2-104) formally satisfy the boundary condition  $T_1 \rightarrow 0$ , as  $r \rightarrow 0$ . The arbitrary constant in the homogeneous equation has been absorbed into  $\hat{K}_T$  and  $K_T^*$ .

The solution procedure involves employing Equations (2-103) and (2-104) to generate starting values for the numerical integration of Equations (2-98) at some small but non-zero value of  $r$ . The equations are integrated to the liquid surface, allowing the evaluation of  $H_4$  and  $H_5$  from Equations (2-101) and (2-102). Substitution of these quantities into Equation (2-100) provides the needed expression in the gas phase boundary conditions. Once  $T_{1s}$  and  $\dot{m}_{f1}$  are determined from the gas phase solution, Equations (2-96), (2-97), and (2-98) allow complete determination of  $T_1$  in the liquid phase.

2.4.3 Quasi-Steady Gas Phase Solution. A number of simplifications are available for the analysis when the gas phase

can be assumed to be quasi-steady. This limit arises since frequency effects appear as  $\omega$  in the gas phase and  $\omega/\delta_f$  in the liquid phase. At atmospheric pressure, for hydrazine,  $\delta_f^{-1}$  has the value 2071, and under these conditions, transient effects in the liquid become important at frequencies substantially below the frequencies where gas phase transients are encountered. Since  $\delta_f$  is proportional to the mean pressure, the gap between the two characteristic frequencies progressively becomes smaller as the pressure increases.

At the quasi-steady gas phase limit,  $\dot{m}_1 = \dot{m}_{f1}$ , a constant. For adiabatic combustion, consideration of the overall energy balance and integration of Equation (2-82) shows that  $\theta_1 = K_1$ , a constant as well. Equation (2-83) can then be simplified to yield

$$L'\{T_1\} = A_3 K_1 + A_4 \dot{m}_1 + A_5 \quad (2-105)$$

where

$$L' = \frac{d^2}{dr^2} + A_1 \frac{d}{dr} + A_2 \quad (2-106)$$

and

$$A_1 = 2 \left( \frac{1}{T_o} \frac{dT_o}{dr} + \frac{1}{r} \right) - \frac{\dot{m}_o}{r^2 T_o} \quad (2-107)$$

$$A_2 = \frac{1}{T_o} \frac{d^2 T_o}{dr^2} + \frac{2}{r T_o} \frac{dT_o}{dr} + \frac{w_o q}{T_o} \left[ \frac{(\delta - n)}{T_o} - \frac{n}{(1 - T_o)} + \frac{E}{T_o^2} \right] \quad (2-108)$$

$$A_3 = - \frac{q n w_o}{T_o (1 - T_o)} \quad (2-109)$$

$$A_4 = \frac{1}{r^2 T_o} \frac{dT_o}{dr} \quad (2-110)$$

$$A_5 = - \frac{q w_o n}{T_o} \quad (2-111)$$

The boundary conditions at  $r = 1$  become

$$D_1 \left( \frac{dT_1}{dr} \right)_{s+} + D_2 T_{1s} = D_3 \dot{m}_1 \quad (2-112)$$

$$F_1 \left( \frac{dT_1}{dr} \right)_{s+} + F_2 T_1 = F_3 K_1 + F_4 \dot{m}_1 \quad (2-113)$$

$$G_1 T_1 = K_1 + G_2 \quad (2-114)$$

where

$$D_1 = T_{os} \quad (2-115)$$

$$D_2 = \left( \frac{dT_o}{dr} \right)_{s+} - \dot{m}_o (1-\beta) - H_4 \quad (2-116)$$

$$D_3 = (1-\beta)T_{os} + L + H_5 \quad (2-117)$$

$$F_1 = - T_{os} \quad (2-118)$$

$$F_2 = - \left( \frac{dT_o}{r} \right)_{s-} + \dot{m}_o \quad (2-119)$$

$$F_3 = \dot{m}_o \quad (2-120)$$

$$F_4 = (1 - T_{os} - q) \quad (2-121)$$

$$G_1 = 1 + \frac{a q L_f}{T_o^2} \exp(-L_f/T_{os}) \quad (2-122)$$

$$G_2 = a q \exp(-L_f/T_{os}) \quad (2-123)$$

The outer boundary condition is  $r \rightarrow \infty$ ,  $T_1 \rightarrow K_1$ .

Again exploiting linearity, define

$$T_1 = \hat{T}_1 + \hat{m}_1 T_1^* + K_1 \bar{T}_1 \quad (2-124)$$

Separating the functions in Equation (2-124) into homogeneous and particular parts

$$\begin{aligned} \hat{T}_1 &= \hat{T}_{1P} + \hat{K} T_{1H} \\ T_1^* &= T_{1P}^* + K^* T_{1H} \\ \bar{T}_1 &= \bar{T}_{1P} + \bar{K} T_{1H} \end{aligned} \quad (2-125)$$

where

$$\begin{aligned} L'\{T_{1H}\} &= 0 & L'\{\hat{T}_{1P}\} &= A_5 \\ L'\{T_{1P}^*\} &= A_4 & L'\{\bar{T}_{1P}\} &= A_3 \end{aligned} \quad (2-126)$$

The parameters  $\hat{K}$ ,  $K^*$  and  $\bar{K}$  are constants which can be selected to satisfy any of the boundary conditions. Since the outer boundary condition can be handled by the asymptotic solution of Equations (2-126), Equation (2-114) was chosen to determine the values of the  $K$ 's. This yields

$$\hat{K} = \left( \frac{G_2}{G_1} - \hat{T}_{1Ps+} \right) / T_{1Hs+} \quad (2-127)$$

$$K^* = -T_{1Ps}^* / T_{1Hs+} \quad (2-128)$$

$$\bar{K} = \left( \frac{1}{G_1} - \bar{T}_{1Ps+} \right) / T_{1Hs+} \quad (2-129)$$

The remaining two boundary conditions at  $r = 1$ , Equations (2-112) and (2-113), can be employed to determine the values of  $\hat{m}_1$  and  $K_1$ .

The result is

$$K_1 = (J_{11} J_{23} - J_{21} J_{13}) / (J_{11} J_{22} - J_{12} J_{21}) \quad (2-130)$$

$$\dot{m}_1 = (J_{13} J_{22} - J_{12} J_{23}) / (J_{11} J_{22} - J_{12} J_{21}) \quad (2-131)$$

where

$$\begin{aligned} J_{11} &= D_1 \left( \frac{dT_1^*}{dr} \right)_{s+} + D_2 T_{1s+}^* - D_3 \\ J_{12} &= D_1 \left( \frac{d\bar{T}_1}{dr} \right)_{s+} + D_2 T_{1s+}^* \\ J_{13} &= -D_1 \left( \frac{d\hat{T}_1}{dr} \right)_{s+} - D_2 \hat{T}_{1s} \\ J_{21} &= F_1 \left( \frac{dT_1^*}{dr} \right)_{s+} + F_2 T_{1s}^* - F_4 \\ J_{22} &= F_1 \left( \frac{d\bar{T}_1}{dr} \right)_{s+} + F_2 \bar{T}_{1s+} - F_3 \\ J_{23} &= F_1 \left( \frac{d\hat{T}_1}{dr} \right)_{s+} - F_2 \hat{T}_{1s+} \end{aligned} \quad (2-132)$$

The derivatives in these expressions are obtained by differentiating Equations (2-125) noting that the K's are constants.

In order to complete the solution, the asymptotic forms of Equations (2-126) at large  $r$  must be solved. Proceeding in the same manner as the zero-order case, the result is

$$r \rightarrow \infty$$

$$\begin{aligned} T_{1H} = \hat{T}_{1P} = T_{1P}^* &= 1 - \exp(-\dot{m}_0/r) \\ \bar{T}_{1P} &= \exp(-\dot{m}_0/r) \end{aligned} \quad (2-133)$$

Equations (2-133) automatically satisfy the outer boundary condition of the gas phase solution.

The solution is obtained by calculating  $D_1, D_2, D_3, F_1, F_2, F_3, F_4, G_1$  and  $G_2$  from the zero-order solution and the solution of the first order liquid phase. The parameters  $A_1 - A_5$  are also available from the zero order solution. Equations (2-133) are used to generate starting values for the differential equations given by Equations (2-126) at some large but finite value of  $r$ . These equations are then integrated to the surface of the droplet. The parameters  $\hat{K}, K^*$ , and  $\bar{K}$  can then be determined from Equations (2-127) to (2-129). When these parameters are ascertained,  $\hat{T}_{1s}, T_{1s}^*$ ,  $\bar{T}_{1s}$ , and the derivatives of these quantities can be determined from Equations (2-125) and their derivatives. Determining the  $J_{ij}$  terms from Equations (2-132) then allows  $K_1$  and  $\dot{m}_1$  to be found from Equations (2-130) and (2-131). If desired,  $T_1$  can then be evaluated as a function of  $r$  from Equation (2-124) for the gas phase (yielding  $T_{1s}$ ) and from Equation (2-96) for the liquid phase.

### 2.5 Wet Bulb Limit Equations

In the early phases of the lifetime of a droplet, and for large droplets having strong decomposition effects, substantial temperature gradients exist within a droplet [30]. The present investigation examines this limit by considering liquid temperatures at the center of the droplet that are lower than the equilibrium surface temperature.

In the later stages of droplet gasification, particularly for small droplets with relatively weak monopropellant decomposition effects, temperatures throughout the droplet approach the liquid surface temperature [30]. This can also occur due to circulation

in the liquid phase; however, this effect is difficult to determine quantitatively. When temperatures throughout the droplet are equal to the surface temperature, droplet conditions are often referred to as combustion at the wet bulb state. In order to cover the complete range of possibilities, the present calculations also consider response at the wet bulb state. In both cases; however, the overall combustion process is assumed to be adiabatic.

The distinction in the determination of property values for the temperature gradient and wet bulb cases may be seen as follows. For adiabatic combustion, the flame temperature is given by the dimensional form of Equation (2-62)

$$T_{\infty 0}^* = (q^* + C_f^* T_i^* - L^*) / C_p^* \quad (2-134)$$

With temperature gradients present,  $T_i^*$  can be specified (as the liquid injection temperature, for example) and the flame temperature can then be obtained from Equation (2-134). The other dimensionless variables are determined from Equations (2-22), and the liquid surface temperature from Equation (2-68).

For wet bulb combustion, liquid temperatures are uniform and  $T_i^* = T_{os}^*$ , and both  $T_i^*$  and  $T_{\infty 0}^*$  are unknown. In this case, Equation (2-134) and the dimensional form of Equation (2-68) are solved simultaneously to yield  $T_i^*$  and  $T_{\infty 0}^*$ , followed by the determination of the dimensionless variables through Equations (2-22).

## CHAPTER III

### STEADY STATE DROPLET RESULTS

#### 3.1 Introduction

The physical property values and the chemical kinetic parameters used in the calculations are representative of hydrazine decomposition. The specific values, summarized in Table 1, are identical to those used by Allison and Faeth [11].

A second order reaction correlates the strand burning rate of hydrazine at pressures above 1 atmosphere [11]. For steady state conditions, the theoretical burning rate is relatively insensitive to variations in the activation energy. However, for oscillatory combustion, the activation energy influences both the amplitude and phase of the combustion response of strands. Allison and Faeth [11] found that the value of  $E^*$  given in Table 1 gave good agreement between theoretical and experimental response determinations over their test range. This value also agrees with earlier values reported for hydrazine decomposition [31]. With the activation energy given, the value of  $B^*$  is found by matching the steady strand burning rates.

#### 3.2 Temperature Distribution

In order to check the accuracy of the zero-order model, predicted and measured liquid surface temperatures were compared as a function of pressure. The theoretical prediction of liquid surface temperatures is independent of geometry under the unity Lewis number assumption. Therefore, the comparison is identical to that made in

Table 1

## Properties Used in the Theoretical Model

Property	Value
$a^*$ (N/m <sup>2</sup> )	$3.0078 \times 10^{10}$
$B^*$ (m <sup>3</sup> /Kg-s)	$8.385 \times 10^{10}$
$C_f^*$ (KJ/Kg-K)	3.0961
$C_p^*$ (KJ/Kg-K)	3.0961
$E^*$ (KJ/Kg-mol)	111700
$L^*$ (KJ/Kg)	1715
$L_f^*$ (KJ/KG-mol)	40794
$Le$	1
$M^*$ (Kg/Kg-mol)	24
$n$	2
$q^*$ (KJ/Kg)	4537
$R^*$ (KJ/Kg-mol-K)	8.3144
$T_i^*$ (K)	298
$T_{\infty 0}^*$ (°C)	1345
$\gamma$	1.126
$\delta$	0
$\lambda_f^*$ (J/m-s-k)	0.390
$\lambda_{\infty 0}^*$ (J/m-s-k)	0.176
$\rho_f^*$ (Kg/m <sup>3</sup> )	1000

REPRODUCIBILITY OF THE  
ORIGINAL PAGE IS POOR

Reference [11] between measured and predicted surface temperatures in the strand combustion case. These results have been replotted and are shown in Figure 2. The agreement is good throughout the pressure range of the measurements (.51-19.8 atm.).

The test conditions shown in Figure 2 involved a liquid temperature of 298°K far from the liquid surface. This is representative of a non-wet bulb condition, with the liquid temperature increasing as the surface is approached. A theoretical calculation for the wet bulb state is also presented in Figure 2, where the liquid temperature is constant. For the wet bulb case, no energy is required to raise the liquid to the vaporization temperature, resulting in a higher surface temperature than the non-wet bulb case (for a given pressure).

Steady state calculations were completed over a range of A (essentially representing droplet size variations) and pressure for both non-wet bulb (with a centerline droplet temperature of 298°K) and wet bulb conditions.

Figures 3 and 4 illustrate liquid and gas phase temperature profiles for non-wet bulb conditions at a pressure of  $10^6 \text{ N/m}^2$  (approximately 10 atm.). Curves are plotted for various values of A. When  $A = 0$ , there is negligible reaction in the gas phase surrounding the droplet, and the process corresponds to simple droplet evaporation. In this case, temperature variations are gradual and the effect of curvature in the spherical coordinate system is important. As A (droplet size) increases at a given pressure, the rate of gasification also increases. The greater liquid flow rate toward the surface of the droplet tends to sweep back the temperature profile

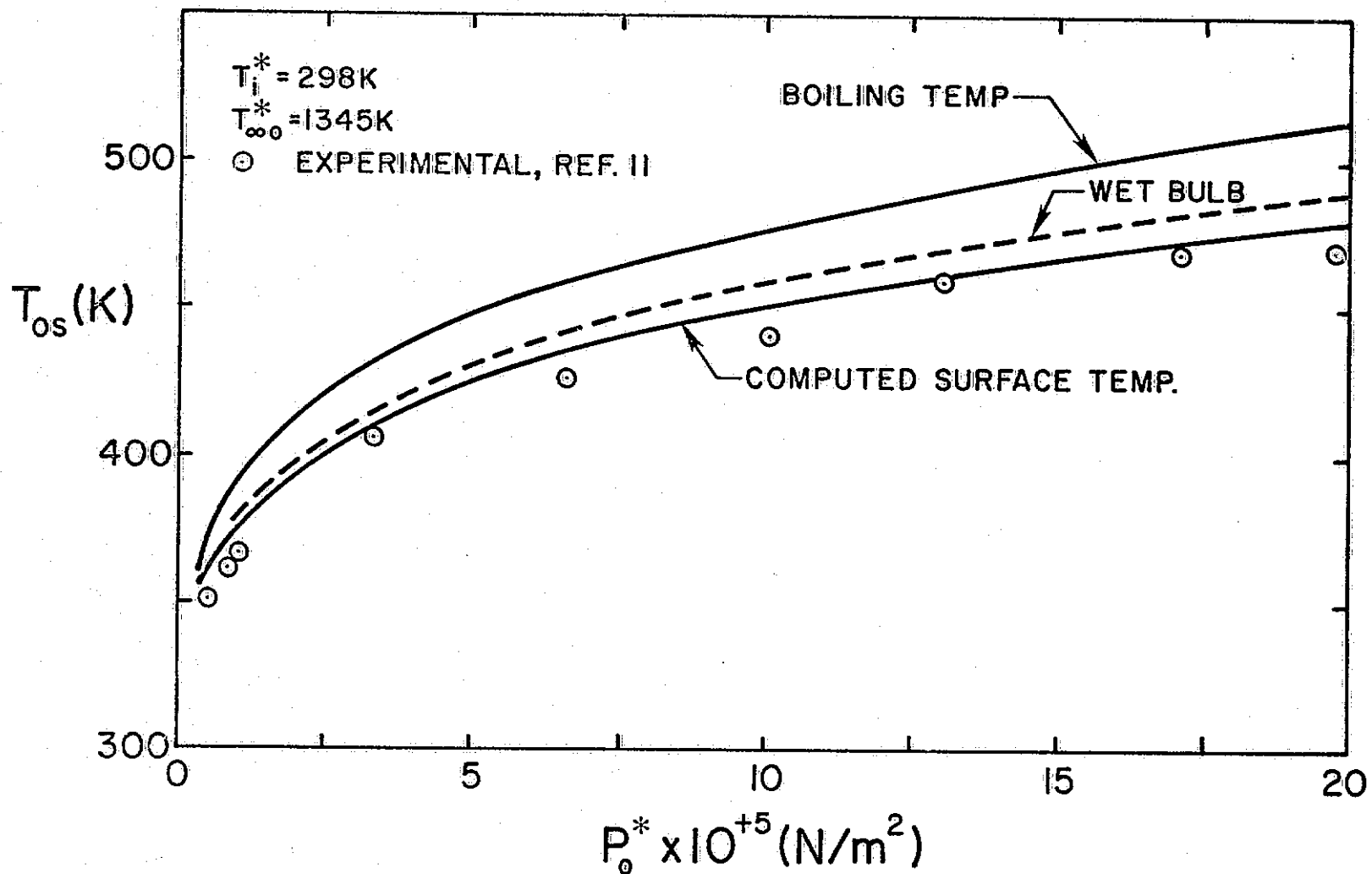


Figure 2 Theoretical and Experimental Liquid Surface Temperatures as a Function of Pressure

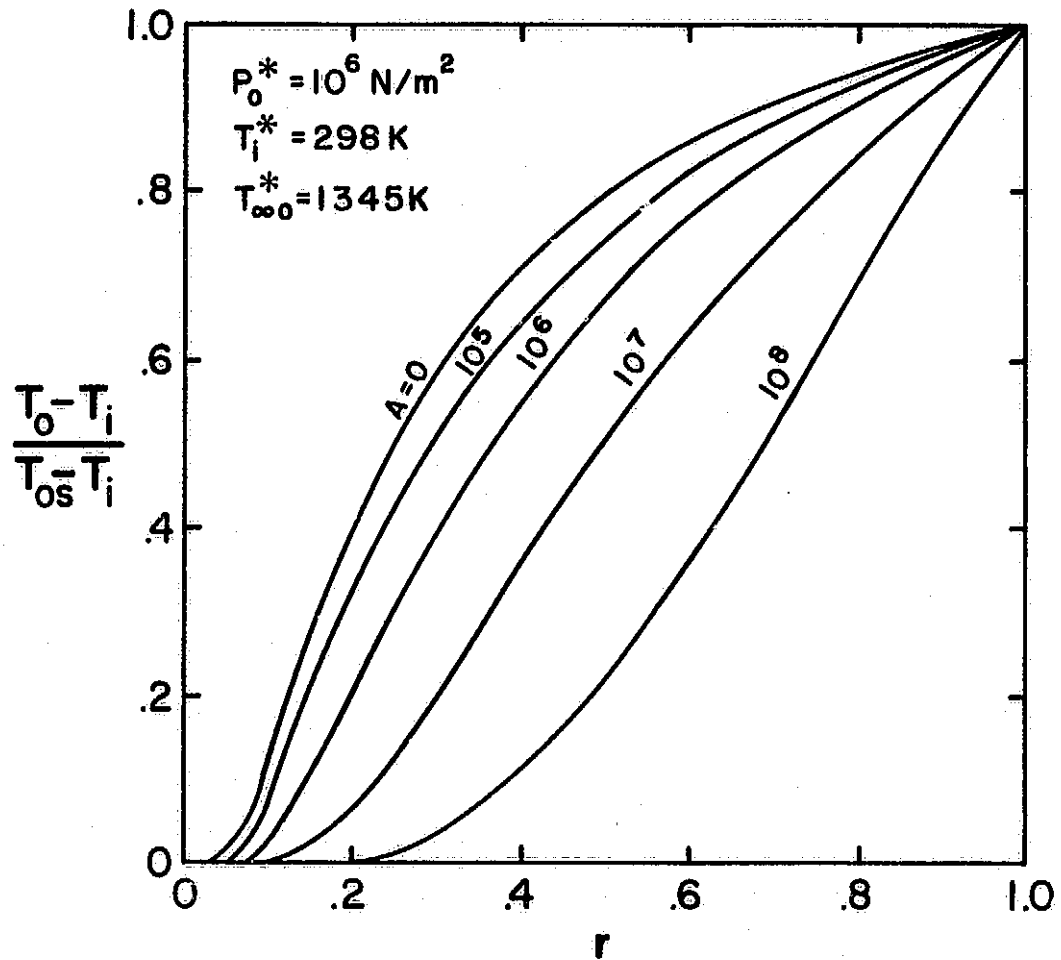


Figure 3 Steady State Liquid Phase Temperatures as a Function of  $A$  at Approximately 10 Atm. Pressure (Non-Wet Bulb Conditions)

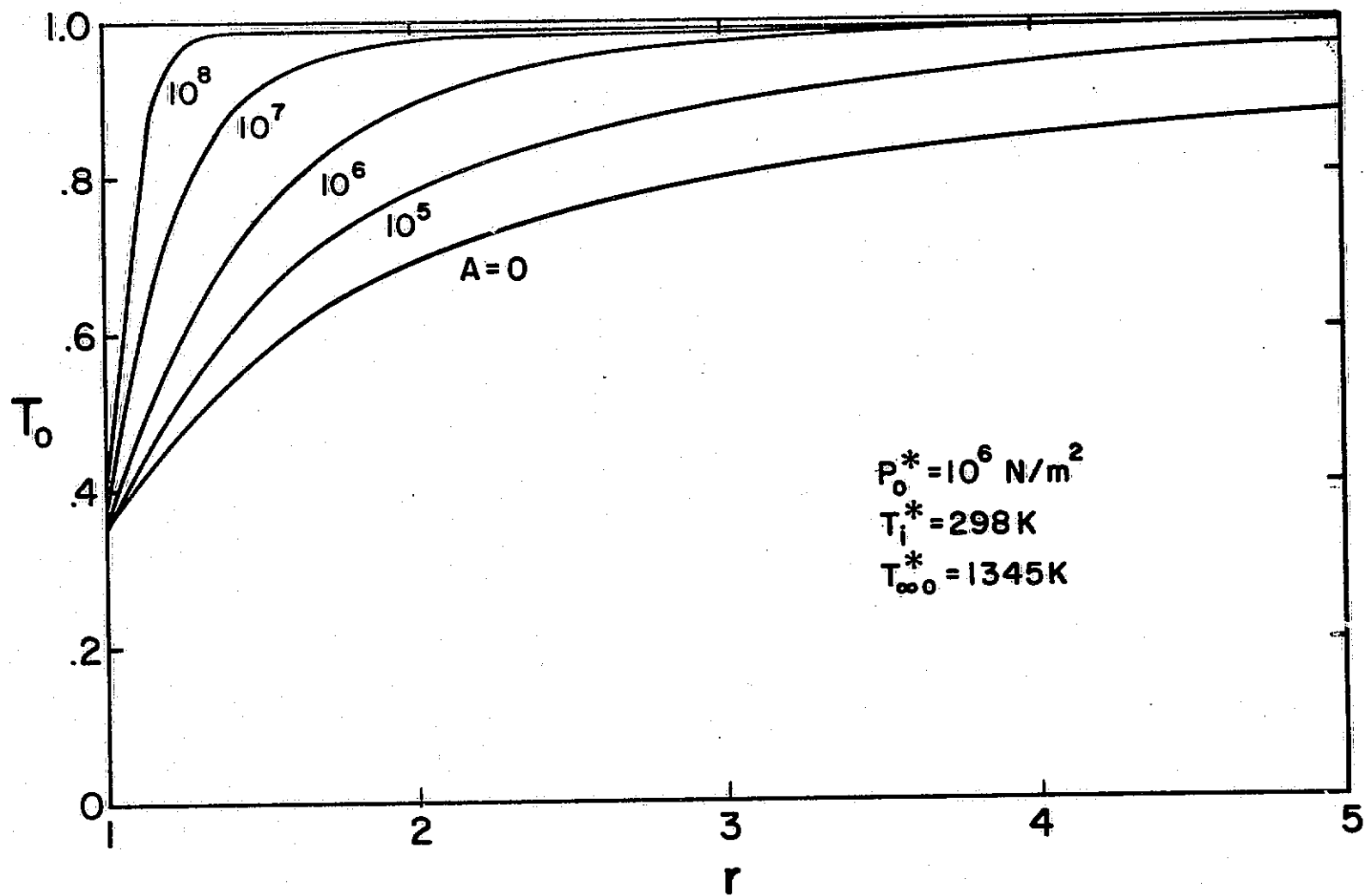


Figure 4 Steady State Gas Phase Temperatures as a Function of A at Approximately 10 Atm. Pressure (Non-Wet Bulb Conditions)

in the liquid phase (Figure 3). The increased reaction rate also causes the combustion zone in the gas phase to approach the liquid surface as shown in Figure 4. Therefore, as  $A$  increases, temperature gradients become confined to the region near the liquid surface and the effect of curvature is reduced. These conditions correspond to the large drop limit, where strand combustion is similar to adiabatic droplet combustion.

Figure 5 shows gas phase temperature distributions for the wet bulb case, with remaining conditions similar to the calculations shown in Figure 4. For wet-bulb conditions the liquid temperature is constant and equal to the surface temperature. These gas phase temperature profiles are similar to the non-wet bulb case, becoming steeper as the value of  $A$  increases. The major difference is the slightly higher temperature at the liquid surface for wet bulb conditions.

Calculations completed for pressures of  $10^5$  N/m<sup>2</sup> and  $10^7$  N/m<sup>2</sup> (approximately 1 and 100 atm.) gave results that are generally similar to those shown in Figures 3-5.

### 3.3 Mass Burning Rates

The mass burning rate of a liquid droplet depends on the size of the droplet (at a given pressure) and approaches two asymptotic limits: the large drop and small drop limit burning rates. The small drop limit represents a droplet vaporizing without reaction, and the large drop limit approximates a one-dimensional liquid strand with the flame very close to the liquid surface. The intermediate drop sizes or transition range constitute the majority of drops that are distributed between the two asymptotic limits.

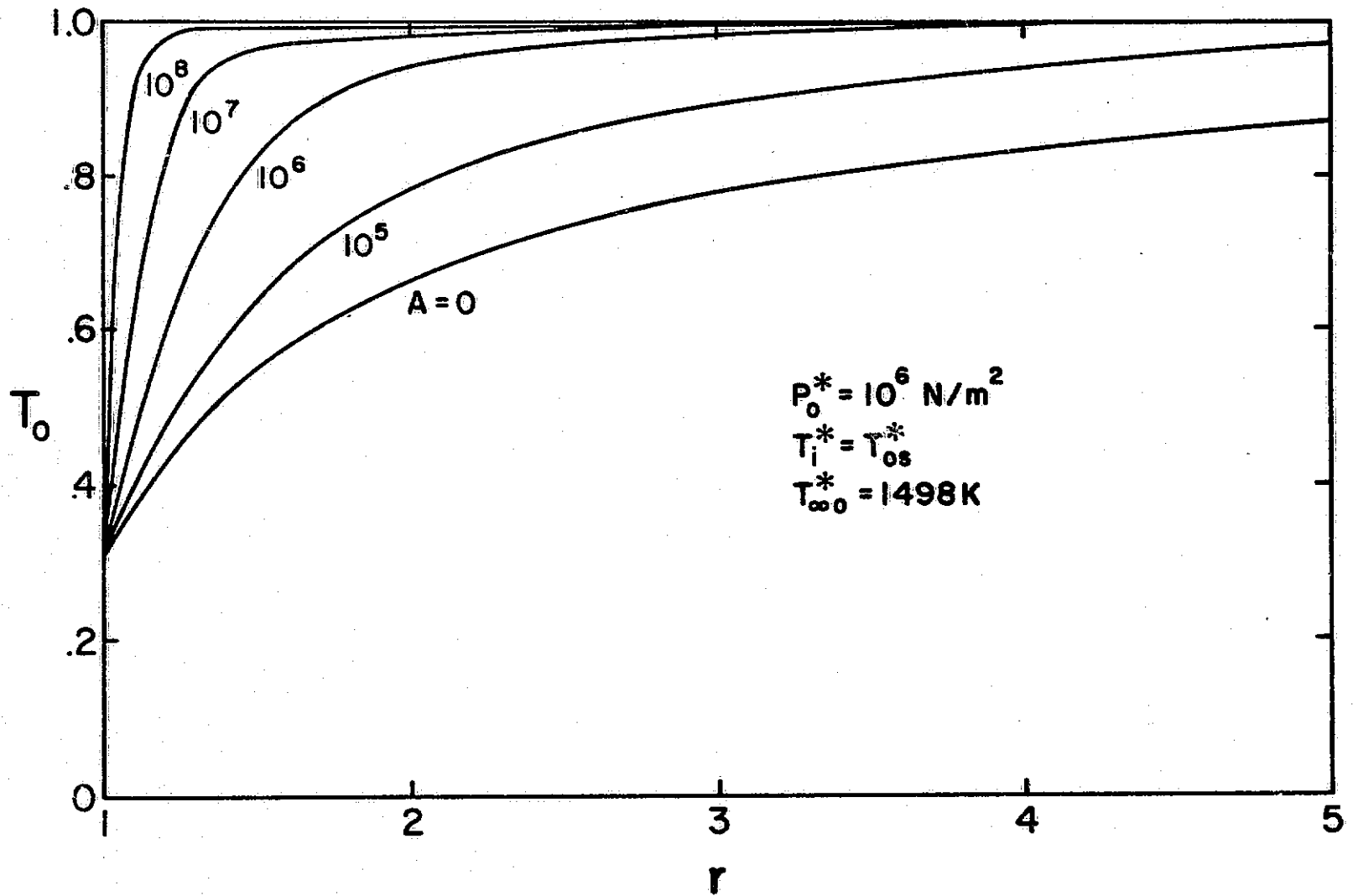


Figure 5 Steady State Gas Phase Temperatures as a Function of A at Approximately 10 Atm. Pressure (Wet Bulb Conditions)

Figure 6 shows the steady state mass burning rates as a function of  $A$  at 1 atmosphere pressure for non-wet bulb conditions. The complete steady state solution clearly approaches the large and small drop limits. In order to plot  $\dot{m}_o$  as a function of  $A$  at the large drop limit, values of  $A_s$  were obtained from the strand combustion calculations [11]. Equation (2-78) then yields the large drop limit mass burning rate,  $\dot{m}_{oLDL}$ , as a function of  $A$ . The small drop limit mass burning rate,  $\dot{m}_{oSDL}$ , is calculated directly from Equations (2-68) and (2-75) and is independent of  $A$ .

An approximation to the complete steady state solution is shown in Figure 6. The approximation was obtained by simply adding the small and large drop mass burning rates at each value of  $A$ , as follows:

$$\dot{m}_o = \dot{m}_{oSDL} + \dot{m}_{oLDL} \quad (3-1)$$

The approximation of Equation (3-1) yields a maximum error of approximately 12% over the entire range of  $A$ . Equation (3-1) will be used later to evaluate spray combustion characteristics since it can be readily integrated to determine droplet lifetimes.

Data on hydrazine combustion was available from experimental work done by Allison and Faeth [9]. This study involved droplet burning in a combustion gas under decomposition conditions, for various droplet sizes, at atmospheric pressure. The data was limited to the ambient temperature range 1660-2530°K; therefore, it was necessary to extrapolate the measurements to the 1345°K ambient temperature of the present study. The values used in the experimental comparison shown in Figure 6 are summarized in Table 2. The agreement

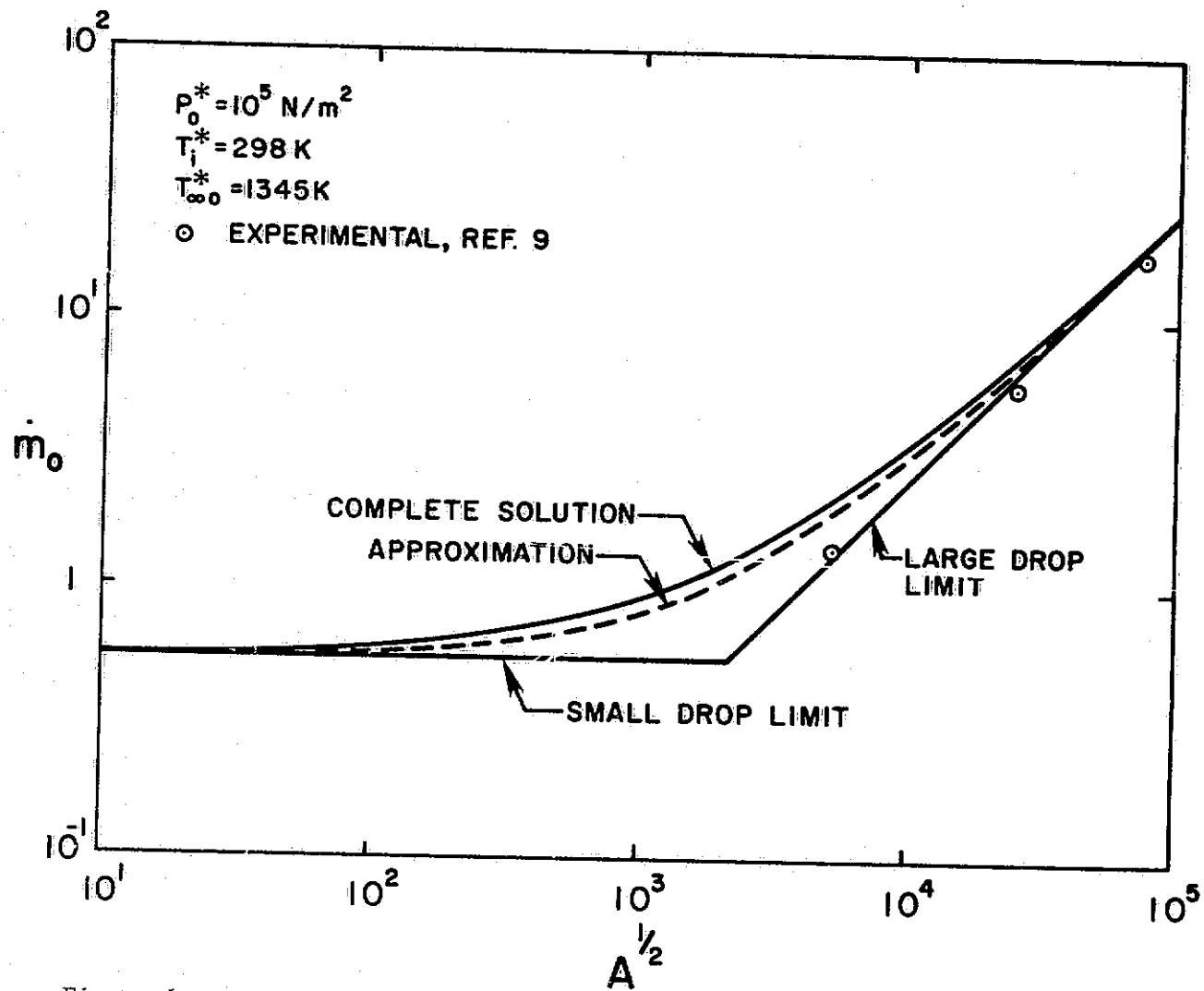


Figure 6 Theoretical and Experimental Steady State Droplet Gasification Rates at Approximately 1 Atm. Pressure (Non-Wet Bulb Conditions)

between the predicted and measured burning rates is seen to be reasonably good, lending confidence to the theoretical model.

Table 2

Steady Droplet Burning Rate Data (Non-Wet Bulb)<sup>a</sup>

$d_s^*$ (diameter) (mm)	$4\pi\dot{m}_O^* \times 10^6$ (Kg/s)
1.3	.70
6.3	1.4
19.1	135

<sup>a</sup>Extrapolated to  $T_{\infty O}^* = 1345K$  from data of Reference [9] at atmospheric pressure. Non-wet bulb conditions,  $T_1^* = 298K$ .

Burning rate results at atmospheric pressure for wet bulb conditions are illustrated in Figure 7. The general behavior is similar to the non-wet bulb conditions; the major difference involves a slight increase in the burning rate throughout the entire range of A.

Theoretical mass burning rates at pressures of 10 and 100 atmospheres were completed and gave results very similar to Figures 6 and 7. In all cases the transition region between the large and small droplet limits falls approximately in the range  $10^4 < A < 10^9$ . The approximation of Equation (3-1), was found to provide a good representation of the data (with maximum errors on the order of 10%) over the entire range of the calculations.

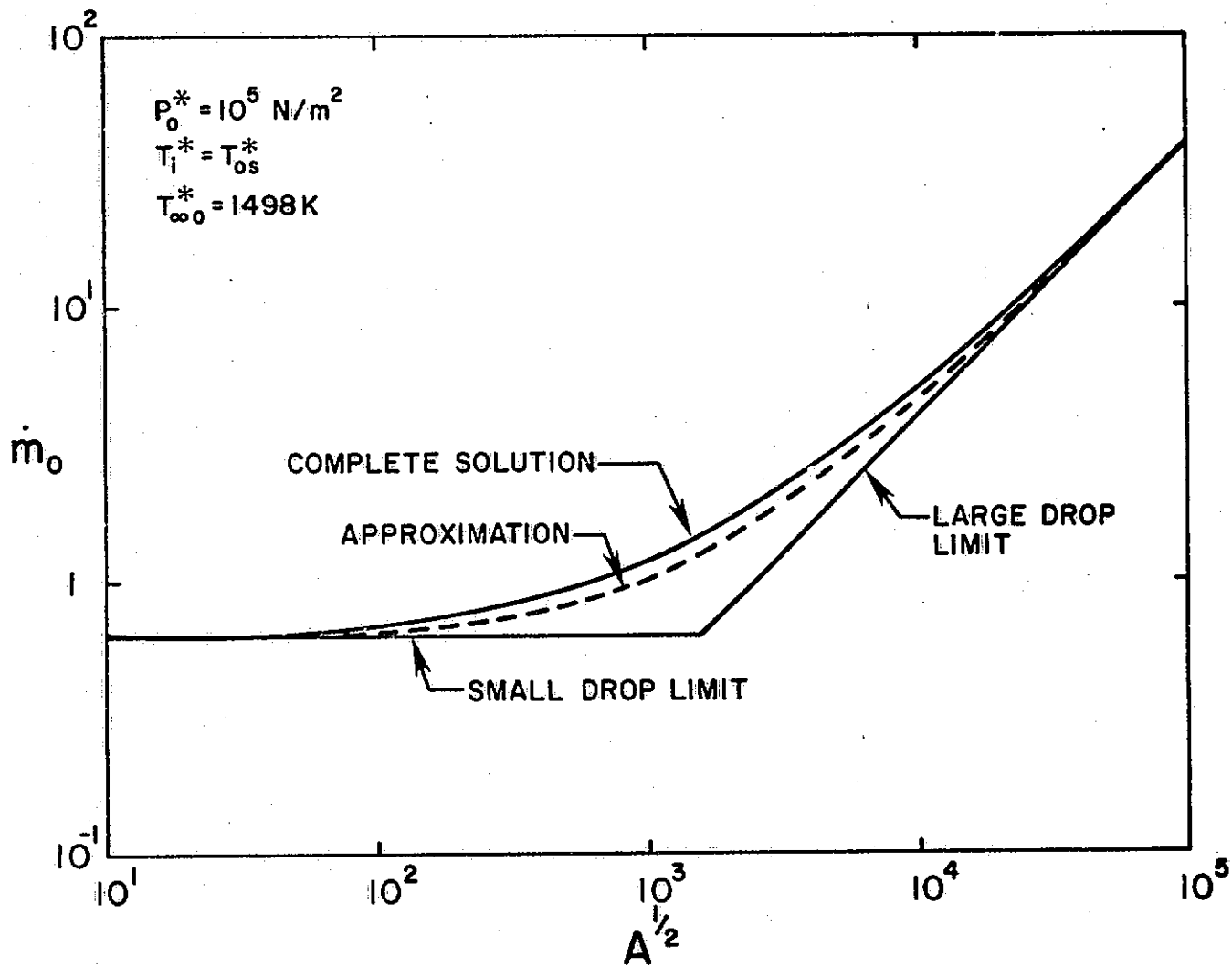


Figure 7 Theoretical Steady State Droplet Gasification Rates at Approximately 1 Atm. Pressure (Wet Bulb Conditions)

In order to employ the approximate burning rate expression, it is necessary to have values for  $\dot{m}_{O_{SDL}}$  and  $A_s$ . These quantities, along with surface temperature predictions, are summarized in Table 3, over a range of pressures, for both wet bulb and non-wet bulb conditions.

Table 3

Summary of Steady State Calculations

$P_o$	$T_i$	$T_{os}$	$T_{os}^*(K)$	$T_{\infty O}^*(K)$	$\dot{m}_{O_{SDL}}$	$A_s$
<u>Non Wet Bulb Conditions</u>						
$10^5$	.221	.278	374	1345	.544	$1.432 \times 10^7$
$10^6$	.221	.335	450	1345	.509	$1.432 \times 10^7$
$10^7$	.221	.418	562	1345	.454	$1.432 \times 10^7$
<u>Wet Bulb Conditions</u>						
$10^5$	.266	.266	376	1417	.603	$6.205 \times 10^6$
$10^6$	.306	.306	457	1498	.629	$2.660 \times 10^6$
$10^7$	.359	.359	582	1623	.668	$8.162 \times 10^5$

With increasing pressure, the surface temperature increases in all cases. As noted earlier, the wet bulb surface temperature slightly exceeds the non-wet bulb surface temperature at each pressure. The nondimensional surface temperatures are lower for the wet bulb condition at a given pressure even though the dimensional surface temperatures are higher. This is due to the fact that at the wet

bulb condition, the flame temperatures and ambient temperatures ( $T_{\infty 0}^*$ ) are also higher. At the non-wet bulb limit, for fixed centerline temperature, the ambient temperature is independent of pressure.

While  $A_s$  is relatively constant with pressure at non-wet bulb conditions,  $A_s$  decreases with increasing pressure for the wet bulb case, significantly increasing the mass burning rates for the larger drops at a given value of  $A$ . This effect is due to increased reaction rates for the higher flame temperatures of wet bulb combustion, at elevated pressures.

At non-wet bulb conditions,  $\dot{m}_{\text{SDL}}$  decreases with increasing pressure due to the reduction in the temperature difference between the ambient gas and the liquid surface. For the wet bulb case, the increased ambient temperature compensates for this effect and there is a slight increase in  $\dot{m}_{\text{SDL}}$  with increasing pressure.

Using the properties of Table 1, the droplet size range corresponding to the transition region (taken to be  $10^4 < A < 10^9$ ) is shown in Table 4. As the pressure increases, the droplet size for the onset of the large drop limit is reduced. Notably, the size range of technological importance for actual combustors falls largely in the transition region. At higher pressures, however, a greater percentage of the droplets present in a spray can be represented by large drop limit results.

Table 4

Droplet Size Range of Transition Region<sup>a</sup>

$P_o^* \times 10^5$ (N/m <sup>2</sup> )	$d_{s_{min}}^* - d_{s_{max}}^*$ ( $\mu$ )
1	25-7500
10	2.5-750
100	.25-75

<sup>a</sup>Corresponding to  $10^4 < A < 10^9$ .

## CHAPTER IV

### FIRST-ORDER RESULTS

#### 4.1 Introduction

At very low frequencies, the liquid and gas phases respond rapidly to changes in the forcing function and a total quasi-steady analysis is sufficient. As the oscillation frequency is increased, the liquid response is not rapid enough as the characteristic frequency of the liquid phase thermal wave is approached, requiring an unsteady analysis of the liquid phase. As the frequency approaches the characteristic frequency of the gas phase thermal wave, both the liquid and gas phases are unsteady. At extremely high frequencies, both the liquid and gas phases are unable to respond at all, and a steady state approximation can be assumed.

In order to analyze response, the burning rate response function is utilized [1]. In the present notation this quantity is

$$P_r = \text{Re}\{\dot{m}_1/\dot{m}_0\} \quad (4-1)$$

where Re denotes the real part; i.e., that portion of the burning rate oscillation that is in-phase with the pressure oscillation. For instability,  $P_r$  must be positive and of order unity (the exact value depends upon the degree of damping present) at a point in the combustion chamber where the pressure is varying. It must be understood that a droplet with  $P_r \geq 1$  will not in itself cause instability, but rather the sum of the responses of all the droplets within the combustion chamber must be greater than the available

damping, in order for the combustion oscillation to grow.

#### 4.2 Small Drop, Low Frequency Limit

This section considers behavior at low frequencies for the small droplet or evaporative limit. Figure 8 illustrates both the wet and non-wet bulb response function,  $P_r$ , and the magnitude of the surface temperature oscillation,  $T_{1s}$ , plotted as a function of pressure. The frequency for this plot is zero so that both the gas and liquid phases are quasi-steady. (The present analysis is not formally valid at  $\omega = 0$ , since the mean droplet size varies during an oscillation at this condition; therefore, the plot should be taken as representative of conditions where it is still valid to assume that both gas and liquid phases are quasi-steady, but with sufficiently high frequency so that changes in mean size can be ignored during a period of oscillation.)

At this condition, the response function is negative, with a relatively small magnitude, and with increasing pressure, the response function becomes more negative. This is in contrast to results for bipropellant combustion where the response function generally approaches zero or a positive limit for small  $\omega$ .

At this low frequency limit, the ambient temperature is constant since there is no transient energy storage in either phase. The surface temperature varies in phase with the pressure oscillation, and its magnitude increases as the pressure increases. This follows primarily from the form of the vapor pressure curve. At the quasi-steady limit

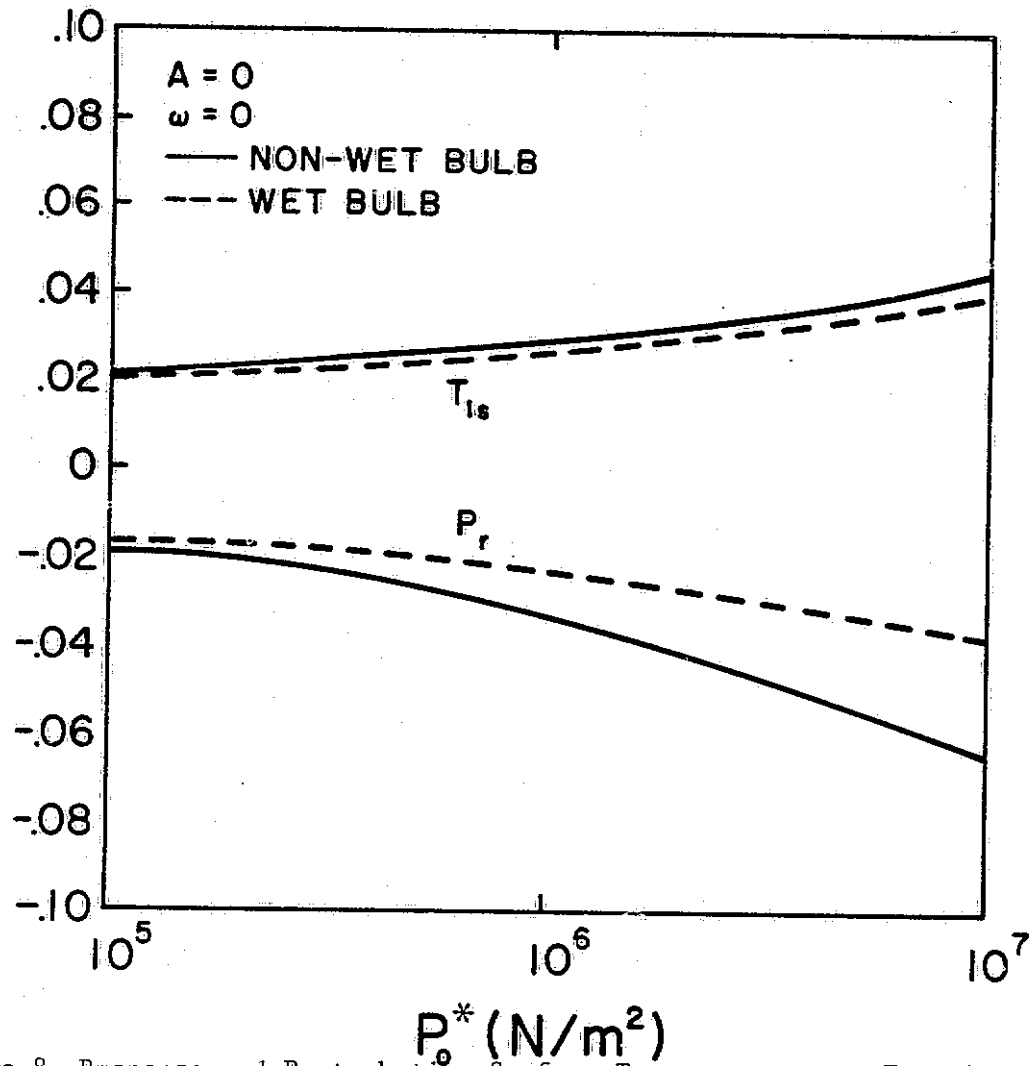


Figure 8 Response and Perturbation Surface Temperature as a Function of Pressure at the Small Droplet Limit for Wet and Non-Wet Bulb Conditions

$$T_{ls} \approx \frac{T_{os}^2}{L_f} \quad (4-2)$$

therefore, since  $T_{os}$  increases with increasing mean pressure,  $T_{ls}$  increases accordingly.

At the same limit, using the results for  $T_{ls}$

$$\dot{m}_1 \approx \frac{-T_{os}^3}{L_f \{q + T_{os} - 1\}} \quad (4-3)$$

This approximate formula indicates negative response at the quasi-steady limit. With increasing pressure,  $T_{os}$  increases, providing a larger negative response.

Physically, the negative response at the totally quasi-steady limit is caused by the fact that the gasification rate decreases as the surface temperature increases (for a constant ambient temperature). Therefore, pressures above the mean result in reduced gasification rates, and pressures below the mean result in increased gasification rates-yielding a negative response. At higher frequencies, energy can be temporarily stored in the liquid or gas phases, causing a fluctuation in the ambient temperature which can compensate for the surface temperature fluctuation. This modifies the response for small droplets as will be discussed later.

#### 4.3 Large Drop Limit

Moving from the evaporative limit (small drop limit) to the large drop limit, much greater response is observed for nonpropellant droplets. Figures 9-11 illustrate the non-wet bulb response as a function of frequency (dimensionless frequency for strand combustion from Reference [11]) for the large droplet limit at mean pressures of

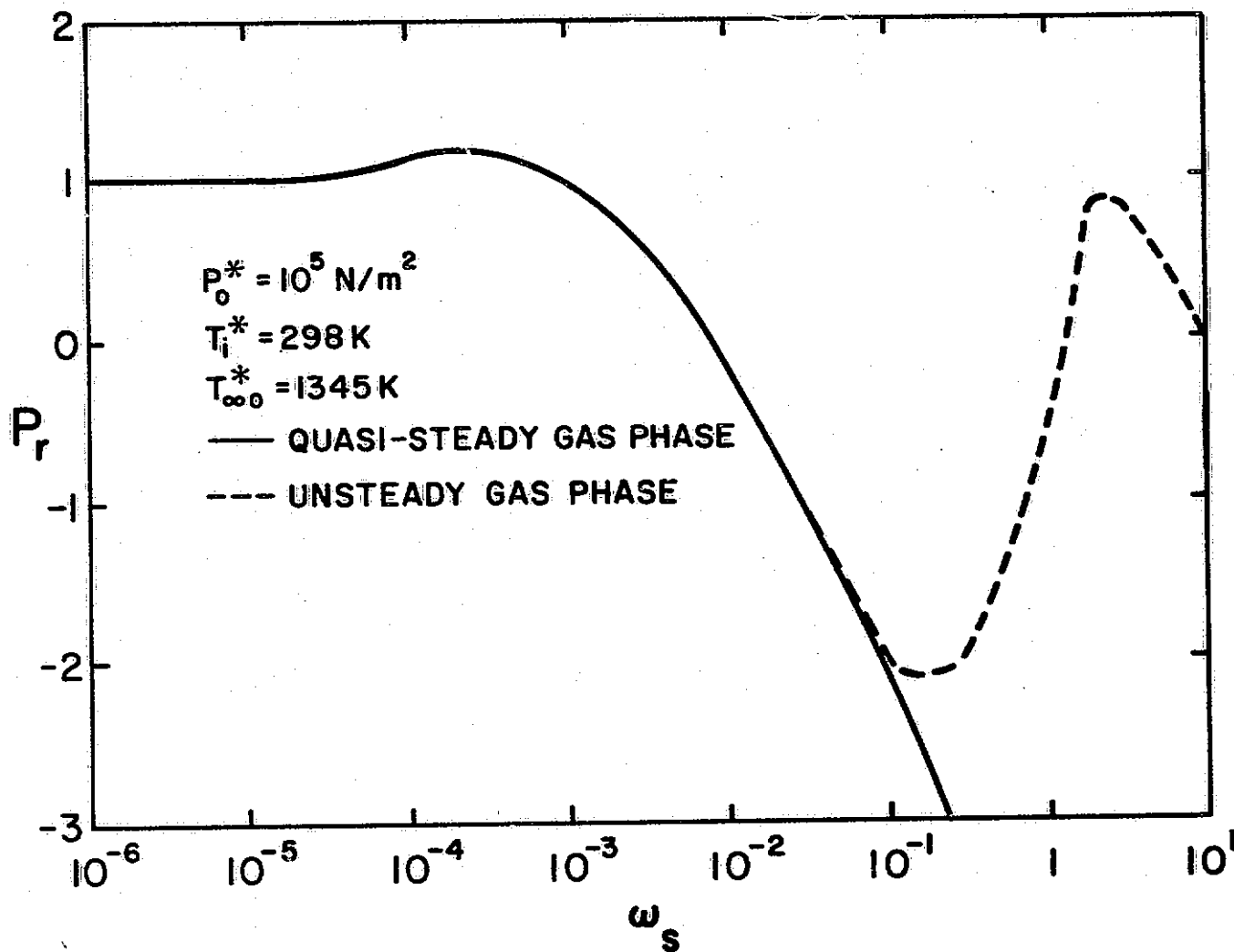


Figure 9 Response as a Function of Frequency at the Large Droplet Limit at Approximately 1 Atm. Pressure (Non-Wet Bulb Conditions)

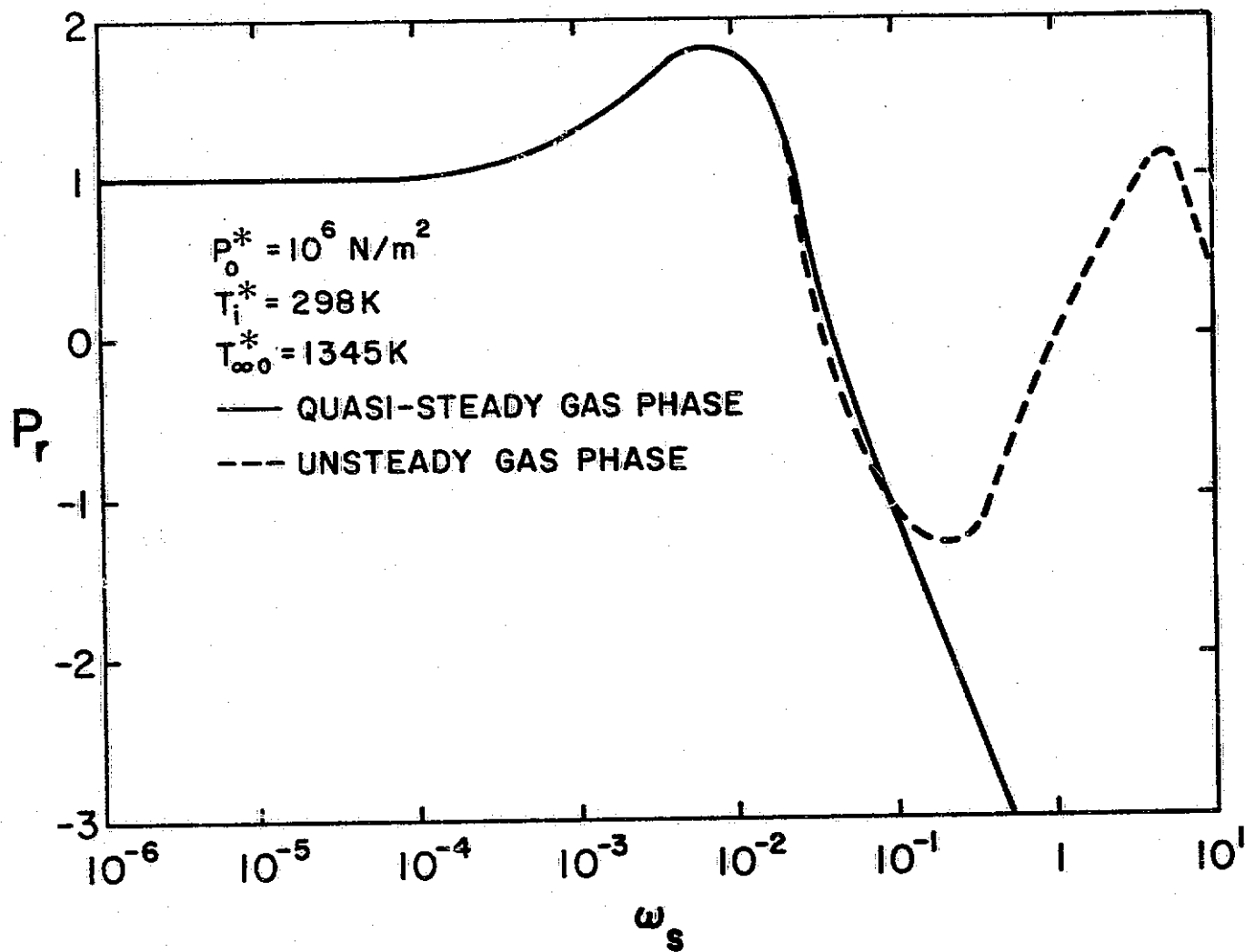


Figure 10 Response as a Function of Frequency at the Large Droplet Limit at Approximately 10 Atm. Pressure (Non-Wet Bulb Conditions)

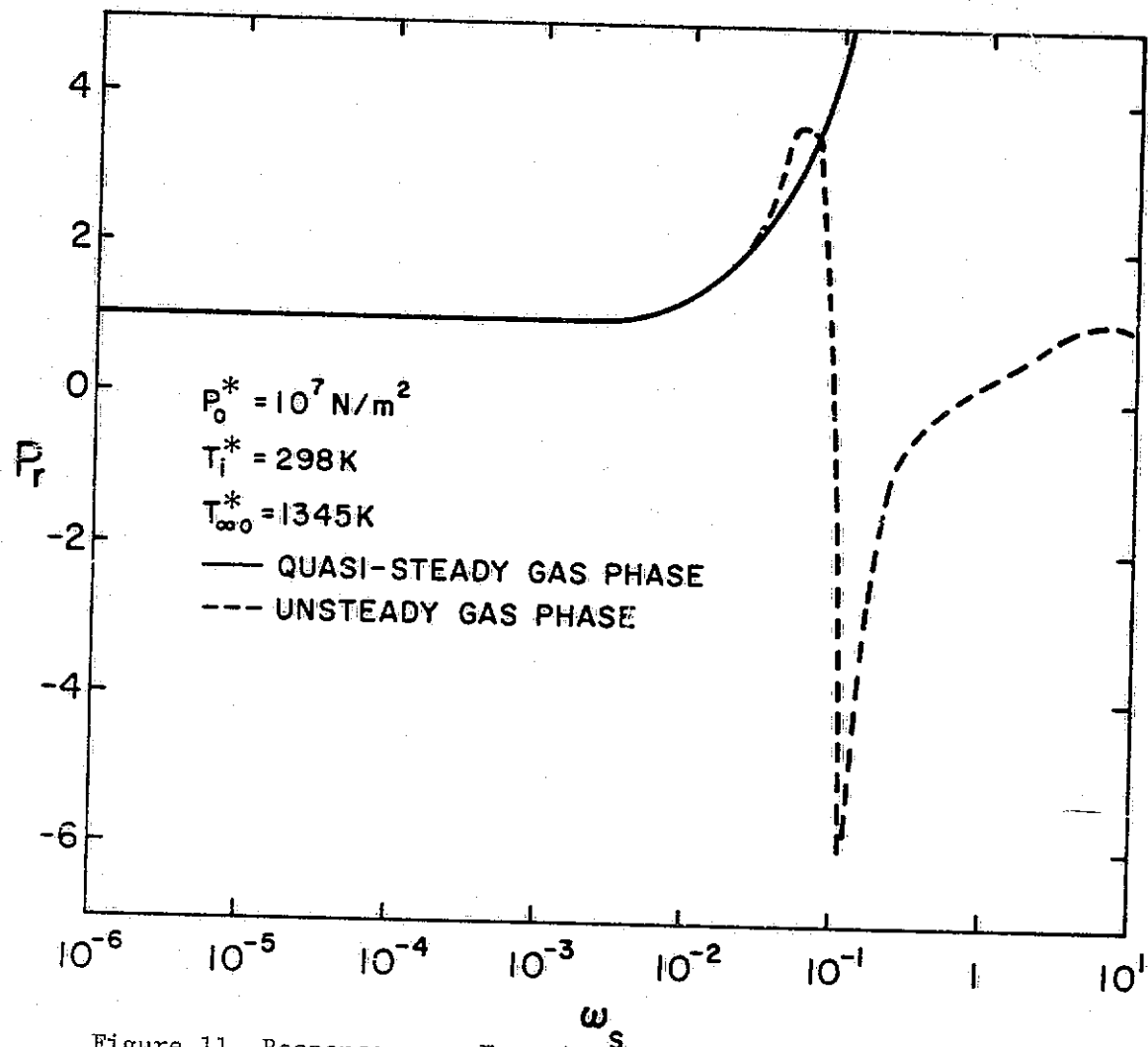


Figure 11 Response as a Function of Frequency at the Large Droplet Limit at Approximately 100 Atm. Pressure (Non-Wet Bulb Conditions)

1, 10 and 100 atmospheres. Figures 12-14 show similar results at wet bulb conditions. In addition to the quasi-steady gas phase approximation, results for the completely unsteady gas phase are also shown. The non-wet bulb results are replotted from the calculations of Reference [11], while the wet bulb results were calculated by the present author.

The conversion of  $r_0$  and  $r_1$ , the strand burning rate and its perturbation, is straight-forward at the large drop limit, namely

$$P_r = \text{Re} \left\{ \frac{\dot{m}_1}{\dot{m}_0} \right\} = \text{Re} \{r_1\} \quad (4-4)$$

since  $r_0 = 1$ . The dimensionless frequency for the strand combustion case,  $\omega_s$ , is related to the present dimensionless frequency by

$$\omega_s = (A_s/A)\omega \quad (4-5)$$

In all cases, the response approaches unity at low frequencies, where both liquid and gas phases are quasi-steady. This follows from the fact that the burning rate is proportional to pressure, under steady conditions, for a second-order reaction [11].

With increasing frequency, at non-wet bulb conditions, a peak is observed in the response plot at frequencies near the characteristic frequency of the liquid phase. Beyond this peak, the quasi-steady gas phase solution gives a continuously declining response. The peak is absent in the wet bulb case, with the response showing a noticeable decline at the liquid phase characteristic frequency. This increasing contrast between the two cases will be discussed later in more detail.

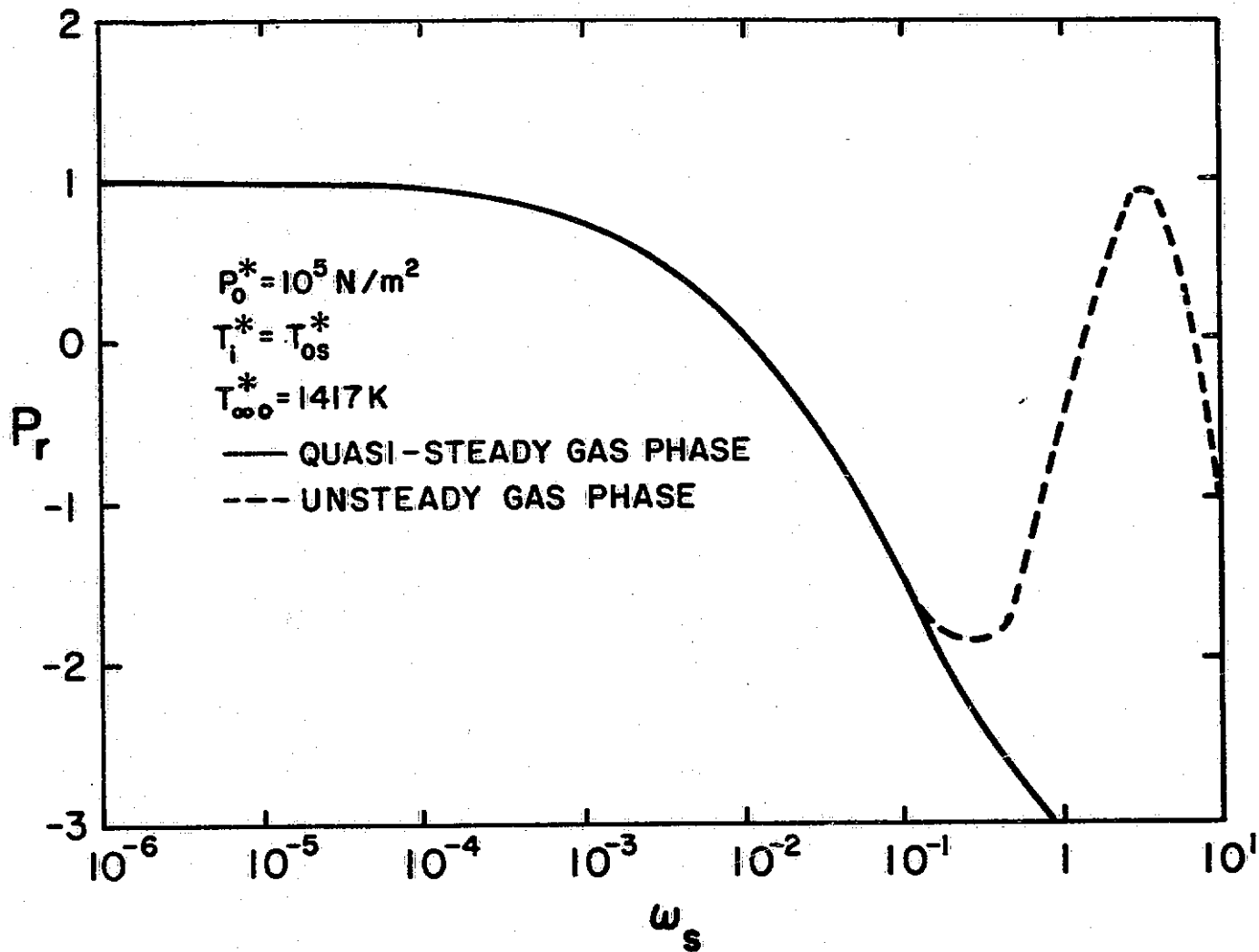


Figure 12 Response as a Function of Frequency at the Large Droplet Limit at Approximately 1 Atm. Pressure (Wet Bulb Conditions)

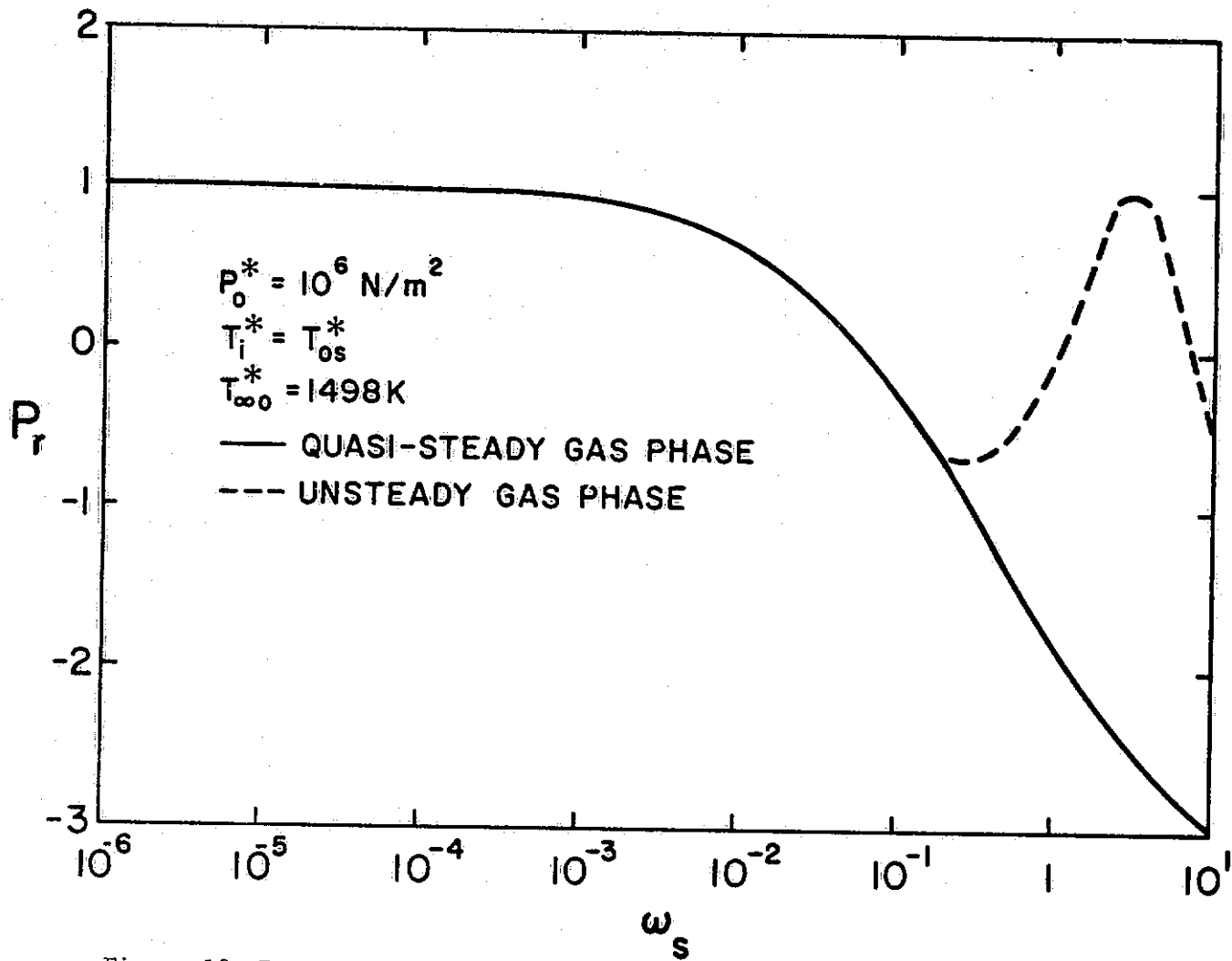


Figure 13 Response as a Function of Frequency at the Large Droplet Limit at Approximately 10 Atm. Pressure (Wet Bulb Conditions)

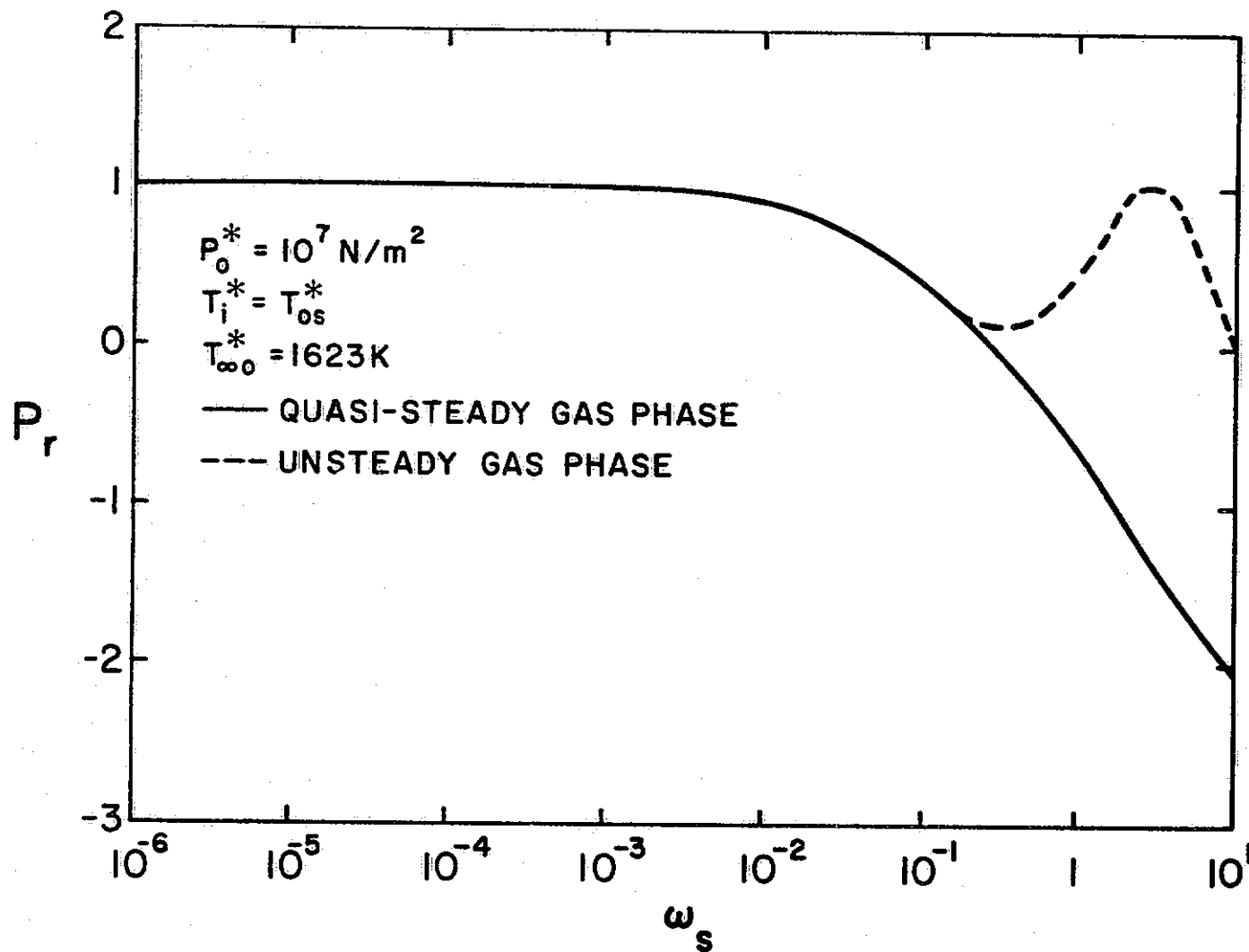


Figure 14 Response as a Function of Frequency at the Large Droplet Limit at Approximately 100 Atm. Pressure (Wet Bulb Conditions)

At higher frequencies, the analysis allowing for transient gas phase effects begins to diverge from the quasi-steady gas phase solution. Substantial differences between the two models are encountered for values of  $\omega_g$  on the order of  $10^{-1}$ , which represents frequencies near the characteristic frequency of the gas phase. At dimensionless frequencies on the order of unity, a second response peak is observed, in all cases, for the complete unsteady gas phase solution. This peak is clearly associated with gas phase transient effects and yields maximum values of  $P_r$  on the order of unity. With increasing pressure, the frequencies of the two response peaks approach one another due to the increase in gas density.

Table 5 lists the frequencies from Figures 9-14 where large droplets have a positive response, the liquid thermal wave characteristic frequencies, and the gas thermal wave characteristic frequencies. In considering this table, it should be recalled that acoustic instability in rocket engine combustion chambers is generally associated with the frequency range 500-30,000 Hz [1]. At pressures below 10 atmospheres, response peaks due to gas phase transient effects largely fall within this range. At pressures above 10 atmospheres, response peaks due to gas phase transient effects decline in importance since they are associated with very high frequencies. In this pressure range, liquid phase phenomena are more significant, providing response peaks in the critical frequency range. Since the pressure range usually encountered in rocket engines is above 10 atmospheres, gas phase transient effects do not appear to be a major factor in causing instability for hydrazine fueled engines. Based on this finding, further analysis in the

Table 5

Critical Frequency Ranges for Hydrazine Strand Combustion

(Non-Wet Bulb Conditions)

Mean Pressure (N/m <sup>2</sup> )	Liquid Thermal Wave Characteristic Frequency (Hz)	Liquid Transient Range (Hz)	Gas Thermal Wave Characteristic Frequency (Hz)	Gas Transient Range (Hz)
10 <sup>5</sup>	0.02	< 1.8	210	270-1,900
10 <sup>6</sup>	2.1	< 84 <sup>a</sup>	2,100	2,100-170,000
10 <sup>7</sup>	210	< 1,800 <sup>a</sup>	21,000	27,000 < <sup>b</sup>

(Wet Bulb Conditions)

Mean Pressure (N/m <sup>2</sup> )	Liquid Thermal Wave Characteristic Frequency (Hz)	Liquid Transient Range (Hz)	Gas Thermal Wave Characteristic Frequency (Hz)	Gas Transient Range (Hz)
10 <sup>5</sup>	0.02	< 2	210	330-1500
10 <sup>6</sup>	1.8	< 130	2,100	2,100-18,000
10 <sup>7</sup>	180	< 6700 <sup>c</sup>	21,000	6,700 <sup>c</sup> -190,000

<sup>a</sup>Liquid transient range ends where transient gas curve intersects P<sub>r</sub> = 0.

<sup>b</sup>Gas transient range begins where second gas transient peak intersects P<sub>r</sub> = 0.

<sup>c</sup>Liquid transient range ends where gas transient range begins, at low point in gas transient curve at approximately P<sub>r</sub> = 0.14.

transition region, between the large and small droplet regimes, was limited to the case of quasi-steady gas phase effects.

The magnitude of the unsteady gas phase response peaks approach unity at elevated pressures; however, these response peaks are smaller in magnitude than the transient liquid phase response peak for the non-wet bulb case. Also, the unsteady gas phase peak occurs near or beyond the maximum probable frequencies that cause instability. Table 6 lists the frequencies where the unsteady liquid and gas phase response peaks occur. At the higher pressures, the unsteady gas phase response peak is outside the critical instability frequency range.

Table 6

Frequencies of the Unsteady Gas and Liquid Phase Response Peaks

Mean Pressure (N/m <sup>2</sup> )	Liquid Transient Peak (Hz)	Gas Transient Peak (Hz)
<u>(Non-Wet Bulb Condition)</u>		
10 <sup>5</sup>	0.04	528
10 <sup>6</sup>	17	11,000
10 <sup>7</sup>	1100 <sup>a</sup>	110,000
<u>(Wet Bulb Condition)</u>		
10 <sup>5</sup>	--	670
10 <sup>6</sup>	--	6,700
10 <sup>7</sup>	--	67,000

<sup>a</sup> Corresponds with first gas phase transient analysis peak.

#### 4.4 Complete Solution

Figures 15-17 show the quasi-steady gas phase non-wet bulb response as a function of frequency at various drop sizes, ranging from the small drop to the large drop limit. As  $A$  increases, the response increases, caused by the combustion zone moving closer to the liquid surface. At an  $A$  of approximately  $10^7$ , a peak in the response curve develops, increasing in magnitude and frequency as the drop size increases, until the large drop approximates the one-dimensional strand near the value of  $A = 10^{10}$ . As the pressure increases, the peaks increase in magnitude and move to higher frequencies. It should be noted that when  $A = 10^{10}$ , transient gas phase effects begin to appear at approximately  $\omega = 6.98 \times 10^1$ . This corresponds to  $\omega_s = 10^{-1}$ .

The quasi-steady wet bulb responses are plotted in Figures 18-20, as a function of frequency for the complete range of drop sizes. As in the non-wet bulb case, the response increases with increasing  $A$ ; however, no response peaks are observed. Droplet combustion response is well approximated by the one-dimensional strand at values of  $A$  greater than  $10^{10}$ .

In order to better understand the difference in the response for the wet and non-wet bulb cases, an investigation of the first-order liquid phase temperature distribution was undertaken.

Figure 21 shows the non-wet bulb perturbation surface temperature, magnitude and phase angle, as a function of frequency for a pressure of 10 atmospheres and  $A = 10^{10}$ . At low frequencies the surface temperature,  $T_{1s}$ , is in-phase with the pressure oscillation. When the frequency increases, a peak occurs in the

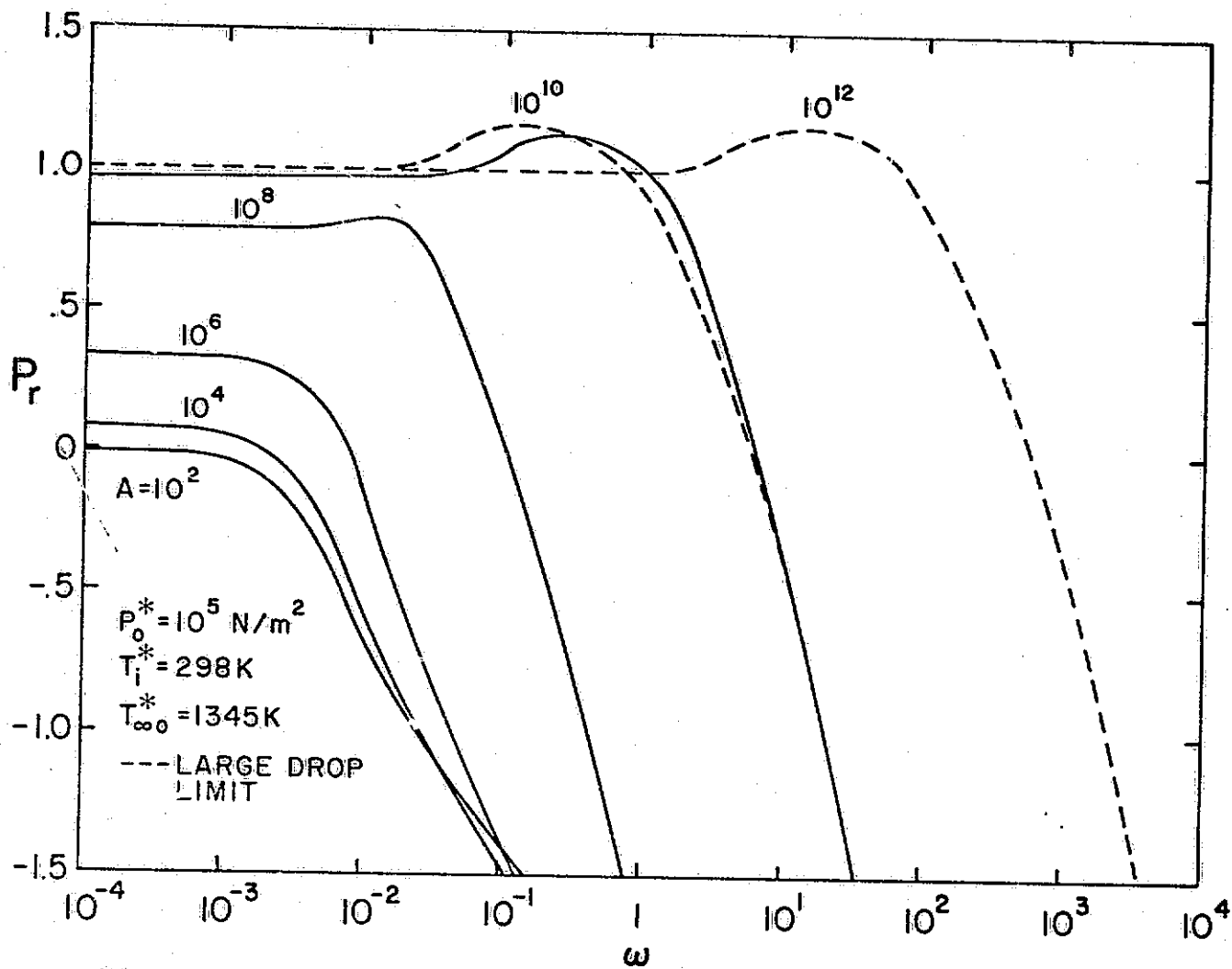


Figure 15 Quasi-Steady Gas Phase Response as a Function of Frequency and  $A$  at Approximately 1 Atm. Pressure (Non-Wet Bulb Conditions)

REPRODUCIBILITY OF THE ORIGINAL PAGE IS POOR

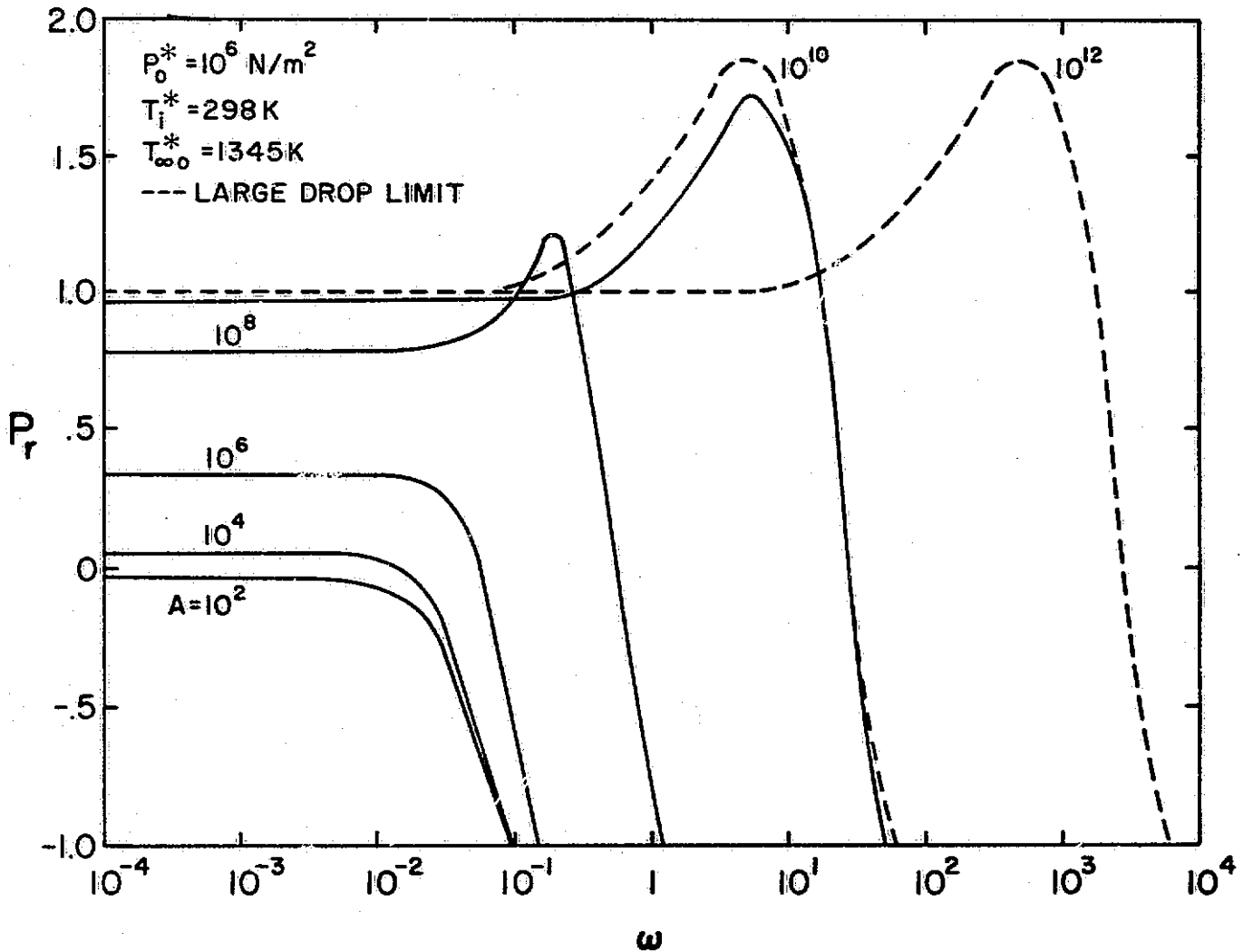


Figure 16 Quasi-Steady Gas Phase Response as a Function of Frequency and A at Approximately 10 Atm. Pressure (Non-Wet Bulb Conditions)

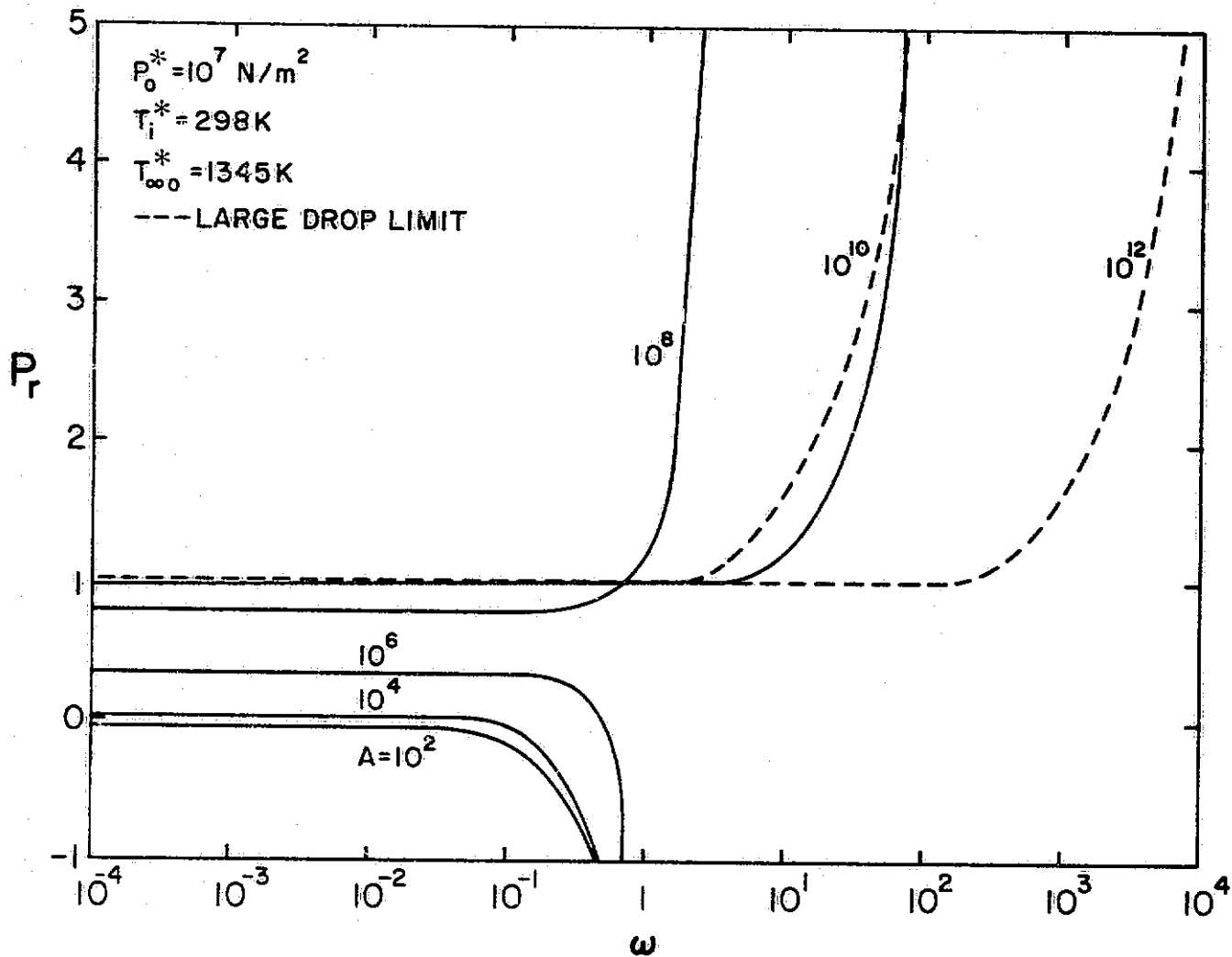


Figure 17 Quasi-Steady Gas Phase Response as a Function of Frequency and  $A$  at Approximately 100 Atm. Pressure (Non-Wet Bulb Conditions)

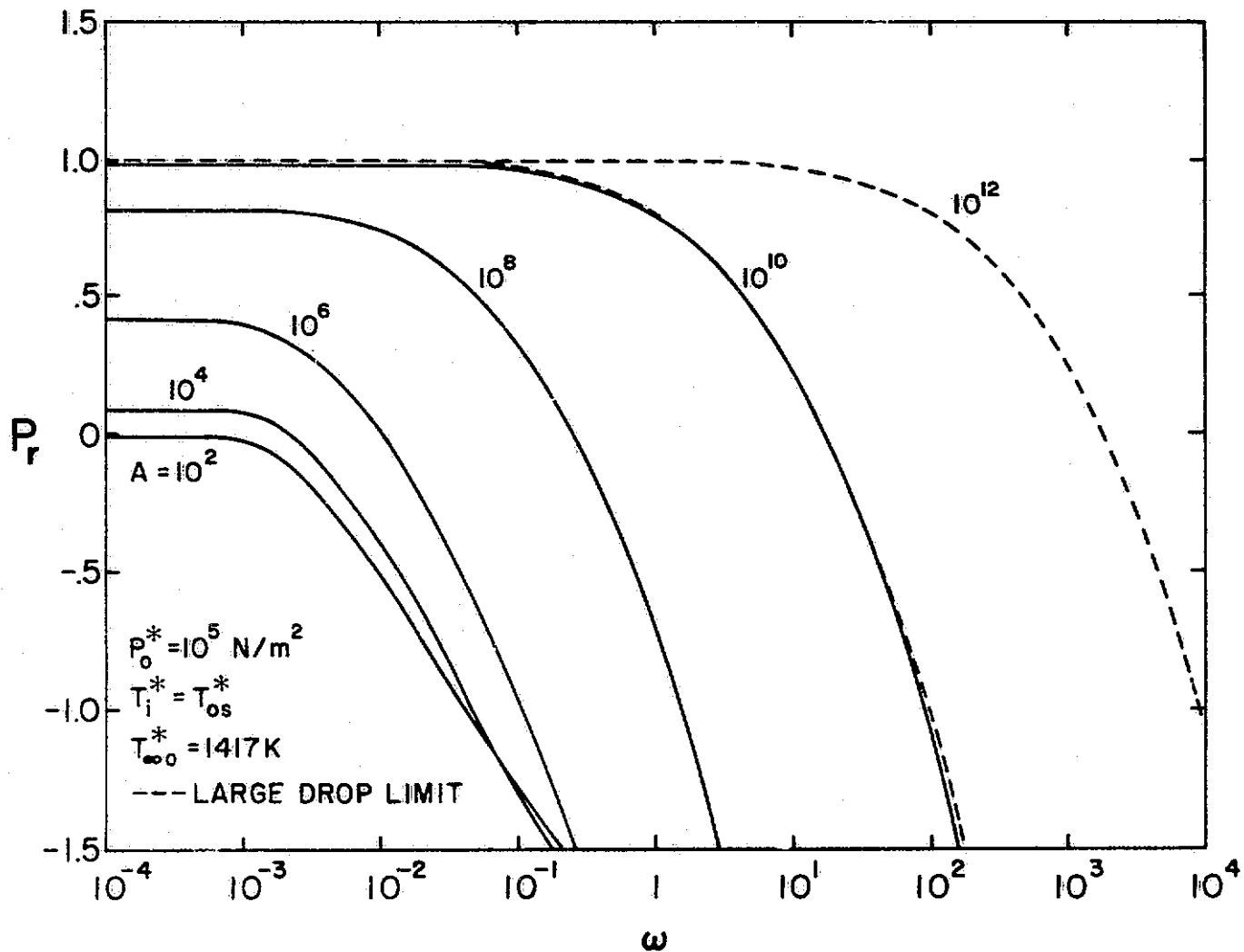


Figure 18 Quasi-Steady Gas Phase Response as a Function of Frequency and A at Approximately 1 Atm. Pressure (Wet Bulb Conditions)

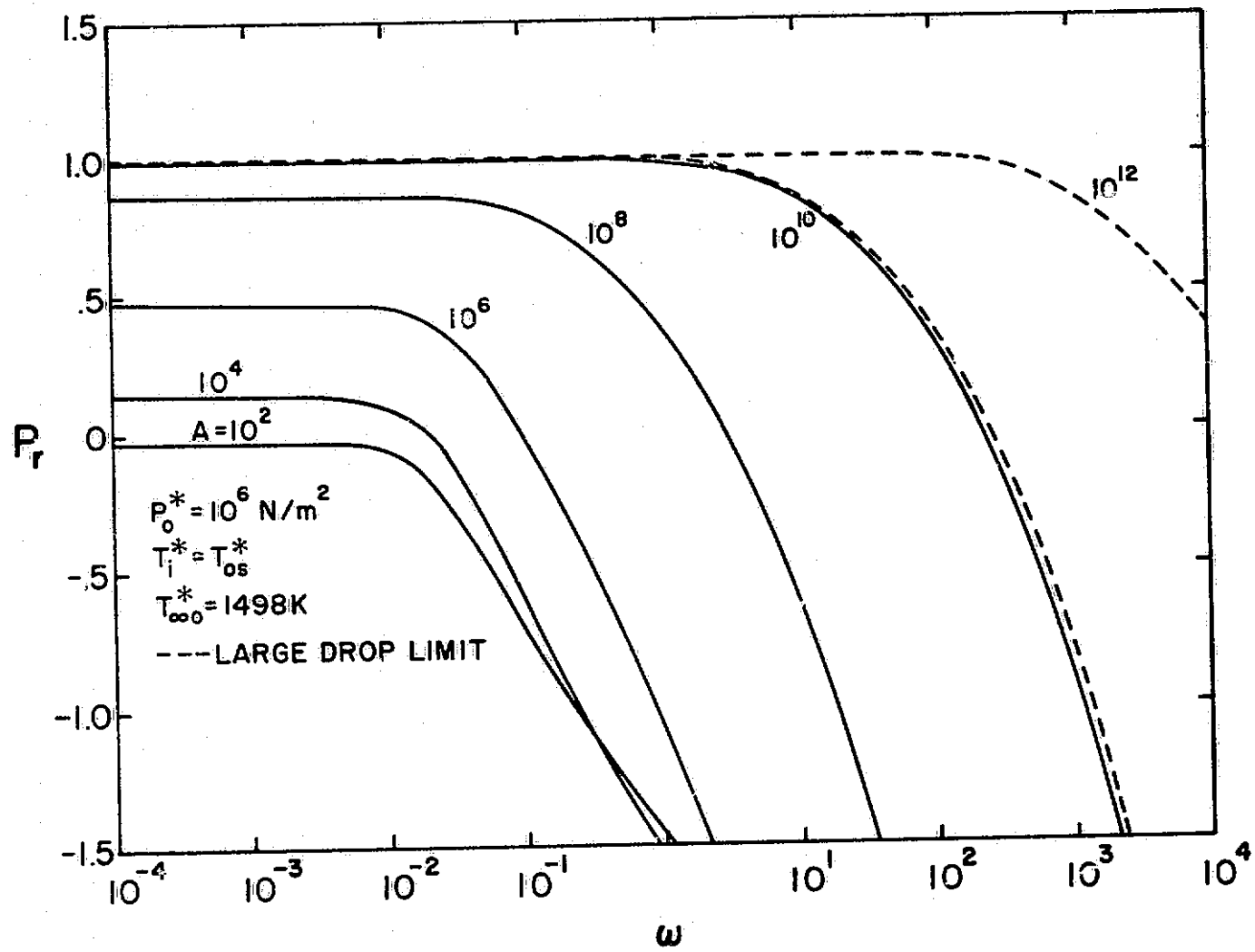


Figure 19 Quasi-Steady Gas Phase Response as a Function of Frequency and A at Approximately 10 Atm. Pressure (Wet Bulb Conditions)

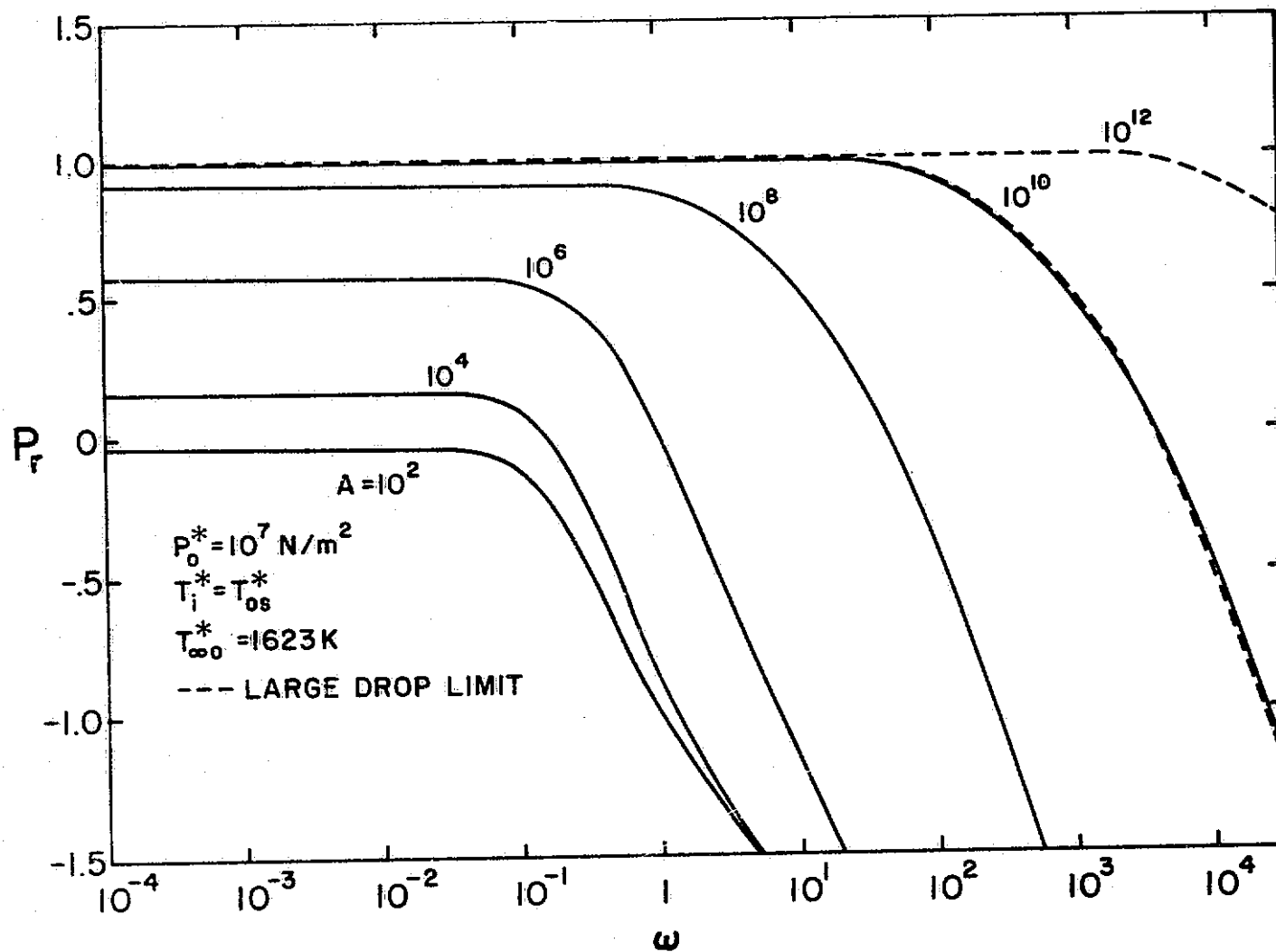


Figure 20 Quasi-Steady Gas Phase Response as a Function of Frequency and  $A$  at Approximately 100 Atm. Pressure (Wet Bulb Conditions)

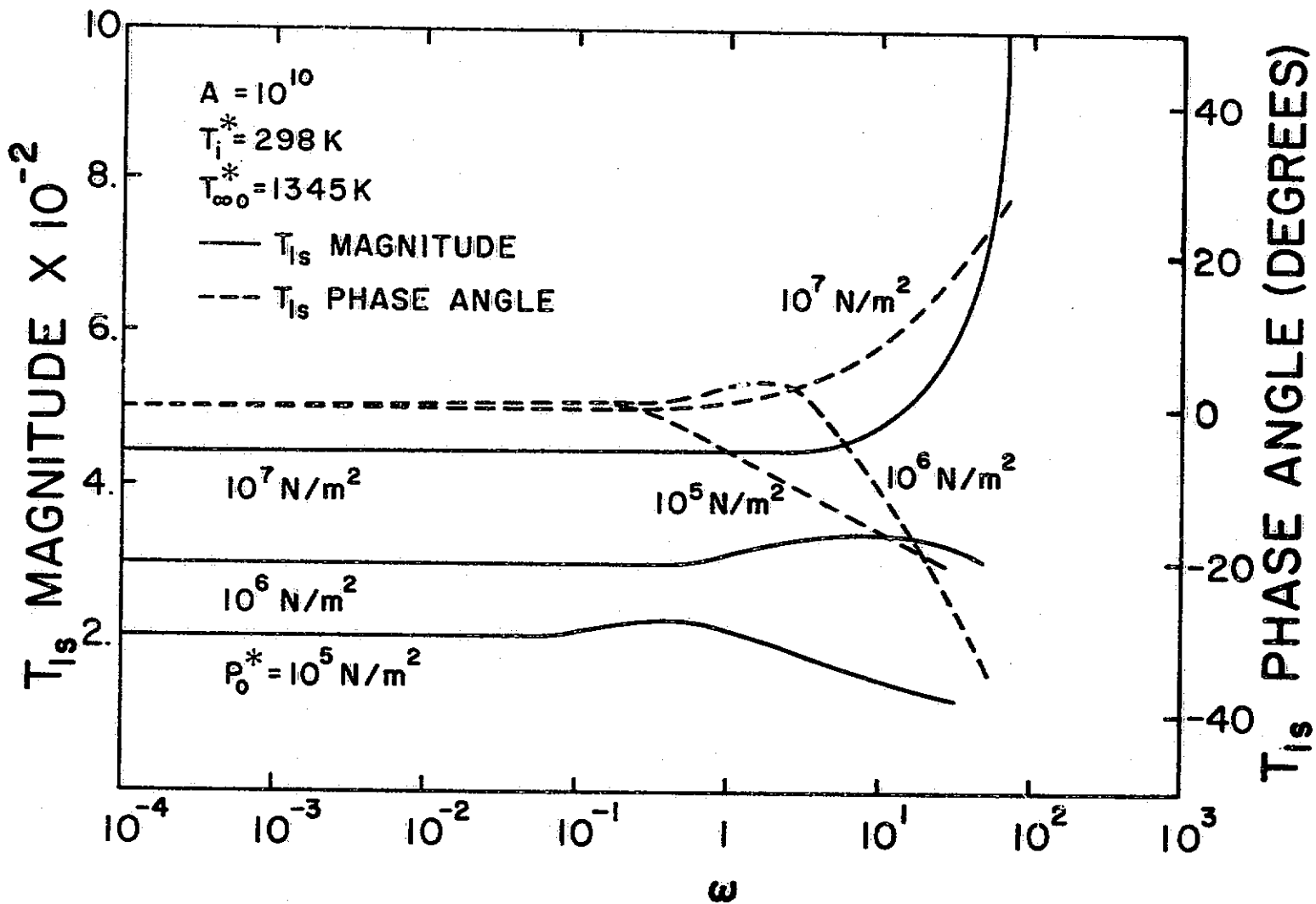


Figure 21 Perturbation Surface Temperature Magnitude and Phase Angle as a Function of Frequency and Pressure (Non-Wet Bulb Conditions)

magnitude of  $T_{1s}$ , which corresponds with the response peak. It is also observed, that when the peak does occur,  $T_{1s}$  leads the forcing function until the peak is reached, while at higher frequencies,  $T_{1s}$  lags the pressure oscillation.

Figure 22 is a plot of the first-order liquid phase temperature distribution near the drop surface for a sinusoidal oscillation at a nondimensional frequency of 1.6, a pressure of 10 atmospheres, and  $A = 10^{10}$ . This plot further illustrates the  $T_{1s}$  phase lead. A frequency of 1.6 corresponds to the maximum phase lead in Figure 21 for the perturbation surface temperature at 10 atmospheres. As the pressure wave oscillates at  $\omega = 1.6$ ,  $T_{1s}$  also oscillates at approximately 4 degrees ahead of the pressure.  $T_{1s}$  is unable to stay in-phase with the pressure oscillation at this frequency because the large values of  $T_{1s}$  induce steep temperature gradients near the liquid surface which act as heat sinks. The increased heat loss from the surface due to this gradient causes the temperature peak to precede the pressure peak for this range of frequencies (and conversely at the minimum pressure and temperature regions).

Figure 23 shows the magnitude and phase angle of the wet bulb perturbation surface temperature as a function of frequency at 10 atmospheres for  $A = 10^{10}$ . It is observed that  $T_{1s}$  never leads the pressure oscillation in this case, in contrast to non-wet bulb conditions (Figure 21).

In order to better understand this phenomena, a plot similar to Figure 22 is introduced. Figure 24 is an illustration of the liquid phase first-order temperature distribution near the drop surface at  $\omega = 50$ , a pressure of 10 atmospheres, and  $A = 10^{10}$ . In

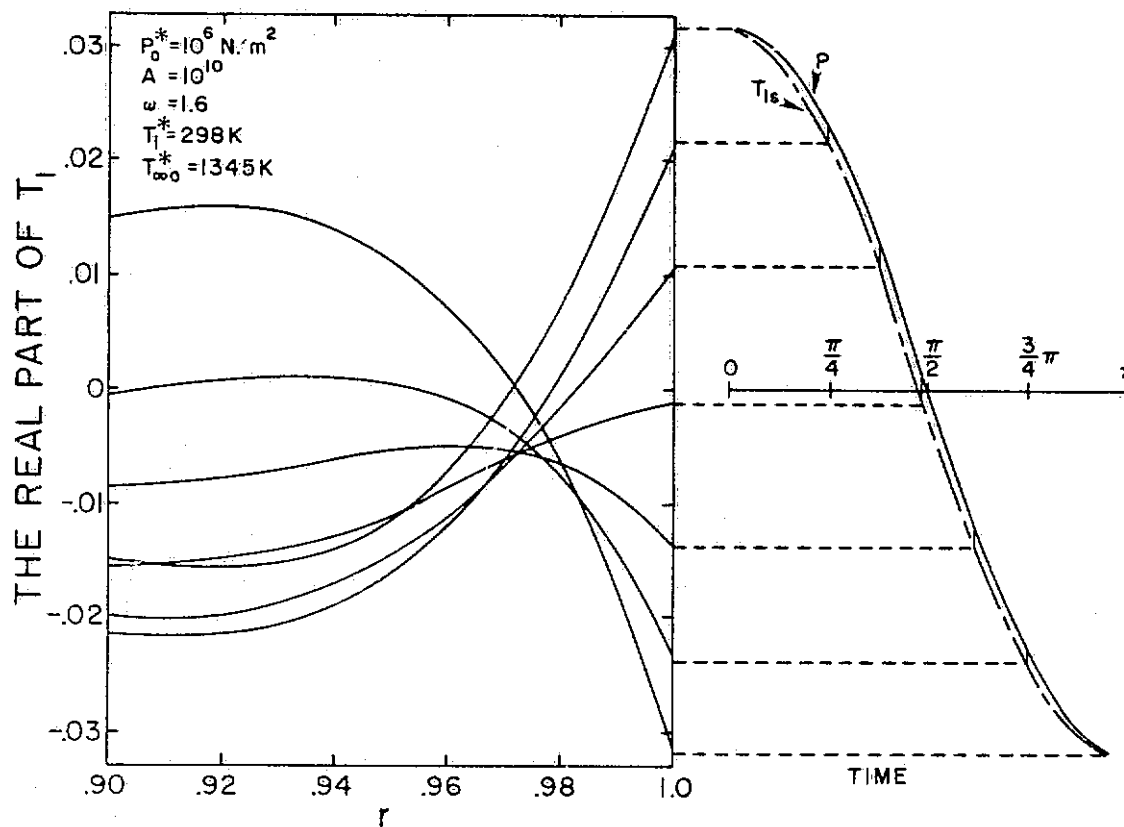


Figure 22 Perturbation Liquid Phase Temperature Distribution for a Sinusoidal Pressure Oscillation and a  $T_{l,s}$  Phase Lead of Approximately 4 Degrees (Non-Wet Bulb Conditions)

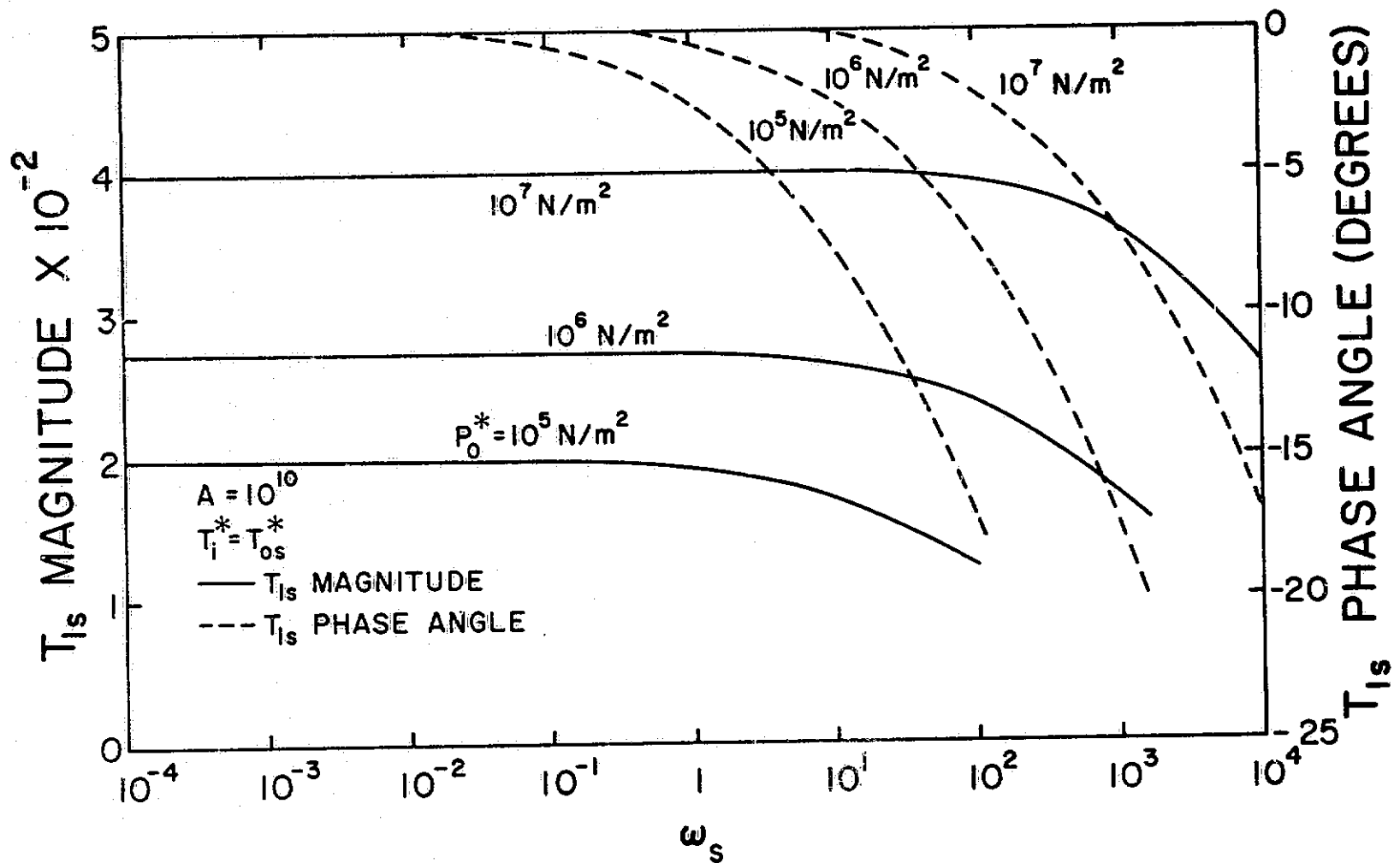


Figure 23 Perturbation Surface Temperature Magnitude and Phase Angle as a Function of Frequency and Pressure (Wet Bulb Conditions)

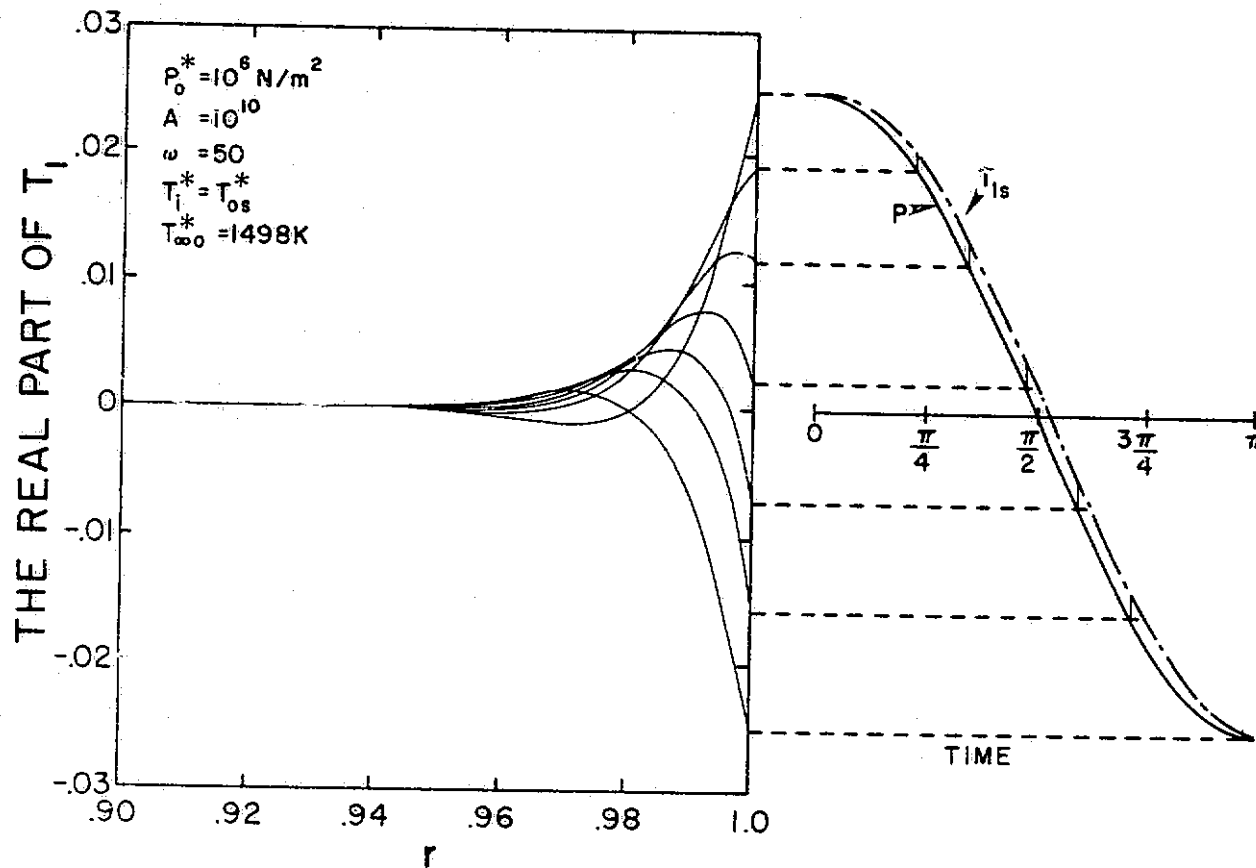


Figure 24 Perturbation Liquid Phase Temperature Distribution for a Sinusoidal Pressure Oscillation and a  $T_{ls}$  Phase Lag of Approximately 5.5 Degrees (Wet Bulb Conditions)

this case  $T_{1s}$  lags the pressure oscillation by approximately 5.5 degrees. The wet bulb case differs from the non-wet bulb condition because of the constant zero-order mean liquid phase temperature, which reduces the steepness of the first-order temperature gradients in the liquid phase near the surface.

The only two types of monopropellant droplets which have been considered, are the wet bulb droplet with a zero mean temperature gradient (constant mean temperature) and the non-wet bulb droplet with a steep mean temperature gradient. For the parameters listed in Table 1, a response peak is observed in the non-wet bulb case, while the opposite is true for the wet bulb case. Under realistic conditions, the droplets will have temperature gradients ranging between the wet and non-wet bulb limits.

From the present study it can be concluded that a response peak will only occur when the mean temperature gradient near the droplet surface has sufficient steepness so that enough energy will flow from the surface towards the center of the drop, causing the perturbation surface temperature to lead the pressure. When the mean temperature gradient is not steep enough, the perturbation surface temperature will never lead the pressure. Also, as the droplet size decreases while it is reacting, the liquid temperature gradient will tend to approach the wet bulb limit; thus, eliminating the response peak.

Once the response peak begins to appear,  $T_{1s}$  leads the pressure wave. As the frequency is increased, the non-wet bulb temperature gradient loses its influence on the droplet surface, enabling the  $T_{1s}$  phase angle to begin to decrease. When the frequency is further

increased, the first-order surface temperature and the pressure wave are again in-phase; thus, the burning rate is maximized and the response peak is reached. Any additional increase in frequency will decrease the response as the lag in surface temperature continues to increase.

CHAPTER V

SPRAY COMBUSTION MODEL

As discussed earlier, a combustion chamber will become unstable when the total response of all the droplets in the spray exceeds the available damping. Using the droplet response results of the previous chapter, an analysis of spray response will not be undertaken.

5.1 Description of the General Model

For the spray combustion model, the spray is assumed to be relatively confined, with the pressure field identical for all parts of the spray.

The open-loop response function for an individual drop is defined on page 130 of Reference [1] as follows:

$$P_r = R_e \left\{ \frac{\dot{m}^* \bar{P}^*}{P^* \bar{m}^*} \right\} \quad (5-1)$$

where  $P^*$  and  $\dot{m}^*$  are the instantaneous perturbations of pressure and burning rate, and  $\bar{P}^*$  and  $\bar{m}^*$  are the respective steady state values.

For a monodisperse spray, Equation (5-1) can be extended to compute the total response of a spray consisting of numerous drops of varying sizes as follows:

$$P_{rt} = R_e \left\{ \frac{\dot{m}_T^* \bar{P}^*}{P^* \bar{m}_T^*} \right\} \quad (5-2)$$

where  $\bar{m}_T^*$  and  $\dot{m}_T^*$  are the respective total steady state and perturbation mass burning rates of all the drops in the spray.

The total number of droplets in a spray,  $N$ , is equal to the droplet injection rate multiplied by the droplet lifetime. The number of droplets in a size increment  $dr_s^*$  is  $Nfdr_s^*$ , where  $f$  is a function of  $r_s^*$ , pressure, and the combustion characteristics. The fraction of droplets in a given interval  $dr_s^*$  is  $fdr_s^*$ .

With these definitions, the total steady state mass burning rate for all drops in the spray is

$$\bar{m}_T^* = \dot{m}_{o_T}^* = \int_0^{\infty} Nf4\pi\dot{m}_o^* dr_s^* \quad (5-3)$$

where  $\bar{m}_o^*$  is the steady state mass burning rate per unit solid angle and is a function of  $r_s^*$  at a given pressure.

The total mass burning rate perturbation is

$$\dot{m}_{l_T}^* = \int_0^{\infty} Nf4\pi\dot{m}_l^* dr_s^* \quad (5-4)$$

where

$$\dot{m}_l^* = \frac{\bar{P}^* \dot{m}^{*'}}{P^{*'}} \quad \dot{m}_{l_T}^* = \frac{\bar{P}^*}{P^{*'}} \dot{m}_T^{*'} \quad (5-5)$$

and  $\dot{m}_l^*$  is the perturbation mass burning rate per unit solid angle and is a function of  $r_s^*$ , frequency, and pressure for the quasi-steady gas phase case.

Substituting Equations (5-3) and (5-4) into Equation (5-2) yields the total spray response,  $P_{rt}$ , for a monodisperse spray

$$P_{rt} = R_e \left\{ \frac{\int_0^{\infty} Nf4\pi\dot{m}_l^* dr_s^*}{\int_0^{\infty} Nf4\pi\dot{m}_o^* dr_s^*} \right\} \quad (5-6)$$

Introducing the dimensionless radius

$$R_s = r_s^*/r_{s0}^* \quad (5-7)$$

where  $r_{s0}^*$  is the radius of the droplet initially injected into the combustion chamber; recalling the definition of the dimensionless mass burning rate from Equation (2-22); and noting

$$Re \{ \dot{m}_l \} = P_r \dot{m}_o \quad (5-8)$$

Equation (5-6) becomes:

$$P_{rt} = R_e \left\{ \frac{\int_0^1 f P_r \dot{m}_o R_s dR_s}{\int_0^1 f \dot{m}_o R_s dR_s} \right\} \quad (5-9)$$

Equation (5-9) can be solved numerically by dividing the spray distribution into finite increments of  $\Delta R_s$  and summing the weighted responses of all the size groups.

When a polydisperse spray (more than one initial size droplet) is injected into the combustion chamber, the overall spray can be thought of as many separate spray sets being injected into the chamber, where each spray set is a monodisperse spray.

The number of droplets from each spray set in an increment  $dr_s^*$  is  $Nfdr_s^*$ , where  $N$  is the total number of droplets in each spray set and is related to the number of drops injected per unit time per set, and  $f$  has the same definition as for a monodisperse spray.

The number of drops injected per unit time in an initial size interval  $dr_{s0}^*$  is  $Igdr_{s0}^*$ , where  $I$  is the total number of drops

injected per unit time, and  $g$  is a function of  $r_{s_o}^*$ , pressure, and the injector. The fraction of droplets injected per unit time in a given interval  $dr_{s_o}^*$  is  $g dr_{s_o}^*$ .

Two new dimensionless radii are defined as follows:

$$R_{s_{ref}} = \frac{r_s^*}{r_{s_o_{ref}}^*} \quad 0 \leq R_{s_{ref}} \leq 1$$

$$R_{s_o_{ref}} = \frac{r_{s_o}^*}{r_{s_o_{ref}}^*} \quad 0 \leq R_{s_o_{ref}} \leq 1 \quad (5-10)$$

where  $r_{s_o_{ref}}^*$  is the largest drop injected into the combustion chamber.

Substituting Equation (5-10) into Equation (5-9) and taking into account the polydisperse spray, gives the following result

$$P_{rt} = R_e \left\{ \frac{\int_0^1 g \left[ \int_0^1 N f P_{r_o} \dot{m}_o R_{s_{ref}} dR_{s_{ref}} \right] dR_{s_o_{ref}}}{\int_0^1 g \left[ \int_0^1 N f \dot{m}_o R_{s_{ref}} dR_{s_{ref}} \right] dR_{s_o_{ref}}} \right\} \quad (5-11)$$

The polydisperse spray can be solved numerically by separating the spray into drop size groups and individual spray sets, by a simple extension of the method used for monodisperse sprays.

The remaining assumptions are similar to those employed in the response analysis. The effect of droplet heat-up is ignored, with temperature gradients assumed to persist in the liquid phase. The effect of convection is also neglected so that specific combustion chamber configurations need not be considered at this point.

The distribution of droplet sizes in the combustion chamber depends upon the range of droplet sizes injected and the steady combustion characteristics of each size. Figure 25 outlines the process, schematically. Each spray set has a total lifetime,  $t_L^*$ . The number of droplets in the chamber originating from a given initial size  $r_{s0}^*$  is equal to the number of droplets of that size injected per unit time, times the lifetime of that size. The number of drops per size group, resulting from a given initial size, is given by the fraction of the lifetime spent within any subsidiary size group.

When more than one size droplet is injected, the additional spray sets can contribute to droplet size groups of the primary spray set as indicated in Figure 25. In this case, the size distribution of the droplets within the spray must be obtained by summing over all drop size groups.

### 5.2 Life History Analysis

As indicated earlier, the time variation of droplet size must be known in order to determine the spectrum of droplet sizes in a spray from the injected size distribution. This can be determined by considering the mass balance of the droplet

$$4\pi r_s^{*2} \rho_f \frac{dr_s^*}{dt^*} = -4\pi \dot{m}^* \quad (5-12)$$

where

$$\dot{m}^* = r_s^* \lambda_{\infty 0}^* \dot{m}/Cp^* \quad (5-13)$$

The dimensionless steady state mass flow rate per unit solid angle for any given sized droplet, can be approximated (as explained

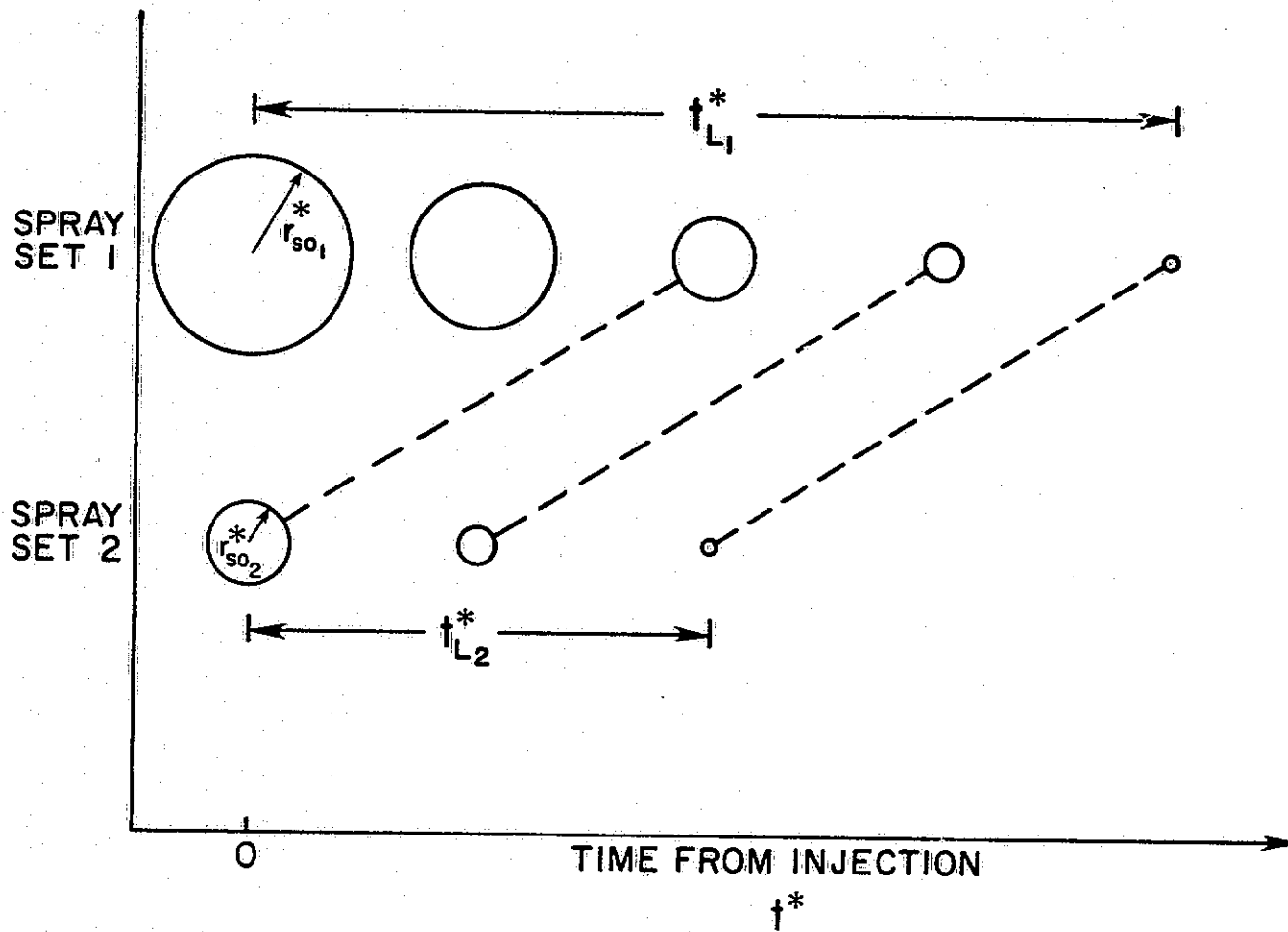


Figure 25 Spray Combustion Model

in Chapter III) by the sum of the small drop limit and the large drop limit mass flow rates as follows:

$$\dot{m}_o = \dot{m}_{o_{SDL}} + \dot{m}_{o_{LDL}} \quad (5-14)$$

The large drop limit mass flow rate is a function of  $A^{1/2}$  from Equation (2-78) and can be transformed into

$$\dot{m}_{o_{LDL}} = \left( \frac{A_o}{A_s} \right)^{1/2} \left( \frac{r_s^*}{r_{so}^*} \right) \quad (5-15)$$

where  $r_{so}^*$  is the initial drop radius,  $A_o$  is the value of  $A$  for  $r_{so}^*$  and the combustion chamber pressure,  $A_s$  is obtained from the one-dimensional strand analysis, and  $\dot{m}_{o_{SDL}}$  is calculated from Equation (2-75). Thus, the mass flow rate of a given sized droplet can be approximated by

$$\dot{m}_o = \dot{m}_{o_{SDL}} + \left( \frac{A_o}{A_s} \right)^{1/2} (R_s) \quad (5-16)$$

In order to put Equation (5-12) into a generalized form,  $R_s$  and

$$\tau = \frac{t^* \lambda_{\infty}^*}{r_{so}^{*2} \rho_f^* C^* p} \quad (5-17)$$

are introduced.

Combining Equations (5-12), (5-13), (5-16), and (5-17) the following relationship is obtained

$$R_s \frac{dR_s}{dt} \left[ \frac{1}{\dot{m}_{o_{SDL}} + \left( \frac{A_o}{A_s} \right)^{1/2} R_s} \right] = -1 \quad (5-18)$$

Separating variables and integrating Equation (5-18), noting that  $\tau = 0$  at  $R_s = 1$ , yields

$$\tau = \frac{(1 - R_s)}{\left(\frac{A_o}{A_s}\right)^{1/2}} + \frac{\dot{m}_{oSDL}}{\left(\frac{A_o}{A_s}\right)} \ln \left[ \frac{\dot{m}_{oSDL} + \left(\frac{A_o}{A_s}\right)^{1/2} R_s}{\dot{m}_{oSDL} + \left(\frac{A_o}{A_s}\right)^{1/2}} \right] \quad (5-19)$$

where  $\dot{m}_{oSDL}$  and  $A_s$  are functions of pressure ( $A_s$  for the non-wet bulb case is relatively constant with pressure for  $E = 10$  and  $n = 2$ ) and  $A_o$  is a given constant depending upon the injected droplet size.

For the limit as  $A_o/A_s$  approaches zero, integrating Equation (5-18) yields

$$\tau = \frac{1 - R_s^2}{2\dot{m}_{oSDL}} \quad (5-20)$$

which represents the size variation for a small droplet.

Setting  $R_s = 0$  in Equations (5-19) or (5-20) yields the dimensionless lifetime  $\tau_L$  for drops originating with a radius  $r_{so}^*$ . The fraction of these droplets in a size range  $R_s' - R_s''$  is then given by

$$F(R_s' - R_s'') = (\tau(R_s'') - \tau(R_s'))/\tau_L \quad (5-21)$$

The response has been determined as a function of  $\omega$  and  $A$ , at a given pressure and injected liquid temperature. These quantities are related to values based upon the injected radius,  $\omega_o$ , and  $A_o$  as follows

$$A_j = A_o R_{s_j}^2, \quad \omega_j = \omega_o R_{s_j}^2 \quad (5-22)$$

for any size group,  $j$ . The response of each size group,  $j$ , is then summed using Equation (5-9) to give the total response. A second weighted sum is required if more than one initial drop size is

injected. In this case a reference size is more convenient and

$$A_j = A_{o_{ref}} \left( \frac{r_{s_j}^*}{r_{so_{ref}}^*} \right)^2, \quad \omega_j = \omega_{o_{ref}} \left( \frac{r_{s_j}^*}{r_{so_{ref}}^*} \right)^2 \quad (5-23)$$

In the following, the reference size has been taken to be the largest droplet size injected, and the total response is calculated from Equation (5-11).

## CHAPTER VI

### SPRAY COMBUSTION RESULTS

#### 6.1 Droplet Burning Time

Employing Equation (5-9), calculations of droplet lifetimes were completed for a range of conditions. Figure 26 shows the nondimensional droplet lifetime as a function of  $A_o/A_s$  and pressure, for both the wet and non-wet bulb cases. At the large drop limit, the dimensionless lifetime is relatively independent of pressure. This is true for a second order reaction, where the burning rate per unit area is proportional to pressure. At the small drop limit for the non-wet bulb case,  $\tau_L$  increases with increasing pressure, due to the reduction in  $\dot{m}_{o,SDL}$  with pressure. For the wet bulb case,  $\tau_L$  decreases with increasing pressure at the small drop limit, since  $\dot{m}_{o,SDL}$  increases with increasing pressure at this condition.

Figures 27 and 28 show the variation of dimensionless radius with dimensionless time and  $A_o/A_s$ ; at a pressure of 10 atmospheres for both non-wet and wet bulb conditions. These figures show that as  $A_o/A_s$  increases,  $\tau_L$  decreases for a given pressure. This is due to the increased gasification rate caused by decomposition near the droplet surface. Results at 1 and 100 atmospheres are similar to Figures 27 and 28.

Table 7 lists the dimensional droplet lifetimes as a function of pressure and initial drop radius.

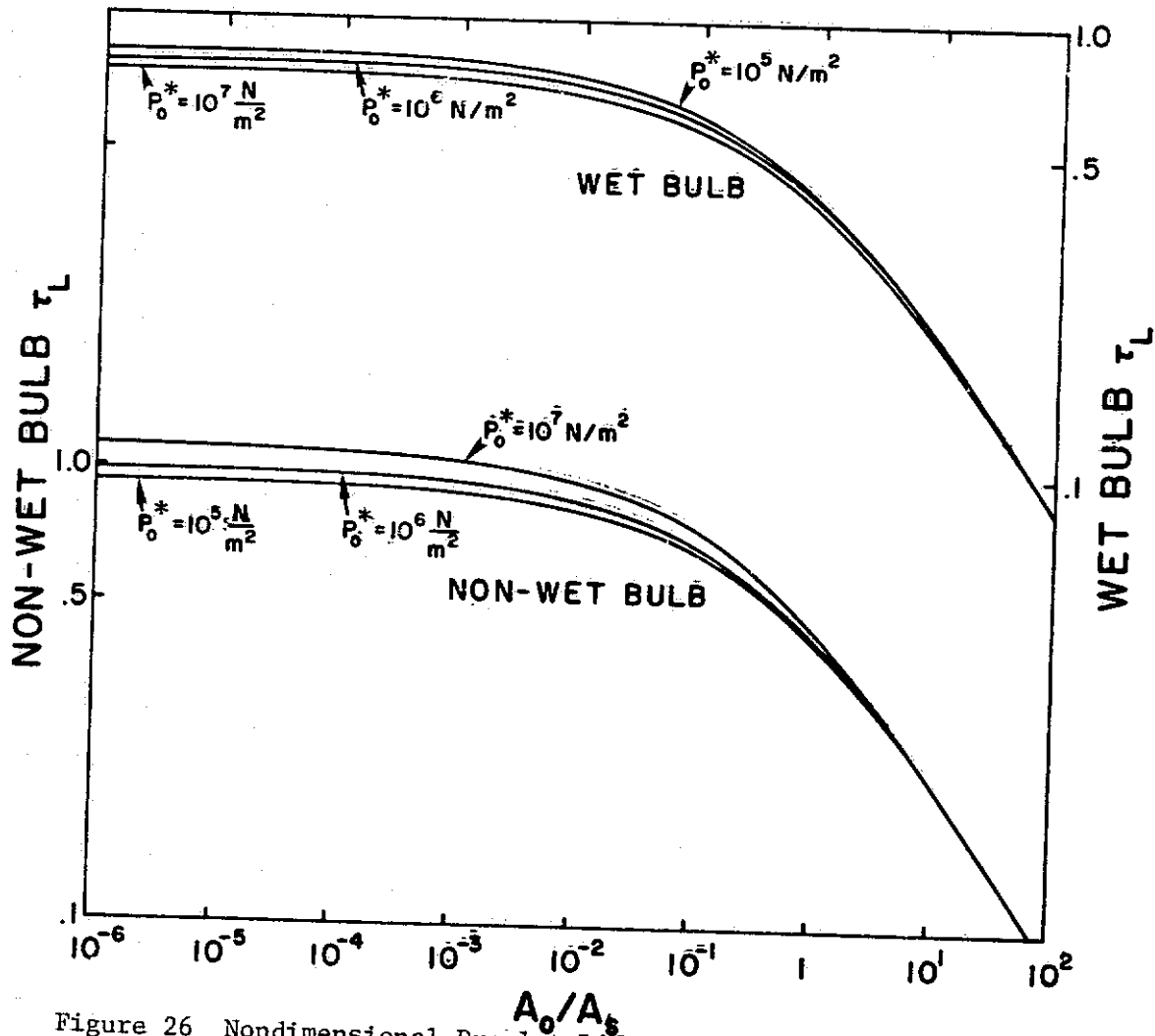


Figure 26 Nondimensional Droplet Lifetimes as a Function of  $A_0/A_s$

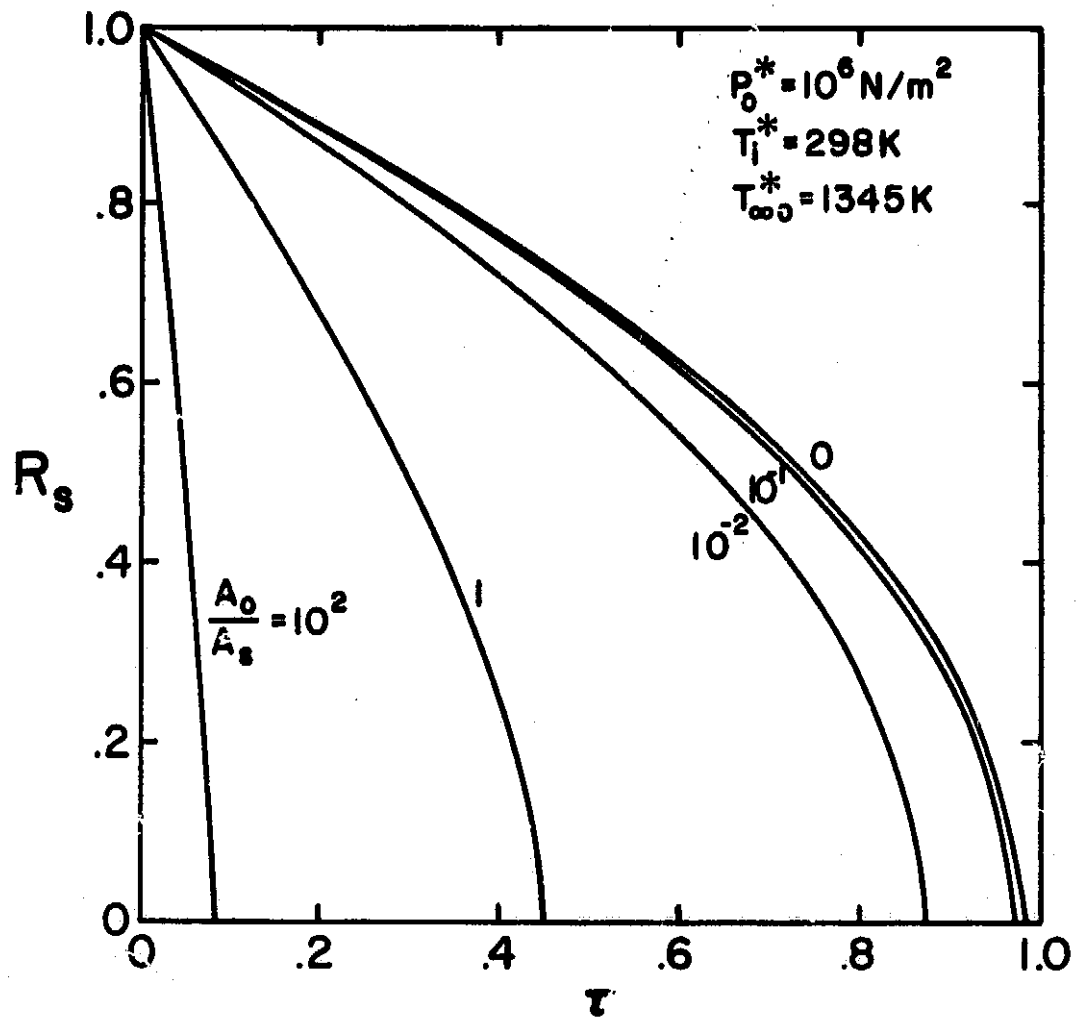


Figure 27 Nondimensional Droplet Burning Time as a Function of Nondimensional Droplet Radius at Approximately 10 Atm. Pressure (Non-Wet Bulb Conditions)

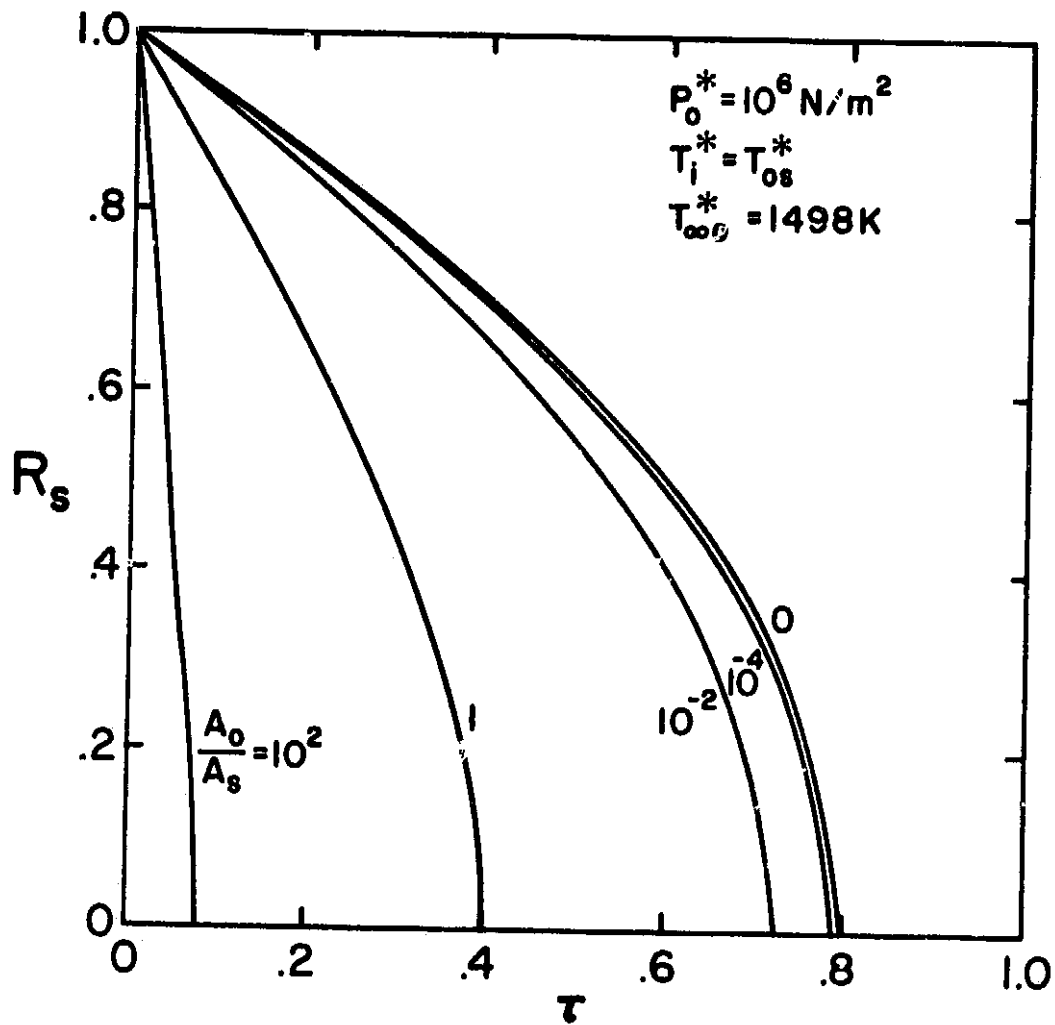


Figure 28 Nondimensional Droplet Burning Time as a Function of Nondimensional Droplet Radius at Approximately 10 Atm. Pressure (Wet Bulb Conditions)

Table 7

Dimensional Droplet Lifetimes as a Function of  
Initial Radius and Pressure

$P^*$ ( $N/m^2$ )	$r_{so}^*$ ( $\mu$ ) = 10	100	1000
<u>(Non-Wet Bulb)</u>			
		(seconds)	
$10^5$	0.00158	0.128	4.79
$10^6$	0.00135	0.0489	0.728
$10^7$	0.000507	0.00734	0.0788
<u>(Wet Bulb)</u>			
		(seconds)	
$10^5$	0.00141	0.109	3.61
$10^6$	0.000955	0.0272	0.361
$10^7$	0.000179	0.0020	0.0229

The wet bulb droplets consistently have shorter lifetimes because of their higher mass burning rates. For all cases, at a given initial radius, the lifetime decreases with increasing pressure. This is caused by the fact that a given radius corresponds to a larger value of  $A$  at higher pressures, yielding a greater mass burning rate. At a constant pressure, the lifetime increases with drop size, which is to be expected.

The response portion of the present analysis is not valid at frequencies having an oscillation period comparable to the lifetime of the droplet. This provides a minimum droplet size that can be

considered by the present analysis. The probable oscillation periods of instability range from  $2 \times 10^{-3}$  to  $3 \times 10^{-5}$  seconds/cycle (corresponding to the 500-30,000 Hz range indicated in Reference [1]). At the oscillation period limit of  $2 \times 10^{-3}$  seconds/cycle, the minimum drop radius is approximately  $13 \mu$  at pressures of 1 and 10 atmospheres, for both wet and non-wet bulb conditions. At a pressure of 100 atmospheres, the minimum drop radius is approximately  $30 \mu$  at the non-wet bulb condition, and approximately  $95 \mu$  for the wet bulb case. At the other limit of  $3 \times 10^{-5}$  seconds/cycle the minimum droplet radius is approximately  $2 \mu$  at all pressures and both wet and non-wet bulb conditions. This indicates that at low frequencies, appreciable response may be generated by droplet lifetime characteristics, a mechanism that has not been considered in the present investigation.

## 6.2 Quasi-Steady Gas Phase Spray Response

If a monodisperse spray is injected into the combustion chamber, the total response,  $P_{rt}$ , is the weighted sum of all drop sizes existing in the chamber. Figure 29 illustrates the non-wet bulb total response of a monodisperse spray as a function of frequency,  $\omega_0$ , for a pressure of 10 atmospheres. The values of  $A_0$  were chosen so that the first drop size group (which has the largest mass fraction) has an  $A$  for which the droplet response has previously been computed. The solid lines correspond to the entire spray while the dashed lines correspond to the situation when it is assumed that all drop sizes are approximated by a constant drop size equal to  $A_0$ . For these two cases, the peaks occur at approximately the same frequency, while the magnitude of the peak is slightly larger when

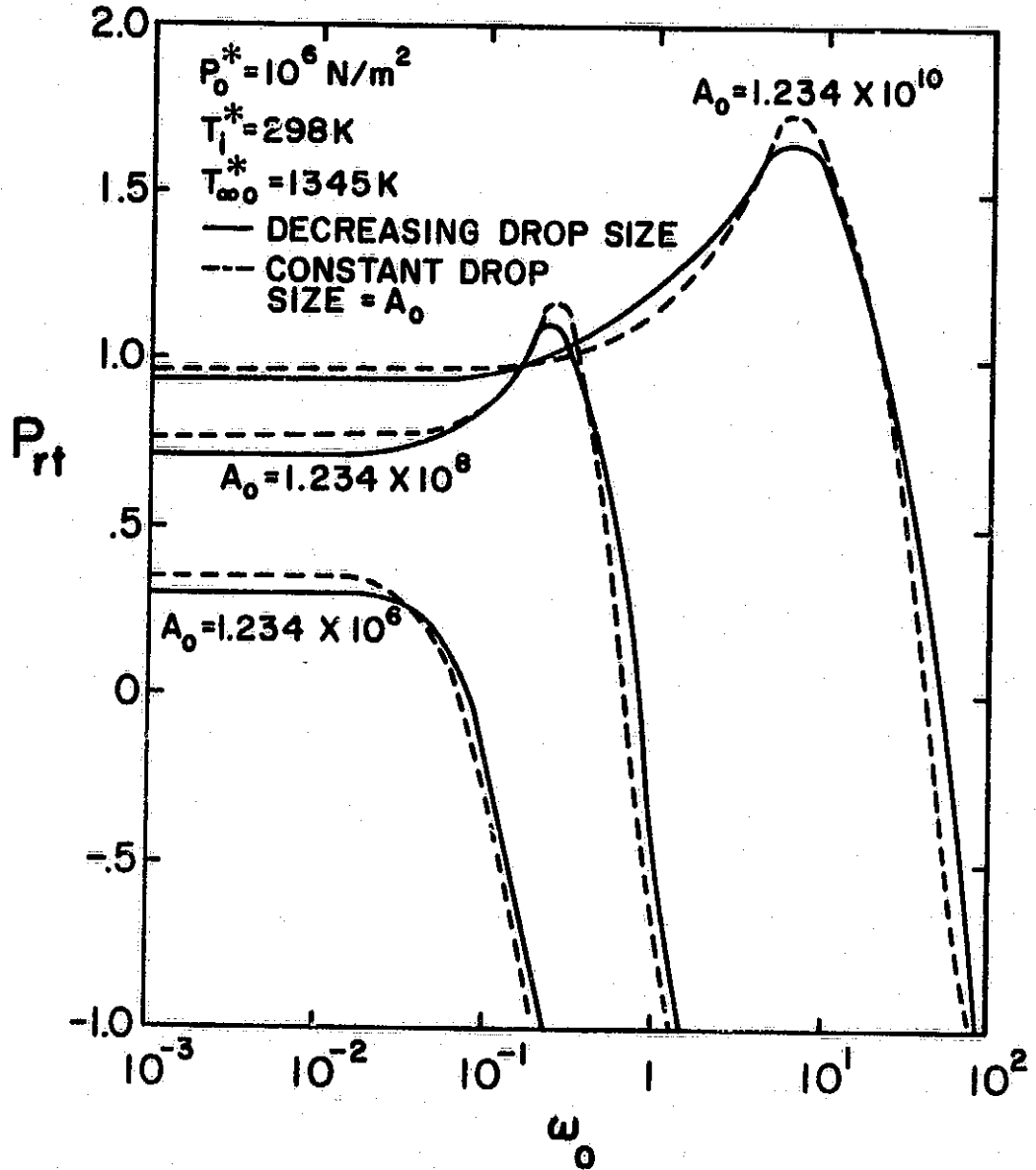


Figure 29 Total Response as a Function of  $\omega_0$  for a Monodisperse Spray at Approximately 10 Atm. Pressure (Non-Wet Bulb Conditions)

the drop size is assumed constant. The reduction in the response peak of the spray is due to the reduced response of the smaller droplets. It should be noted that for the case when the drop size is constant at  $A_o = 1.234 \times 10^{10}$ , transient gas phase effects begin to appear at approximately  $\omega_o = 6.98 \times 10^1$ . This corresponds to  $\omega_s = 10^{-1}$ .

Figure 30 is the wet bulb total response for a monodisperse spray as a function of  $\omega_o$  at 10 atmospheres pressure. The same conclusion can be drawn as from the non-wet bulb case. The total responses at pressures of 1 and 100 atmospheres for both wet and non-wet bulb conditions give similar results. The shapes of the total response curves in Figures 29 and 30 are very similar to the shape of the individual response curves for  $A_o$ . In all cases, five drop size groups were used, in which approximately 60% of the total mass occurred in the first group.

When a polydisperse spray is introduced into the combustion chamber, the spray is separated into discrete spray sets, each with its own  $A_o$ . The smaller initial drop size spray sets are placed in the corresponding size groups of the largest spray set as shown in Figure 25. The responses are weighted and summed, and the total response is obtained.

Figure 31 is a plot of a non-wet bulb polydisperse spray at a pressure of 10 atmospheres, consisting of three spray sets with  $A_o$ 's of  $1.234 \times 10^{10}$ ,  $1 \times 10^9$ , and  $1.234 \times 10^6$ . The response from each size group is weighted and summed in order to obtain the total response. The mass fractions of the spray sets and injection rates are varied, as listed in Figure 31. The total responses are greater

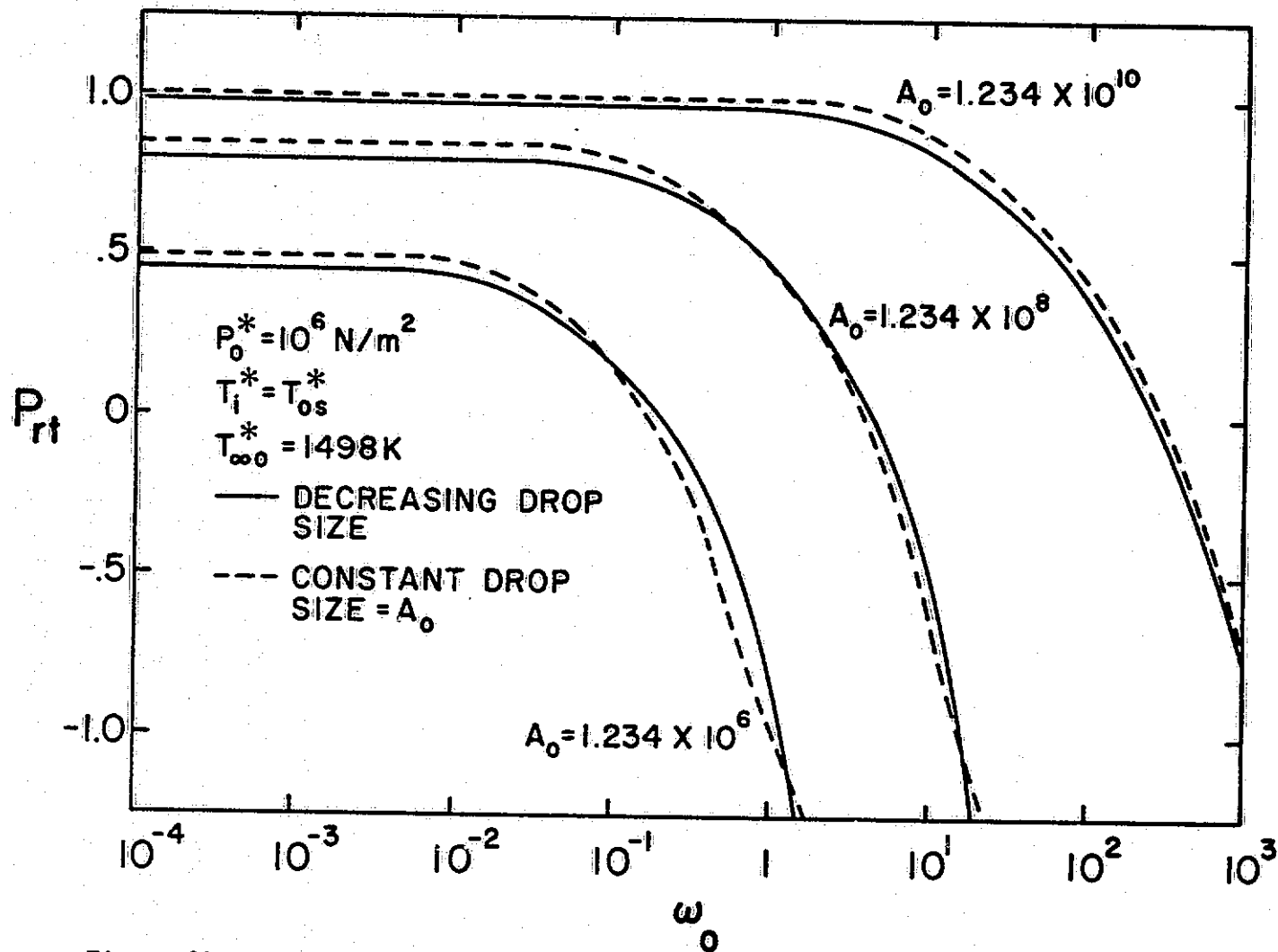
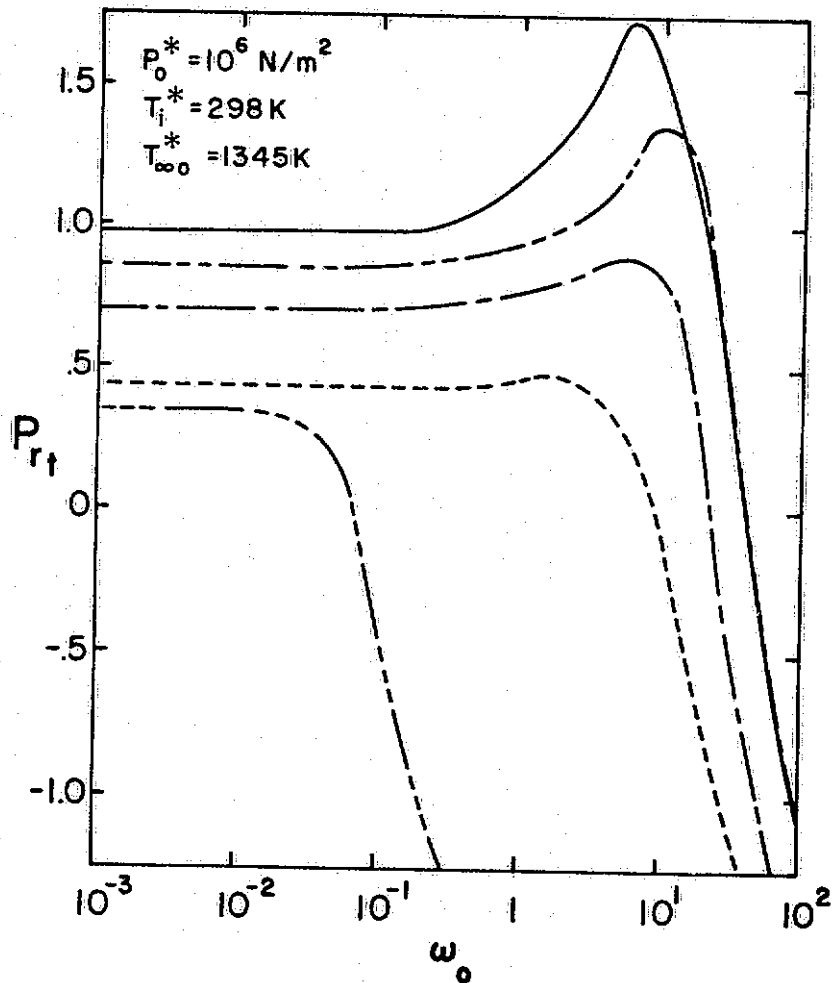


Figure 30 Total Response as a Function of  $\omega_0$  for a Monodisperse Spray at Approximately 10 Atm. Pressure (Wet Bulb Conditions)



$A_0 (\times 10^8)$	% MASS IN CHAMBER			% DROPS/SEC. INJECTED			% MASS/SEC. INJECTED		
	123	10	.0123	123	10	.0123	123	10	.0123
—	100 <sup>a</sup>	0	0	100 <sup>a</sup>	0	0	100 <sup>a</sup>	0	0
- - -	10	30	60	.001	.053	99.946	.1	1.4	98.5
- · - · -	60	30	10	.005	.315	99.68	3.4	7.7	88.9
- - -	49.5	49.5	1.0	.05	4.98	94.97	11.47	51.78	36.75
- - -	0	0	100 <sup>a</sup>	0	0	100 <sup>a</sup>	0	0	100 <sup>a</sup>

<sup>a</sup> ALL DROPS IN THE SPRAY ARE AT A CONSTANT SIZE  $A_0$

Figure 31 Total Response as a Function of  $\omega_0$  for a Polydisperse Spray at Approximately 10 Atm. Pressure for Varying Spray Set Mass Fractions and Injection Rates (Non-Wet Bulb Conditions)

than unity when the larger  $A_0$  spray sets comprise about 30% of the injected spray mass. The results indicate, however, that even a very small percentage of large drops in the injected spray can result in substantial response. Findings at other pressures for both wet and non-wet bulb conditions are similar; however, for the wet bulb case, no peaks greater than unity are observed.

## CHAPTER VII

### SUMMARY AND CONCLUSIONS

#### 7.1 Summary

The present study considered the steady state combustion and oscillatory response of a single monopropellant droplet subjected to imposed pressure oscillations, followed by an estimation of the characteristics of an entire spray. The specific objectives of the study are as follows:

1. Develop a mathematical model for the burning of a liquid monopropellant droplet for both steady state and oscillatory pressure conditions.
2. Theoretically investigate the steady state droplet burning for both wet and non-wet bulb conditions; and compare the results with available measurements.
3. Investigate the theoretical burning response for wet and non-wet bulb conditions.
3. Develop a mathematical model for one-dimensional, quasi-steady spray combustion, and calculate the overall spray combustion response for both wet and non-wet bulb conditions.

The present theoretical model is an extension of the one-dimensional strand model developed by Allison and Faeth [11]. The major assumptions in the analysis are: a one-step, irreversible gas phase reaction, conventional low pressure phase equilibrium at the liquid surface; constant liquid phase physical properties, and

variable gas phase physical properties. The present calculations were based on the reaction and the physical property characteristics of hydrazine.

A limitation of the work involves neglecting forced convection, yielding a spherically symmetric flow field. It is believed that low droplet velocities represent a critical condition for instability [1], and forced convection is of minor importance when the reaction zone is very near the surface [25, 26], a condition where the response for monopropellants is greatest.

The theoretical approach employs the use of a perturbation analysis in which the amplitude of the imposed pressure oscillation is taken as the small perturbation parameter.

The oscillatory (first-order) solution involves a transient liquid and both transient and quasi-steady gas phase effects. The results indicated that most of the transient gas phase effects lie outside the probable instability range at realistic combustion chamber pressures. Therefore, the spray response calculations were confined to conditions where a quasi-steady gas phase is valid.

Finally, a one-dimensional quasi-steady spray combustion model is developed in which the spray is divided into size groups, and the response is weighted and summed over all groups, to give the total spray response.

## 7.2 Conclusions

This section is divided into three parts: steady state combustion, oscillatory combustion, and spray combustion.

7.2.1 Steady State Combustion. The major conclusions of the steady state portion of this study are as follows:

1. The theoretical droplet surface temperatures are identical to the measured and predicted strand values from Reference [11].
2. Steady state droplet mass burning rates can be divided into three regions: large, intermediate, and small drop regions. The large drop region can be approximated by a one-dimensional strand, while the small drop region is similar to a small drop evaporating in absence of reaction. Most drop sizes of technological importance fall within the intermediate region ( $10^4 < A < 10^9$ ).
3. At the non-wet bulb small drop limit, the burning rate decreases with increasing pressure because the higher pressures raise the surface temperature, while the ambient temperature is constant. The reduced temperature difference between the liquid surface and the ambient gas causes a reduction in the droplet gasification rate.
4. The wet bulb small drop limit burning rate increases with pressure. This is caused by the increase in the ambient temperature with pressure, which compensates for the increase in surface temperature.
5. At all pressures, the wet bulb burning rate is higher than the non-wet bulb case. This is due to the fact that the wet bulb droplet has a higher ambient temperature, and from the fact that the heat conducted back into the wet

REPRODUCIBILITY OF THE  
ORIGINAL PAGE IS POOR

bulb droplet goes only into vaporizing the liquid, not in heating the droplet liquid.

7.2.2 Oscillatory Combustion. The major conclusions of the oscillatory portion of this study are as follows:

1. At the small drop limit, the response is negative and becomes more negative with increasing pressure. This results from the gasification rate decrease as the surface temperature increases for a constant ambient temperature. (The wet bulb response is less negative than the non-wet bulb case.) Therefore, pressures above the mean result in reduced gasification rates while pressures below the mean result in increased gasification rates - yielding a negative response.
2. The large drop limit results give good agreement with the one-dimensional strand results of Reference [11].
3. At the non-wet bulb large droplet limit, response peaks occur near the characteristic frequency for the liquid and gas phase thermal waves. With increasing pressure, these liquid and gas phase peaks approach each other and increase in magnitude.
4. At the wet bulb large drop limit, no response peaks occur from liquid transient effects.
5. As the drop size decreases, the response also decreases.
6. The transient gas phase response is not a major contributor to combustion instability at the frequencies and pressures where instability has a high probability

of occurring. Thus, a quasi-steady gas phase analysis can be assumed in most instances.

7. A response peak will occur only when the mean temperature gradient near the droplet surface has sufficient steepness, so that enough energy will flow from the surface towards the center of the drop, causing the perturbation temperature to lead the pressure. When the mean temperature gradient is not steep enough, (which occurs near the wet bulb case for properties used in the present calculations) the perturbation surface temperature will lag behind the pressure at all frequencies.

7.2.3 Spray Combustion. The major conclusions of the spray combustion portion of the study are as follows:

1. The total response of a polydisperse spray is less than the response of the largest droplet injected.
2. Relatively small numbers of injected large drops greatly influence the spray by adding a substantial response.
3. A spray response of order unity, due to the liquid phase thermal wave, has been observed, indicating that this is a viable mechanism for producing combustion instability.
4. At high pressures and low frequencies (on the order of 500 Hz) the large burning rates of monopropellant droplets provide droplet lifetimes near the cycle period for drop sizes of technological importance. Under these conditions, droplet lifetime effects contribute to the response; thus, this phenomena should be investigated next.

## BIBLIOGRAPHY

1. Harrje, D. T. (Ed.), Liquid Propellant Rocket Combustion Instability, NASA SP-194, 1974.
2. Allison, C. B., "Hybrid and Decomposition Combustion of the Hydrazine Fuels," NASA CR-72977, July 1971.
3. Allison, C. B., "Burning Rate Response of Liquid Monopropellants to Imposed Pressure Oscillations," NASA CR-134541, January 1974.
4. Fendell, F. E., "Finite Rate Burning of a Monopropellant Droplet in a Stagnant Atmosphere," Astronautica Acta, Vol. 11, No. 6, 1965, pp. 418-421.
5. Williams, F. A., "Theory of the Burning of Monopropellant Droplets," Combustion and Flame, Vol. 3, December 1959, pp. 529-544.
6. Spalding, D. B., and Jain, V. K., "Theory of the Burning of Monopropellant Droplets," A.R.C. Technical Report No. 20-176, Current Paper No. 447, 1958.
7. Jain, V. K., "The Theory of Burning of Monopropellant Droplets in an Atmosphere of Inerts," Combustion and Flame, Vol. 7, March 1963, pp. 17-27.
8. Tarifa, C. S., del Notario, P. P., and Moreno, F. G., "Combustion of Liquid Monopropellants and Bipropellants in Droplets," Eighth Symposium (International) on Combustion, Williams and Wilkins, Baltimore, 1962, pp. 1035-1056.
9. Allison, C. B., and Faeth, G. M., "Decomposition and Hybrid Combustion of Hydrazine, MMH, and UDMH as Droplets in a Combustion Gas Environment," Combustion and Flame, Vol. 19, No. 2, October 1972, pp. 213-226.
10. Lorell, J., and Wise, H., "Steady State Burning of a Liquid Droplet. I. Monopropellant Flame," The Journal of Chemical Physics, Vol. 23, No. 10, October 1955, pp. 1928-1932.
11. Allison, C. B., and Faeth, G. M., "Open-Loop Response of a Burning Liquid Monopropellant," AIAA Journal, Vol. 13, No. 10, October, 1975, pp. 1287-1294.
12. Crocco, L. and Cheng, S. I., Theory of Combustion Instability in Liquid Propellant Rocket Motors, AGARDograph No. 8, Butterworths Scientific Publications, London, 1956.
13. Crocco, L., "Research on Combustion Instability in Liquid Propellant Rockets," Twelfth Symposium (International) on Combustion, The Combustion Institute, Pittsburgh, 1969, pp. 85-99.

14. Crocco, L., "Theoretical Studies on Liquid Propellant Rocket Instability," Tenth Symposium (International) on Combustion, The Combustion Institute, Pittsburgh, 1965, pp. 1101-1128.
15. Priem, R. J., and Heidmann, M. F., "Propellant Vaporization as a Design Criteria for Rocket-Engine Combustion Chambers," NASA TR R-67, 1960.
16. Priem, R. J., and Guentert, D., "Combustion Instability Limits Determined by a Non-Linear and a One-Dimensional Model," NASA TN D-1409, 1962.
17. Priem, R. J., "Influence of the Combustion Process on Stability," NASA TN D-2957, 1965.
18. Williams, F. A., "Response of a Burning Fuel Plate to Sound Vibrations," AIAA Journal, Vol. 3, No. 11, November 1965, pp. 2112-2124.
19. Strahle, W. C., "Periodic Solutions to a Convective Droplet Burning Problem: The Stagnation Point," Tenth Symposium (International) on Combustion, The Combustion Institute, Pittsburgh, 1965, pp. 1315-1325.
20. Strahle, W. C., "Unsteady Reacting Boundary Layer on a Vaporizing Flat Plate," AIAA Journal, Vol. 3, No. 6, June 1965, pp. 1195-1198.
21. Strahle, W. C., "New Considerations on Causes for Combustion Instability in Liquid Propellant Rockets," Combustion Science and Technology, Vol. 2, August 1970, pp. 29-40.
22. Heidmann, M. F., and Wieber, P. R., "Analysis of Frequency Response Characteristics of Propellant Vaporization," AIAA Paper No. 66-604, 1966.
23. T'ien, J. S., and Sirignano, W. A., "Unsteady Thermal Response of the Condensed-Phase Fuel Adjacent to a Reacting Gaseous Boundary Layer," Thirteenth Symposium (International) on Combustion, The Combustion Institute, Pittsburgh, 1971, pp. 529-539.
24. T'ien, J. S., "Oscillatory Burning of Solid Propellants Including Gas Phase Time Lag," Combustion Science and Technology, Vol. 5, 1972, pp. 47-54.
25. Faeth, G. M., "Monopropellant Droplet Burning at Low Reynolds Numbers," Combustion and Flame, Vol. 11, No. 2, April 1967, pp. 167-174.
26. Faeth, G. M., "Flame Zone Development of Monopropellant Droplets," Combustion and Flame, Vol. 12, No. 5, October 1968, pp. 411-416.

27. Williams, F. A., "On the Assumptions Underlying Droplet Vaporization and Combustion Theories," The Journal of Chemical Physics, Vol. 23, No. 1, July 1960, pp. 133-144.
28. Bird, R. B., Stewart, W. E., and Lightfoot, E. N., Transport Phenomena, John Wiley and Sons, Inc., New York, 1960.
29. Faeth, G. M., "High Pressure Liquid Monopropellant Strand Combustion," Combustion and Flame, Vol. 18, No. 1, February 1972, pp. 103-113.
30. Faeth, G. M., "Prediction of Pure Monopropellant Droplet Life Histories," AIAA Journal, Vol. 8, No. 7, July 1970, pp. 1308-1314.
31. McHale, E. T., Knox, B. E., and Palmer, H. B., "Determination of Kinetics of Hydrazine Using a Single-Pulse Shock Tube," Tenth Symposium (International) on Combustion, The Combustion Institute, 1965, pp. 341-351.